UNSTEADY CLEAVAGE CRACK PROPAGATION IN SODIUM CHLORIDE CRYSTALS

A study of microstructural characteristics

LELIA S. DE WAINER

A thesis submitted to the University of Warwick in support of an application for admission to the degree of Doctor of Philosophy.

Physics Department, University of Warwick
Crystallography Div. Argentine Atomic Energy Commission

June 1976

DECLARATION

This thesis is submitted to the University of Warwick in support of my application for admission to the degree of Doctor of Philosophy.

It contains an account of my own research work carried out at the Physics Department of the University of Warwick from October 1967 to October 1968, and at the Crystallography Division of the Argentine Atomic Energy Commission, from November 1968 to July 1975 under the general supervision of Mr. G.A. Bassett and the local supervision, in Buenos Aires, of Dr. M.E.J. de Abeledo.

The research work described in this thesis is the result of my own independent research activity except where the assistance of collaboration is specifically acknowledged.

Some of the work has been published previously and a copy of the original communication reprinted from a scientific journal, and a Xerox copy of the abstracts of communications read at a scientific conference are included at the end of the thesis.

This work has not been used previously in whole or in part in a degree thesis submitted to this or any other university.

[redacted]

Lelia Schmirgeld de Wainer

Buenos Aires

June 1976

Summary

The knowledge of dislocation mechanisms by which plastic deformation may relax the stresses concentrated at the tip of a cleavage crack in crystals is of fundamental importance to control fracture in materials of technological application.

A propagating crack leaves, on the cleavage surfaces, characteristic traces due to the multiplication and movement of dislocations nucleated ahead of the crack tip, as discussed in chapter 1.

One of the purposes of this thesis is to make a comprehensive study of the changes in surface markings accompanying accelerations and decelerations of a propagating cleavage crack in alkali halides, and to relate the resulting plastic deformation with these surface structures.

With this aim in mind, the regions limited by successive stopped crack fronts are studied by several techniques, described in chapters 2 and 5. These techniques comprise a wide range of magnification: from macromethods like optical microscopy to micromethods like electron microscopy of decorated replicas, which allow the observation of monoatomic structures.

In this connexion a new technique, described in chapter 3,is developed which permits, in most cases, the determination of the sign of elementary steps. This technique constitutes an important advance since possible modifications of cleavage structures due to the heat-

activated movement of dislocations are avoided and the resolution attainable by decoration is improved.

The results of these complementary experiments are described in chapter 4.

X-ray topography studies are particularly efficient to determine the slip systems activated by the propagating crack as discussed in chapter 5.

From these chapters an integral picture of the phenomena accompanying unsteady crack propagation is envisaged. Dislocation mechanisms responsible for the formation of the cleavage structures are discussed in chapter 6.

The possibility of quantitative measurements which would allow a theoretical analysis of the subject is discussed in chapter 7.

ACKNOWLEDGEMENTS

The first part of this work has been carried out in the Physics Department of the University of Warwick and I am grateful to Professor A.J. Forty and to Mr. G.A. Bassett for making the facilities of the laboratory available to me. It has been completed in the Crystallography Division of the Argentine Atomic Energy Commission and I am grateful to Dr. G. Videla for permission to continue this research.

I would like to extend my sincere gratitude to Mr. G.A. Bassett who introduced me to the subject of cleavage in ionic crystals. I am indebted to him for his valuable help and advice, his continuous interest and encouragement during the whole period in which this work was carried out.

I would also like to thank Professor Forty for his interest and valuable suggestions and to Dr. Abeledo and Ing. E.E. Galloni for their advice and continuous interest.

I express my gratitude to Lic. M.A.R. de Benyacar for many valuable discussions and her unfailing encouragement.

Thanks are also due to Lic. V. Miguez for her collaboration in the preparation of the etched specimens and to Lic. E. Manghi for her collaboration during studies with X-ray diffraction topography and for the use of her apparatus at the Argentine Armed Forces Scientific and Technological Research Laboratories (CITEFA).

I gratefully acknowledge many members of the Crystallography Division staff, particularly Miss S. Cordeyro for help in various ways, and to Miss J. Boretto for carrying out the typing of this manuscript.

Finally my thanks are due to the Overseas Development Ministry of the British Government and to the Argentine Government for a technological assistance grant during the first year of this research.

TABLE OF CONTENTS

LIST OF ILLUSTRATIONS

Chapter 1

Introduction

1.1. General

The knowledge of the mechanisms controlling fracture in solids is a topic of technological interest as there is an ever increasing demand for improved high strength engineering materials: alloys, ceramics or glasses. Among these mechanisms, those by which the propagation of cracks can be stopped are of particular interest.

It has long been recognized that in crystalline materials plastic deformation can accompany the propagation of a crack otherwise regarded as brittle. Under favourable conditions, this plastic flow can slow down a crack or impede its propagation.

The purpose of the research to be described in this thesis is to make a comprehensive study of the surface structures associated with plastic deformation accompanying the propagation of cleavage cracks in ionic crystals for a wide scale of crack propagation velocities. It is particularly relevant to this approach to review the work on aspects of the discontinuous propagation of cleavage cracks in ionic crystals.

It is impossible to start such a survey without mentioning some of the salient points of bulk fracture mechanics, but it is beyond the scope of this work either to review the vast literature in this field accumulated in the last thirty years or to present an historic account of the evolution of knowledge on the subject.

In 1920 Griffith (1) established the basis of fracture mechanics analysis. He was the first to recognize the importance of pre-existing flaws or small cracks, in the fracture of isotropic

materials. He calculated the critical stress σ_c necessary to propagate a pre-existing crack of length c in an elastic isotropic material by minimizing the potential energy

$$\sigma_c > K\sqrt{\frac{2E\gamma}{\pi c}}$$

E = Young's modulus

γ : surface energy per unit area

K : elastic constant of the material; it depends upon the way in which the body is stressed.

This equation was derived using macroscopic thermodynamical arguments, but from an analysis of interatomic forces Orowan (2) demonstrated that when a crystal is loaded in tension with a stress equal in magnitude to that given by Griffith equation, the stress concentration at the tip of the crack reaches the theoretical strength at which fracture is bound to occur.

Griffith equation can be used even for crystalline anisotropic materials if the surface energy term γ is modified to include the contribution of both plastic deformation (3) γ_p and the energy of formation of cleavage steps γ_c (4)

$$\gamma_e = \gamma + \gamma_p + \gamma_c$$

Besides, once fracture has started, the kinetic energy of the propagating crack must be taken into account. Mott(5) was the first to point out that the sum of the kinetic, elastic and surface energies must be conserved as the crack spreads.

The surface energy of the Griffith equation depends on temperature and strain rate. Stroh (6) took into account this dependence

and proposed a model for a propagating crack which shows a transition from brittle to ductile behaviour as the temperature is raised; his model is a development of one previously proposed by Gilman (3).

A knowledge of the stress field around a crack tip is essential to understand plastic relaxation and crack propagation. Rice (7) and others (8) working on strain fields in elastic-plastic and strain hardening solids, applied a contour integral method to find the stress and strain distribution around crack tips.

Recently Andrews (9) developed a fracture mechanics theory which gives fracture criteria for solids without limitations as to their linearity, elastic behaviour, or infinitesimal strain. He suggests that his theory is the only one in which the unloading of elastic materials is taken into account, while previous workers, i.e. Rice, consider only the loading of materials (non-linear elastic situation).

1.1.2. Unsteady cleavage crack propagation

The ability of a cleavage crack to propagate in a crystalline material depends upon the relationship between the orientation of the cleavage plane and the orientation of the planes in which slip can occur in that particular structure. If the stresses concentrated ahead of the crack tip have a non vanishing component on these slip planes, some plastic relaxation of the elastic strain energy stored up in the crystal will occur.

Gilman (10) and Forty (11) were the first to show that these resolved shear stresses are large enough to nucleate dislocations just ahead of slowly moving cracks in lithium fluoride and sodium chloride single crystals, even in dislocation-free regions of the crystals.

They showed that the velocity of propagation of the crack

relative to the rate at which the surrounding structure can deform plastically is of fundamental importance in determining the amount of plastic flow that will accompany crack propagation. Furthermore Gilman et al. (12) derived a critical crack propagation velocity of 6×10^3 cm/seg below which plastic relaxation of the stresses concentrated at the tip of a cleavage crack should occur in lithium fluoride crystals. Similarly Forwood (4) derived a value of 10^4 cm/seg for sodium chloride crystals. Further work by Forwood and Lawn (14) confirmed by Burns and Webb (15) showed that slip on longitudinal slip systems (defined in Fig. 1.1) does occur above that critical velocity for lithium fluoride crystals.

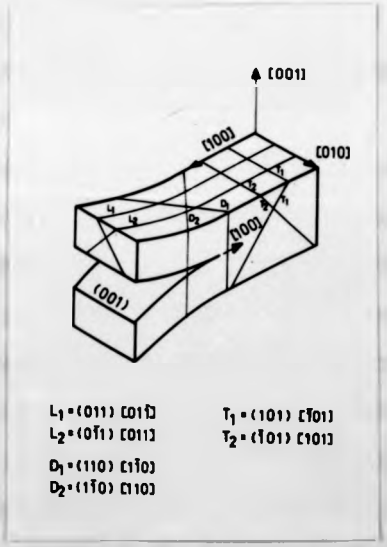

Fig. 1.1. Relationship between longitudinal and transverse slip planes for a (001) crack propagating in the [100] direction.

L_1 L_2 = longitudinal systems

T_1 T_2 = transverse systems

D_1 D_2 = diagonal systems

By the use of different techniques Forty (11) and Gilman (16) found that the regions of the cleavage surfaces where a cleavage crack has stopped are marked by a zone of intense plastic deformation due to the presence of multitudes of dislocation half-loops; in the case of the face centered cubic ionic materials on which they were working the loops lie in the {110} planes. These loops are created ahead of the crack tip and are severed as the crack proceeds. The edge components of the dislocation loops lie parallel to the surface a few microns below it and are responsible for the polygonization observed in the deformation bands. Small cleavage steps stem from the deformation bands and originate in the screw components of the dislocation loops. (13).

Crack propagation velocity is also of fundamental importance in determining the mode of plastic deformation.

From X-ray topography studies of lithium fluoride single crystals, Forwood and Lawn (14) observed that the longitudinal and transverse slip systems are active for a crack propagating at low velocities, while only the longitudinal systems appear for fast cleavages. Deformation bands in lithium fluoride crystals were found to be formed by dislocation loops of both transverse and longitudinal systems by Burns and Webb (17), though they only mention longitudinal systems in more recent work (15).

There is no agreement in the literature about the relationship between cleavage steps and plastic deformation. On one hand Forwood and Lawn (14) related the origin of the transverse mode of deformation to the presence of high cleavage steps. On the other hand, Burns and Webb (17) found that the slip observed in their X-ray topography experiments is not appreciably affected by cleavage steps.

Several mechanisms involving dislocation movement have been

proposed to explain plastic deformation during crack propagation. Based on ideas due to Washburn, Gorum and Parker (18), Burns and Webb (19) proposed a model in which dislocation loops are pushed along by the stresses ahead of the crack tip and can be thus carried over for distances of the order of centimeters.

From fracture dynamics analysis they suggested that the number of dislocations carried over by the stresses around a crack tip is a characteristic parameter of the local plastic flow at the crack tip during cleavage. They measured the surface energy and the plastic deformation contribution to the effective fracture surface energy. They observed the dynamics of cleavage of lithium fluoride crystals with high speed cinematography and dislocation mechanisms of dissipation were deduced from studies of etch pit patterns. Besides, they observed decorated replicas of lithium fluoride cleavage surfaces in the electron microscope. They suggested that the surface structure associated with a hesitating crack is characterized by a vey high density of elementary steps parallel to the [100] crack propagation direction (longitudinal steps). They suggested that neighbouring steps are of alternate signs and form pairs similar to the V's observed for cleavages propagating at high velocities. It is proposed in their paper that 90 % of those elementary steps are not associated with dislocations running with the crack tip and do not contribute to plastic deformation.

It is generally accepted that a typical V or lightning pattern is the microscopic surface structure left by a cleavage crack running at high velocity in a direction slightly off the [100] direction in sodium chloride, magnesium oxide and lithium fluoride crystals. Dislocation processes associated with the lightning structure aroused the interest

of several authors, i.e. Bethge (20), Forwood and Forty (21), Robins et al. (22), Levi (23), Burns and Webb (15). It is agreed that one of the arms of such V's is formed as a cleavage step and the other is related to dislocation motion when it is parallel to [100] .No agreement in the interpretation of this structure is found when both arms follow irrational directions.

Some other features associated with discontinuous cleavage crack propagation are worth mentioning.

Transverse fracture markings generated by unsteady cleavage velocities have been considered in detail by Burns (24) who correlated the positions of the transverse markings with the nodes of the flexural vibrations in crystals cleaved with a double angle wedge, mounted on a heavy pendulum.

Plastic deformation occurring during cleavage of composite sodium chloride crystals containing precipitates in the form of gold platelets was thoroughly studied by Forwood (21). He proposed that a suitable distribution of particles of a second phase is effective in slowing down or even impeding a cleavage crack not only because of direct interaction but mainly because of the plastic deformation blunting the tip of the crack.

When studying the cleavage mode of fracture the healing process cannot be overlooked. This healing process occurs because the elastic stresses concentrated at the tip of a crack relax into the surrounding crystal lattice and the front of the crack retreats. Forty (12) and Forty and Forwood (25) studied the perfection and amount of healing for naturally and artificially healed cracks in lithium fluoride and sodium chloride crystals.

This review is by no means an exhaustive one but it gives an idea on the salient features of the available information and the variety of approaches by which unsteady crack propagation has been studied in alkali halide crystals. Nevertheless it shows the lack of a comprehensive description of all and every one of the surface markings which are left in a cleavage surface by an unsteady cleavage crack; to fill this gap is one of the aims of this thesis. It is also evident the necessity to study changes in cleavage markings related to accelerations and decelerations of cleavage cracks for a wide range of velocities and to correlate observations obtained on a macroscale with those obtained in a microscale (specially at an atomistic level) in order to check the dislocation mechanisms which have been proposed to explain some surface structures and to propose new mechanisms which could account for the outstanding cleavage structures observed.

It was considered most suitable for the above mentioned purposes to study by different techniques (see chapter 2) the regions of cleavage surfaces enclosed between successive stopped crack fronts on sodium chloride crystals.

1.2. Selection of model material and techniques

Sodium chloride single crystals are particularly suitable to study cleavage crack propagation in semi-brittle materials. They are representative of a number of crystals having identical structures, differing only in the ions that compose them. Moreover, alkali halides have been considered as a model material for the study of simple ceramics. Their mechanical behaviour is similar to that exhibited by face centered cubic metals: they show a stress-strain curve where three stages of work

hardening can be recognized. It has the following advantages:

a) It is transparent so that it is possible to observe in the optical microscope the development of the stress birefringence patterns introduced by plastic deformation. Crack propagation can also be followed in the optical microscope.

b) It has perfect cleavage and surface markings can be used to follow the progress of a crack in a macroscale in the optical microscope and in a microscale through the study of decorated replicas in the electron microscope.

c) High purity and doped crystals can be easily grown from the melt.

d) Dislocations and plasticity have been extensively studied by means of different techniques so that a wide range of experimental information and theoretical calculations are already available.

In a macroscale, optical microscopy is a simple and efficient technique to follow crack propagation, while X-ray topography provides useful information on the activated slip systems in a deformed crystal.

Two techniques are particularly efficient to give complementary information on a microscale: chemical etching of surfaces and electron microscopy of decorated replicas. This last technique is a powerful tool that permits observation of steps of monoatomic height. A study of the structure of cleavage surfaces at an atomic level provides invaluable information on the mechanisms involved in the cleavage process.

1.3.1 Dislocations and plasticity in sodium chloride.

Sodium chloride crystals have a face centered cubic lattice with two interpenetrating networks of Na^+ and Cl^- ions (Fig. 1.2).

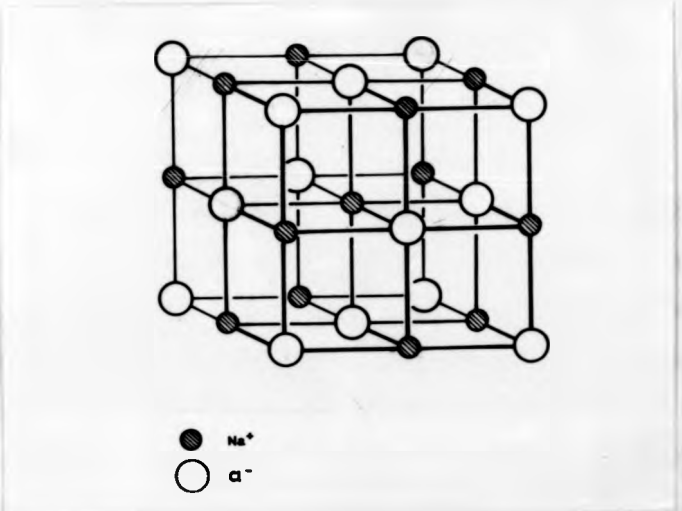

Fig. 1.2. Sodium chloride structure.

It has perfect cleavage along {100}and poor cleavage has been observed along {110} planes.

Single crystals usually slip on close packed planes. Accordingly, {100} should have been the preferred slip plane for sodium chloride crystals. However, already in 1930 Buerger (27) showed that sodium chloride deforms predominantely by slip on {110} planes in a $\langle\bar{1}10\rangle$ direction, this direction being that of rows of like ions. He also showed that limited slip on {100} planes can also occur at high stresses in a <110> direction. But not all sodium chloride-like structures prefer to slip on {110} planes; for example lead telluride primary glide plane is {100}and silver chloride shows pencil glide.

Buerger found a correlation between primary glide planes and ionic polarizabilities: slip along {100} is associated with high polarizabilities, slip along {110} with low polarizabilities; with intermediate values both {100} and {110} may function as slip planes.

Gilman (28) based on ideas due to Buerger made a comprehensive study on the plastic anisotropy of crystals with the sodium chloride structure. He determined that the stresses for {100} $\langle\bar{1}10\rangle$glide in lithium fluoride are much higher than the stresses for {110} $\langle\bar{1}10\rangle$ glide at the same temperature, while measurements in the series of potassium halides indicated that {100} glide is favoured by increasing polarizabilities of the ions. Huntington, Dickey and Thomson (29), taking into account the interionic forces explicitely, calculated the energies of dislocations in sodium chloride.

From their results Gilman (28) concluded that the glide planes in sodium chloride-like crystals seem to be determined by the structure of the cores of the glide dislocations. Recently Granzer et al. (30) performed improved atomistic calculations of the core configuration and core energy of edge dislocations in ionic crystals of the rock-salt structure. Their calculations were carried out using non linear elasticity theory outside the core of the dislocation together with improved interaction potentials inside the dislocation core. They calculated the total interaction energy for the core of {110} $\langle\bar{1}10\rangle$ and {100} $\langle\bar{1}10\rangle$dislocations by adding the electrostatic energy, the repulsion energy from a Born-Mayer-Huggins potential, the Van der Waals energy and for the first time, the polarization energy. The ratios of the core energies of edge dislocations in {100} and {110} planes in lithium fluoride, sodium chloride and silver chloride, according to Granzer et al. are given below:

$\frac{E\ \{100\}}{E\ \{110\}}$ = 2.02 for LiF = 1.6 for NaCl = 1.12 for AgCl

These calculations explain theoretically earlier results on the plastic anisotropy of sodium chloride- like crystals.

There are six equivalent {110} planes in sodium chloride crystals which can be grouped into three pairs. Planes belonging to a pair intersect obliquely (Fig. 1.3.). Which of these six equivalent slip planes are active for each deformation experiment depends on the geometry of the specimen, the type of deformation (torsion, compression, etc) and the direction in which the load is applied.

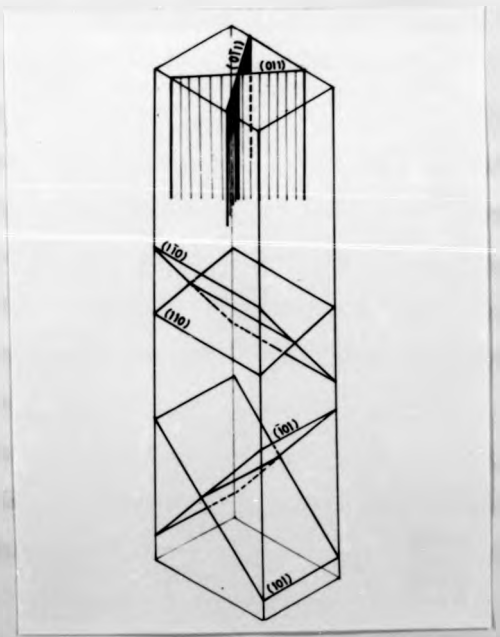

Fig. 1.3. Equivalent {110}planes in NaCl crystals

Cross-slip of the screw components of dislocations moving on {110} planes is known to occur in {100} , {111} (31) and {112}(32) planes in sodium chloride with decreasing facility. Unlike face centered cubic metals, cross-slip of dislocations cannot take place on the orthogonal (conjugate) {110}planes because the Burgers' vector of a dislocation in a {110}plane is perpendicular to the {$\bar{1}$10}conjugate plane. {110} <$\bar{1}$10> dislocations multiply in alkali halide crystals by a multiple cross-slip mechanism, first suggested by Koehler (33) and later developed and observed experimentally by Gilman and Johnston (34) for lithium fluoride crystals. While cross-slipping, screw dislocations leave behind a trail of various defects generally known as debris. They are mainly dislocation dipoles and point defects.

Macroscopic plasticity as well as dislocation interactions have been extensively studied for sodium chloride crystals deformed in compression along <100> and along <110> by different complementary techniques such as: study of etch pit bands, stress birefringence patterns, interferometry, bulk density measurements, stress-strain curves (35), latent hardening experiments (36), X-ray topography (37), analysis of slip-line traces by electron microscopy of shadowed replicas (31), transmission electron microscopy (37), analysis of surface structures in decorated replicas (4), etc.

From the vast amount of information so derived, a brief review of the salient features will be given. Macroscopic slip behaviour and its relationship to dislocation creation and interaction will be first considered.

As observed by Davidge and Pratt (35), the stress-strain curves for sodium chloride crystals deformed in compression along<100> show three different stages of work hardening.

Although the general features of the curve are similar to those for face centered cubic metals, the hardening mechanisms are different if the same stage is studied for both materials. In stage I in sodium chloride crystals the slope of the stress-strain curve is similar to that in stage II for face centered cubic metals, the stress being proportional to the square root of the density of dislocations.

Four of the six {110} <$\bar{1}$10> systems (38) are equally stressed when a crystal is loaded along <100> but initially only the two with the shortest slip distance are active; one of these soon becomes inactive and acts as a barrier to dislocations of the primary system. From etch pit studies and electron microscopy observations most of the authors conclude that sodium chloride deforms macroscopically in single glide.

Hardening in stage I has been ascribed to interactions with blocking obstacles, to the interaction between dislocations on orthogonal systems, to the creation of debris during multiplication of dislocations of the primary slip system and to the interaction with sessile jogs on screw dislocations (39). Opinions on the relative contribution of each of these interactions to work hardening in this stage are not coincident.

Stage II is characterized by the activation of oblique slip systems in sodium chloride crystals. There is a very high work hardening rate in this stage. There is general agreement that this high rate of work hardening can be explained by the interaction of dislocations of the oblique systems with the debris (mainly with the dislocation dipoles) left by the multiple cross-slip of dislocations of the primary slip systems.

In stage III, noticeable cross-slip of dislocations in {100} ,

{111} planes have been observed. The decreased work hardening rate found is explained by the macroscopic cross-slip of correlated groups of screw dislocations around obstacles.

The difference in behaviour between alkali halides and face centered cubic metals is the result of the difference in the type of bonding. The electrostatic repulsion is responsible for the large stacking fault energy found in ionic crystals as well as for the large secondary slip stresses; it favours multiple cross-slip and therefore the production of debris and explains the high work hardening rates observed.

It has been established (40) that work hardening in sodium chloride is athermal in nature but it depends on the temperature and strain rate.

Though sodium chloride crystals prefer to slip on the {110} planes with the shortest slip path (42), the shape of a specimen does not seem to alter noticeably the features of the stress-strain curve as can be deduced by comparing the results obtained by Matucha (31) and Strunk (37) for specimens with a square cross-section and those of Davidge and Pratt (35) for specimens with a rectangular cross-section.

Dislocation behaviour and plastic deformation are similar for other ionic crystals with the rock-salt structure, i.e. lithium fluoride. Lithium fluoride crystals show in many aspects (such as dislocation velocities, multiplication of dislocations by multiple cross-slip, etc) a behaviour similar to that of sodium chloride crystals. Although previously it was believed that lithium fluoride crystals show only one stage of work hardening, Fotedar and Stoebe (41) have shown that depending upon temperature, purity of the crystals, strain rate and specimen geometry, the stress-strain curve of lithium

fluoride single crystals can be also separated into three stages of work hardening. They have also demonstrated that impurities suppress the three stage work hardening behaviour of lithium fluoride, giving only one stage with a work hardening rate an order of magnitude higher than that of stage I in pure crystals. In contrast to the sodium chloride behaviour, in lithium fluoride crystals specimen geometry (42) has a similar effect to that of impurity content. In effect, specimens with a rectangular cross-section do not show a transition to stage II work hardening.

1.3.2. Electrical effects in ionic crystals.

Alkali halide structures are built up of ions of opposite charge, and, as a consequence, complicated electrical effects are associated with the presence of dislocations. Among them, Gyulay-Hartley and Stepanow effects are related to modifications in the electrical properties of deformed crystals. Joffé and Rehbinder's effects are associated with mechanical properties of deformed crystals and their surface characteristics.

In sodium chloride-like structures edge dislocations,

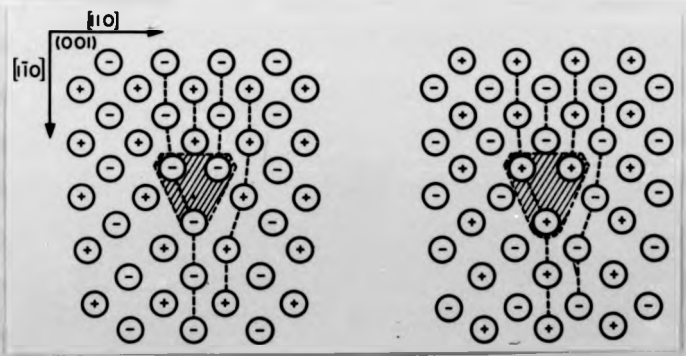

Fig. 1.4. Emergence points in the (001) plane of edge dislocations in the NaCl structure. After Amelinckx(43).

formed by an extra pair of planes (see Fig. 1.4) (43) and screw dislocations (44) (see Fig. 1.5) introduce a net charge on the surface at their point of emergence.

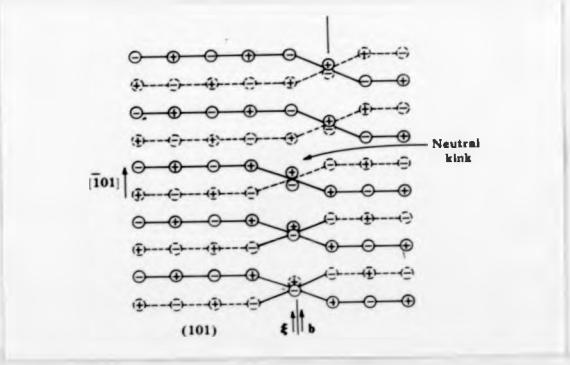

Fig. 1.5. View normal to a screw dislocation lying on a (101) glide plane with a kink configuration. After Hirth and Lothe (44).

Besides, reactions between dislocations may generate charged jogs (45) and point defects, and interactions between dislocations and charged point defects should occur to balance the charge distribution.

Elementary jogs in edge dislocations carry half-integer charges and therefore cannot be neutralized by point defects (46); as these jogs are glissile, edge dislocations carry their charges while gliding through the crystal. Both edge and screw dislocations can transport charge but only screw dislocations (44) can transport charge along their length. Conservative jog and kink motion along a dislocation line provides a mechanism for the exchange of charge between the crystal interior and the external surfaces.

When a sodium chloride crystal built up of singly charged

ions is deformed, there are, for a dislocation gliding in a {110} plane, twelve possible intersections with dislocations from the {110} <$\bar{1}$10> slip systems. Intersections of {110} <$\bar{1}$10> dislocations with dislocations of the orthogonal system are a source of neutral jogs, while intersections with dislocations on oblique {110} planes give rise to charged jogs (36).

Charges on the jogs are balanced by charges on the point defects formed so as to give charge neutrality.

Charged kinks are formed on screw dislocations gliding on {110} planes when they are pulled out of their slip plane until they are perpendicular to the crystal surface. A point defect of charge e can be accommodated at the dislocation by the creation of two new elementary jogs or kinks; thus dislocations can acquire charges at the surface. This might be related to the Joffé effect, which will be discussed in section 1.4.1.

1.4. Influence of the environment on the plastic behaviour of alkali halides.

The mechanical properties of single crystals of alkali halides are greatly influenced by the environment of the crystal. Organic molecules, charged ions, gases, etc. can be adsorbed by the crystal surfaces and modify the plastic behaviour, in particular they can pin the point of emergence of dislocations.

Westwood performed extensive studies and his review (48) of this subject contains detailed discussions on the significant effects of adsorbed species on hardness and on the mobility of dislocations in the near-surface layers of non-metallic crystals.

The influence of adsorbed gases was studied by Aerts and Dekeyser (49) who found that strain-stress curves of sodium chloride

crystals which were previously heated at 300 °C at a pressure of 10 atmospheres in an hydrogen and argon atmosphere were identical to that obtained for crystals which had not been exposed to a gas treatment. On the contrary they found that crystals submitted to a similar treatment in a nitrogen atmosphere were harder.

Particularly relevant to the research described in this thesis is the presence of water.

1.4.1. Influence of water and of water vapor on the plastic deformation of sodium chloride.

The influence of water on the plastic deformation of sodium chloride crystals has long been known. Nabarro (50) cites a paper by Engelhardt written in 1867 stating that brittle rock-salt crystals become ductile when wet. Joffé studied extensively this effect which is named after him. He attributed this effect to the dissolution of surface crack where brittle fracture would be started when the crystal is stressed. Another interpretation of this phenomenon was based on the idea that water dissolves away the embrittled surface layer formed by adsorbed gases and thus enhances ductility.

The Joffé theory was criticized on the basis that it could not explain the re-embrittlement usually observed when the crystals are aged in humid air, after water immersion.

Stokes et al. (51) demonstrated that the re-embrittlement occurs as a consequence of the stress concentration arising at the small cubic crystals which precipitate on the crystal surface after drying. They showed that if the crystal is chemically polished and then carefully rinsed with organic solvents so that no saturated water solution remains on the surface and it is carefully handled so as to avoid damaging the crystal surface, it remains ductile after

standing for several months in dry air.

Even the presence of small quantities of water vapor in the atmosphere in which cleavage is performed can influence the surface structures left by cleavage in sodium chloride crystals as shown by Bethge (20) and Jaunet et al. (52). Huches et al. (53) made a quantitative study of the relationship between the relative humidity at which cleavage is performed and the surface structures observed by electron microscopy of decorated replicas. They showed that when $p/p_o < 0.2$ few cleavage and slip steps appear, separated by flat regions. When the relative humidity increases, the angles between surface steps become rounded. At a critical value $p/p_o \leq 0.4$, the whole surface pattern rearranges and a high density of entangled steps appears. When $p/p_o \simeq 0.75$ surface steps suddenly disappear.

Relative humidity in most laboratories is 40% or higher. So the sensitivity of sodium chloride to water vapor is a problem which can not be disregarded.

R. 1. References

(1) Griffith A.A., Phil. Trans. Roy. Soc. A 221, 163, (1920).

(2) Orowan E., Welding Journal Res. Suppl. 34, 157 , (1955).

(3) Gilman J.J., J. Appl. Phys. 27, 1262, (1956).

(4) Forwood C.T., Ph.D. Thesis, Bristol University (1966).

(5) Mott N.F., Engineering 165, 16, (1948).

(6) Stroh A. N., J. Mech. Phys. Solids 8, 119, (1960).

(7) Rice J. R., J. Appl. Mech. 35, 379, (1968).

(8) Rice J. R., Rosengren G. F., J. Mech. Phys. Solids 16, 1 (1968).

(9) Andrews E. H., J. Mat. Sci. 9, 887, (1974).

(10) Gilman J. J., J. Appl. Phys. 27, 1262, (1956).

(11) Forty A. J., Proc. Roy. Soc., A 242, 392, (1957).

(12) Gilman J.J., Knudsen C., Walsh W.P., J. Appl. Phys. 29, 601,(1958).

(13) Gilman J.J., Trans. A.I.M.E. 310, June (1958).

(14) Forwood C. T., Lawn B. R., Phil. Mag. 13, 595 (1966).

(15) Burns S. J., Webb W. W., J. Appl. Phys. 41, 2086, (1970).

(16) Gilman J. J., Trans. A.I.M.E. 209, 449, April (1957).

(17) Burns S. J., Webb W. W., Trans. A.I.M.E., 236, 1165 (1966).

(18) Washburn J., Gorum A.E., Parker E. R., Trans. A.I.M.E. 215,230 (1959).

(19) Burns S. J,.Webb W.W., J. Appl. Phys. 41, 2078 (1970).

(20) Bethge H., Phys. Stat. Sol. 2, 3 and 775, (1962).

(21) Forwood C. T., Forty A.J., Phil. Mag. 11, 1067 (1965).

(22) Robins J.L., Rhodin T.N., Gerlach R. L., J. Appl. Phys. 37, 3893 (1966).

(23) Levi L., Phil. Mag. 28, 427 (1973).

(24) Burns S. J., Phil. Mag. 18, 625 (1968).

(25) Forty A. J., Forwood C. T., Trans. Brit. Ceram. Soc. 62, 715 (1963).

(26) Tertsch ,Zs. Kr., 96, 38 (1932).

(27) Buerger M. J., Am. Min. 15, 174 and 226 (1930).

(28) Gilman J. J., Acta Met. 7, 608 (1959).

(29) Huntington H. B., Dickey J. E., Thomson R. ,Phys. Rev. 100, 1117 (1955).

(30) Granzer F., Belzner V., Bucher M., Petrasch P., Teodosin C ., J. Phys. Suppl. 11-12, 34, 359 (1973).

(31) Matucha K.H., Phys. Stat. Sol. 26, 291 (1968).

(32) Strunk H., Phys. Stat. Sol. A 28, 119 (1975).

(33) Koehler J. S., Phys. Rev. 86, 52 (1952).

(34) Johnston W. C., Gilman J. J., J. Appl. Phys. 31, 632 (1960).

(35) Davidge R. W., Pratt P. L., Phys. Stat. Sol. 6, 759 (1964).

(36) Kear B. H., Silverstone C. E., Pratt P. L., Proc. Brit. Ceram. Soc., 6 , 269 (1966).

(37) Strunk H. Thesis, Stuttgart University (1973).

(38) Pratt P. L., Acta Met., 1, 103 (1953).

(39) Evans A. G., Proc. Brit. Ceram. Soc. 15, 113, (1970).

(40) Evans A. G., Pratt P. L., Phil. Mag. 21, 951 (1970).

(41) Fotedar H.L., Stoebe T. G., Phil. Mag. 859 (1971).

(42) cited in Fotedar H. L., Srinivasan M., Wilson D. A., Stoebe T. G., Mat. Sci. Eng. 7, 272 (1971).

(43) Amelinckx S., Suppl. Vol 7, Series X, Nuovo Cimento. 569 (1958).

(44) Hirth J. P., Lothe J., Theory of Dislocations, p. 358, Mc.Graw Hill (1968).

(45) Seitz F., Phys. Rev.80, 239 (1950).

(46) Eshelby J. D., Newey C. W. A., Pratt P. L., Lidiart A. B., Phil. Mag. 3, 75 (1958).

(47) Kear B. H., Taylor A., Pratt P. L., Phil. Mag. 4, 665 (1959).

(48) Westwood A. R. C., in Microplasticity, ed. C. J. Mc.Mahon jr. John Wiley and Sons (1968) p. 365.

(49) Aerts E., Dekeyser W., Acta Met. 4, 557 (1956).

(50) cited in Nabarro, Theory of Crystal Dislocations, Oxford, Clarendon Press, (1967), page 292.

(51) Stokes R. J., Johnston T. L., Li C.H., Trans. A.I.M.E. 218, 655 (1960).

(52) Jaunet J., Sella C., Trillat Jl. J., Comptes Rendus, 258, 135 (1964).

(53) Hucher M., Oberlin A., Wyart J., C. R. Acd. Sc. Paris 258, 6473 (1964).

Chapter 2

EXPERIMENTAL

2.1. Apparatus

2.1.1. Introduction

The presence of water has a marked influence on the deformation of sodium chloride crystals as described in section 1.4 . Even atmospheric water can become an important problem when studying microscopic features of plastic deformation at an atomic scale. Bethge (1), Huches M, Oberlin, Wyart, et al.(2) (see section 1.4.1) have shown that cleavage or slip steps of atomic height rearrange or dissolve after a few minutes exposure to humid air. No elementary steps remain after keeping the crystal for a short time at 75% relative humidity. This value is quite common in Buenos Aires climate.

A dry-box had to be designed so that all stages of specimen preparation could be carried out in an atmosphere below 10% relative humidity.

2.1.2. Description of apparatus

A dry-box was constructed from lucite and made sufficiently large for all the experimental operations to be conducted in the dry environment.

Fig. 2.1 shows the dry-box and part of the equipment used to prepare and study the specimens. The relative humidity content inside the dry-box is kept between 5 to 10% by a flow of dry N_2 obtained by controlled electrical resistance heating of liquid nitrogen. The gas obtained in this way is warmed to room temperature by circulation

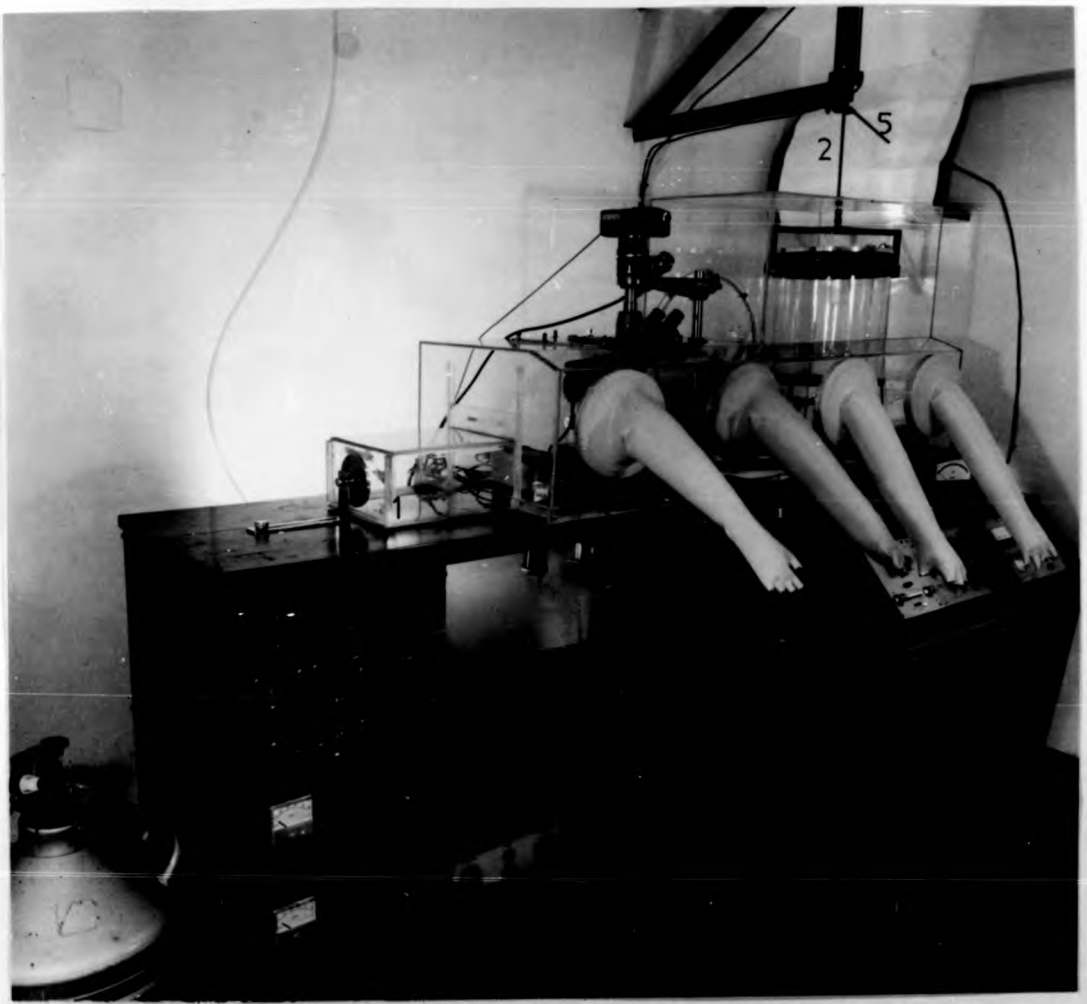

Fig. 2.1. Dry-box and equipment used to prepare the specimens.

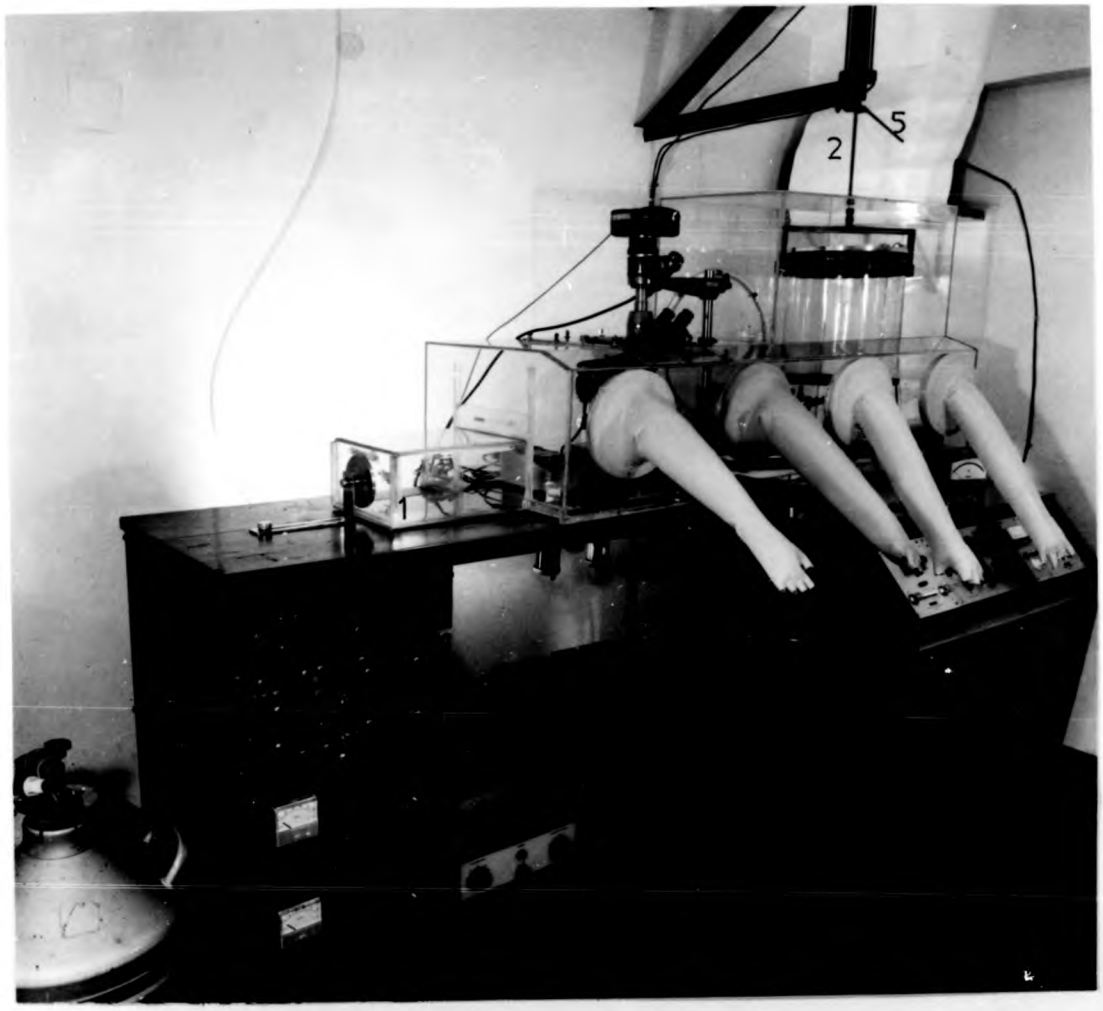

Fig. 2.1. Dry-box and equipment used to prepare the specimens.

through a coil immersed in heated oil.

It was necessary to minimize the liquid nitrogen consumption because it is expensive and the supply is highly limited in the Research Area of Buenos Aires Atomic Energy Commission. This was accomplished by lowering the relative humidity of the dry-box to 30% with dry air, and only then letting the dry nitrogen flow until working conditions are attained. The dry-air flow is obtained from a large compressor* (Fig. 2.2) followed by a double column autoregenerating drying system** filled with Beckman dryer. It is necessary for the dry air to flow overnight in the dry-box to reach the required operating humidity by noon the next day.

A hair hygrometer is used to measure the relative humidity. Samples and elements are introduced into and removed from the dry-box through the buffer chamber (N°1 in Fig. 2.1) that can be isolated from the main box.

There is a Vickers*** M15c optical microscope inside the dry-box. The microscope is fitted with an automatically operated camera (with a Vickers*** J35 automatic exposure unit). The binocular head and photographic system remain outside the dry-box. Just under the binocular head a tight fitting latex membrane keeps the dry-box isolated.

---

* Speedway compressor
De Angelis S.A.
ARGENTINA

** Gilberco

*** Vickers Limited
England

Fig. 2.2. Compressor and double column autoregenerating drying system.

The Dry-box contains the bell-jar of an Edwards E 12E* vacuum coating unit. As the bell-jar of the coating unit is too cumbersome and heavy to handle inside the dry-box, a system was designed to lift it up and lower it down from the outside. A pneumatic system was constructed with a small compressor and an air cylinder bellows** valve. A sliding rod (N°2 Fig. 2.1) is fitted to the bell-jar with a brass ring clamp. The pneumatic system is controlled with handles N°3 and 4 (see Fig. 2.1). A clamp (N°5 Fig. 2.1) is used to keep the bell-jar lifted while everything is adjusted for the preparation of the replicas.

To obtain most of the decorated replicas used in this research, it is necessary to heat the specimen and perform gold and carbon evaporations without breaking the vacuum (see section The coating unit is provided with only two sets of transformers and rheostats. It was then necessary to modify the coating unit, by introducing a new set of transformer and rheostat.

There is enough room between the optical microscope and the coating unit to store all the necessary tools and materials, to cleave, etch and manipulate the crystals without difficulty.

To propagate a cleavage crack, the special device shown in

---

* Edwards High Vacuum
Manor Royal, Crawley, Sussex
England

** Bellows Valvair
Fobosa S A
Uruguay

Fig. 2.3 was used. In this apparatus the specimen rests parallel to the plane of the crack on a stage of adjustable height; a wedge of approximately 17° is slowly inserted into the opening of the crack through a rod connected to a screw which is driven manually. To observe the propagation of the cleavage crack under the optical microscope, a window is provided in the base of the cleavage jig. It was necessary to chrome-plate the bronze cleavage jig in order to prevent corrosion by the sodium chloride crystals.

2.2. Experimental procedure

Hilger & Watts* sodium chloride and lithium fluoride crystals were used throughout this work. The supplied blocks were successively cleaved until small prisms of approximately 15 mm long by 5 mm wide by 3 mm thick were obtained. Freshly cleaved prisms were prepared before running each experiment. This ensured that the external faces of the prisms have not suffered hardening or softening from long exposures to dry nitrogen or humid air (see sec. 1.4).

A cleavage crack is introduced in these prisms by inserting a single edge razor blade with a very light hammer. The propagation of the crack is then continued with the cleavage apparatus described in section 2.1.1 and observed under the optical microscope.

The propagation of the crack is stopped several times and the instantaneous positions of each stopped crack front are recorded with the photographic camera.

---

* Hilger & Watts
Analytical Division
Rank Precision Industries
England

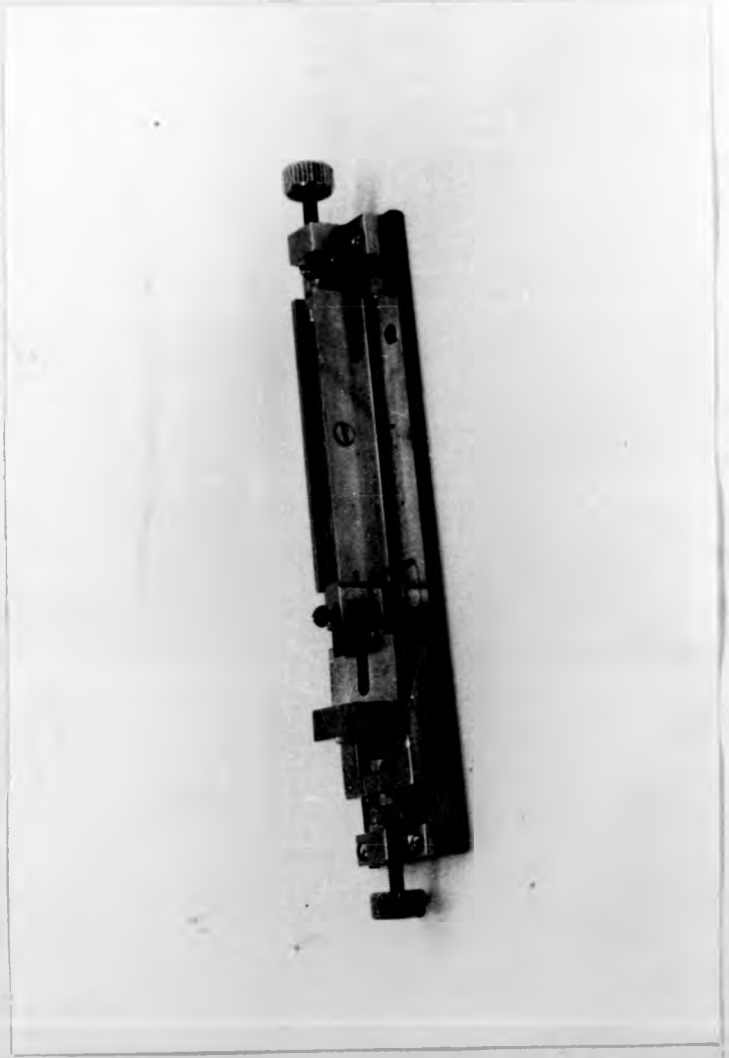

Fig. 2.3. Cleavage jig.

When the cleavage is completed one cleavage half is transferred to the coating unit where a decorated replica of the surface is prepared for further observation in the Philips EM 300* electron microscope as will be seen in section 2.2.2.

The other cleavage half is then available for complementary study by other tecniques: etching to reveal the presence of dislocations (see section 2.2.3), X-ray topography to study the activated slip systems (see chapter 5).

In addition, lateral (010) cross-sections of crystals with stopped (001) cleavage cracks were studied by optical and electron microscopy.

A crystal with a (001) stopped cleavage crack is cleaved laterally along a (010) plane (Fig. 2.7) with a sharp stroke to avoid, as far as possible, secondary deformation of the crystal.

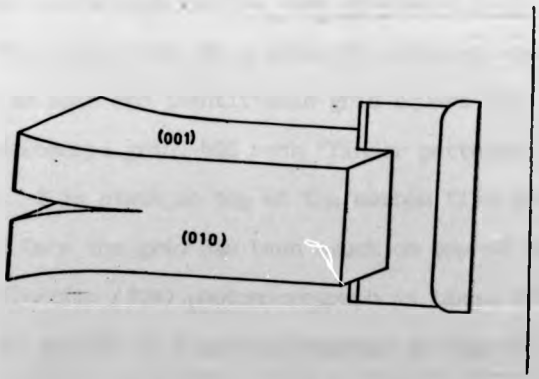

Fig. 2.7 lateral (010) cross-section of a NaCl crystal with a stopped (001) cleavage crack.

Replicas of the newly created lateral surfaces are also studied by electron microscopy.

---

* N.V. Philips Gloeilampenfabrieken
Eindhoven - The Netherlands

2.2.1. Optical microscopy

The propagation of the crack is observed under the optical microscope with reflected white light.

Fig. 2.4 is a photomicrograph showing 2 stopped crack fronts AA, BB the interference pattern between the reflections from the two newly created surfaces can be seen.

A zone including one or more stopped crack fronts is selected for each crystal under the optical microscope; 100x photomicrographs are taken all along the boundary of the internal interference patterns. Cleavage steps and cleavage markings in this zone and in neighbouring areas are recorded for further identification of the selected area in both halves of the crystal.

A decorated replica is prepared by evaporating gold and carbon successively on the cleavage surface of the crystal intended for electron microscopy studies (see section 2.2.2).

To ensure that the previously selected area of the crystal appears in an open and identifiable grid square (50μ x 50μ) an electron microscope grid, 400 mesh "finder patterns" (Grids & Graticules *) is stuck on top of the carbon film under the optical microscope. Once the grid has been stuck on top of the replica, a low magnification (30x) photomicrograph is taken (Fig. 2.5) It is necessary to include in a photomicrograph an edge of the crystal in order to determine the relationship among the main crystallographic directions, the crack propagation direction and the grid bars.

The selected areas of the specimen are carefully

---

* Grids & Graticules Ltd.
London - England

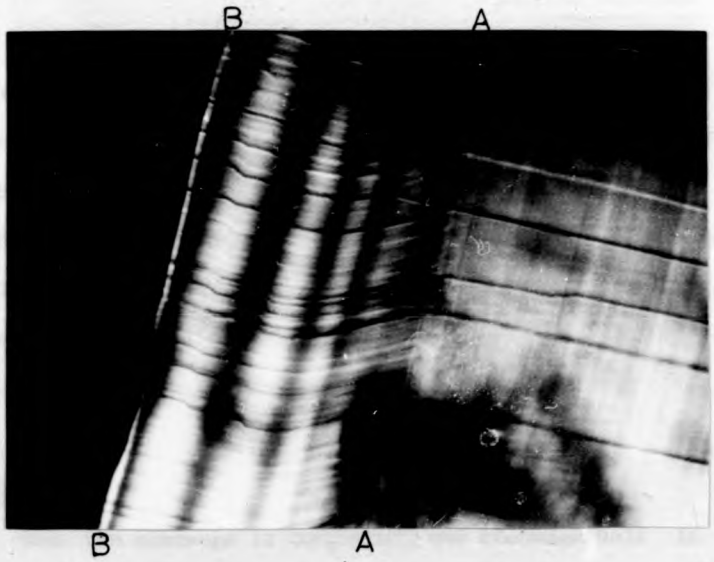

Fig. 2.4. Optical micrograph of a stopped (001) cleavage crack in a NaCl crystal. AA, BB, stopped crack fronts. Magn. x 110.

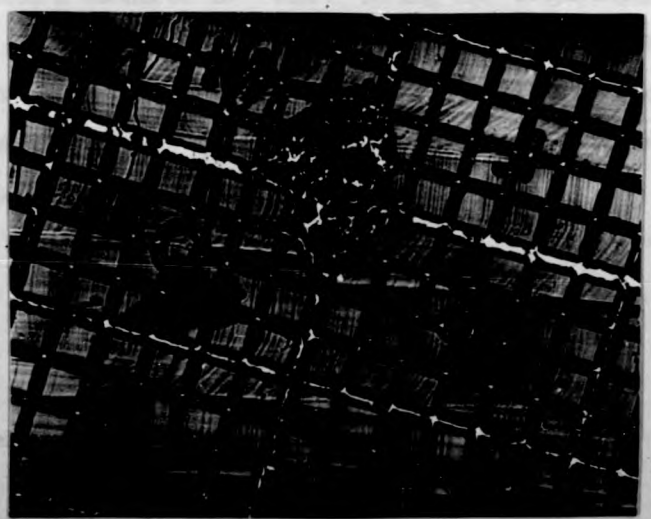

Fig. 2.5. Photomicrograph of an electron microscope grid stuck on top of a replica of a NaCl cleavage surface. Magn. x 110.

photographed once the important crystallographic directions are determined. Every important feature in the free area of each square of the grid is sketched in an enlarged drawing of the grid (Fig. 2.6). With a complete set of photomicrographs and the drawing, it is possible later to identify every area of the replica studied in the electron microscope and relate it to the macrostructure of the cleavage surface.

2.2.2. Replicas

When the cleavage is completed, one cleavage half is transferred to the coating unit where a decorated replica (see section 1.2) of the cleavage surface is prepared.

The crystals are decorated with gold, which is evaporated from a V-shaped tungsten filament placed perpendicularly above the specimen, under a vacuum of 10^{-5} Torr. During the evaporation the crystals are placed on a molybdenum boat where they are heated to about 100°C. The temperature of the specimen is measured with a 1605 Comark* electronic thermometer and a chromel-alumel thermocouple "sealed" in a test sodium chloride crystal lying on the molybdenum boat very close to the specimen. It was found by experiment

---

* Comark electronic thermometer

Comark

England

photographed once the important crystallographic directions are determined. Every important feature in the free area of each square of the grid is sketched in an enlarged drawing of the grid (Fig. 2.6). With a complete set of photomicrographs and the drawing, it is possible later to identify every area of the replica studied in the electron microscope and relate it to the macrostructure of the cleavage surface.

2.2.2. Replicas

When the cleavage is completed, one cleavage half is transferred to the coating unit where a decorated replica (see section 1.2) of the cleavage surface is prepared.

The crystals are decorated with gold, which is evaporated from a V-shaped tungsten filament placed perpendicularly above the specimen, under a vacuum of 10^{-5} Torr. During the evaporation the crystals are placed on a molybdenum boat where they are heated to about 100°C. The temperature of the specimen is measured with a 1605 Comark* electronic thermometer and a chromel-alumel thermocouple "sealed" in a test sodium chloride crystal lying on the molybdenum boat very close to the specimen. It was found by experiment

---

* Comark electronic thermometer
Comark
England

that the amount of gold to produce good decoration under the described experimental conditions is the same that would produce a uniform film 3A thick (2 mg. at a 10 cm. distance). A carbon film is then evaporated about room temperature on top of the gold nuclei, without breaking the vacuum.

After both evaporations are completed the specimen is transferred back to the optical microscope where the selected area to be studied in the electron microscope is located.

An electron microscope grid is then stuck on top of the Carbon film as was explained in section 2.2.1. A solution of 0,3 mg. of neoprene in 100 ml. toluene (3) was found suitable to stick the grid to the Carbon film. For this purpose the grid is soaked in the solution and the excess is drained gently with filter paper. Extreme care must be taken to place the grid on the replica so that the selected zone falls exactly on an open area of approximately 50μ x 50μ. It is particularly important to avoid the contamination of the replica by the sticking solution due to the sliding of the grid over the replica.

Once the grid has been stuck on top of the replica the selected area of the specimen is carefully photographed in the optical microscope (see section 2.2.1 and Fig. 2.6).

At this stage the specimen is removed from the dry-box.

The replica technique is tedious and time consuming and it was necessary to elaborate the customary simple stripping and washing methods, to ensure, as far as possible, that an unbroken replica film spans all the open squares of a grid.

Fig. 2.7 illustrates the apparatus in which the replica

that the amount of gold to produce good decoration under the described experimental conditions is the same that would produce a uniform film 3A thick (2 mg. at a 10 cm. distance). A carbon film is then evaporated about room temperature on top of the gold nuclei, without breaking the vacuum.

After both evaporations are completed the specimen is transferred back to the optical microscope where the selected area to be studied in the electron microscope is located.

An electron microscope grid is then stuck on top of the Carbon film as was explained in section 2.2.1. A solution of 0.3 mg. of neoprene in 100 ml. toluene (3) was found suitable to stick the grid to the Carbon film. For this purpose the grid is soaked in the solution and the excess is drained gently with filter paper. Extreme care must be taken to place the grid on the replica so that the selected zone falls exactly on an open area of approximately 50μ x 50μ. It is particularly important to avoid the contamination of the replica by the sticking solution due to the sliding of the grid over the replica.

Once the grid has been stuck on top of the replica the selected area of the specimen is carefully photographed in the optical microscope (see section 2.2.1 and Fig. 2.6).

At this stage the specimen is removed from the dry-box.

The replica technique is tedious and time consuming and it was necessary to elaborate the customary simple stripping and washing methods, to ensure, as far as possible, that an unbroken replica film spans all the open squares of a grid.

Fig. 2.7 illustrates the apparatus in which the replica

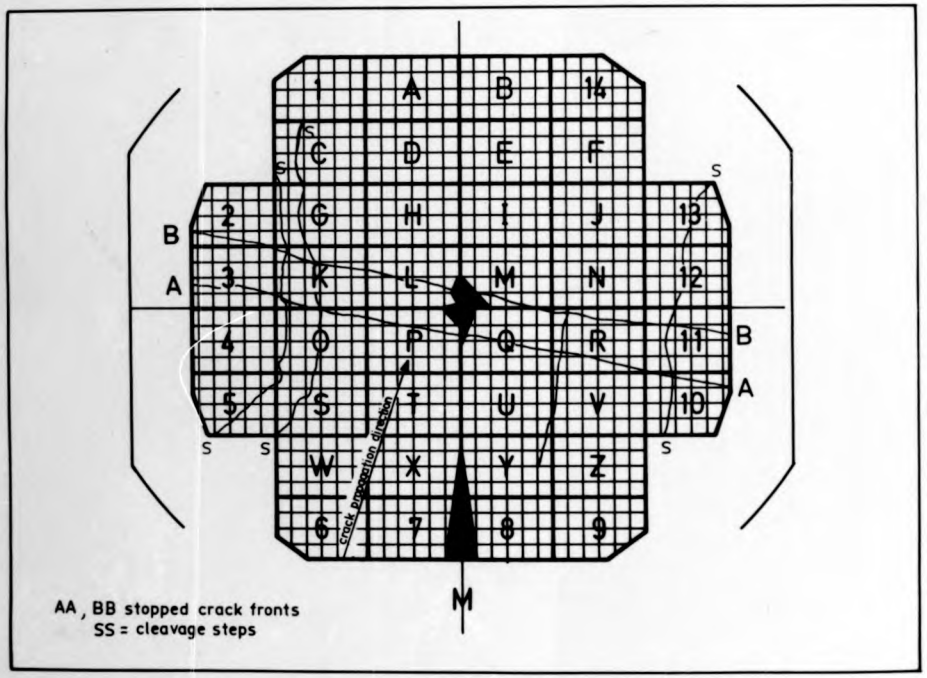

Fig. 2.6. Sketch of main features of the replica on an enlarged drawing of the grid

with the grid attached to it, is stripped from the crystal by floating in double distilled water. The apparatus consists of a glass funnel and a Buchner funnel plus a three-way stopcock which allows differents paths for the circulating water. A coarse woven metal mesh support is placed on the flat perforated plate of the Buchner funnel (Fig. 2.8). Double distilled water is allowed to flow from the glass funnel into the Buchner funnel through its stem until it is almost full.

The edges of the replica are scored with a razor blade and the crystal with the replica on top is lowered gently at an angle into the water (see Fig. 2.9). The replica film is detached from the crystal as the water penetrates between the gold-carbon film and the crystal surfaces; finally the replica with the grid remains floating on the water surface.

It is necessary to rinse carefully the decorated replica because some sodium chloride is dissolved in the stripping process and may contaminate the specimen. In order to rinse the film, the water is let out of the Buchner funnel drop by drop so that the water surface is not disturbed. Before the specimen touches the metallic support, the water flow is reversed and fresh clean water is allowed to enter the Buchner funnel from the glass one. This process must be repeated three or four times. In the last stage the decorated replica with the grid stuck on top is permitted to rest on the metal support. In every step the water must flow drop by drop to avoid breaking the film. The replica is left to dry on the metal support.

It is then ready to be transferred to the electron microscope.

Shadowed replicas were selected as a suitable technique to

Fig. 2.8. Apparatus used to strip and wash the replica films.

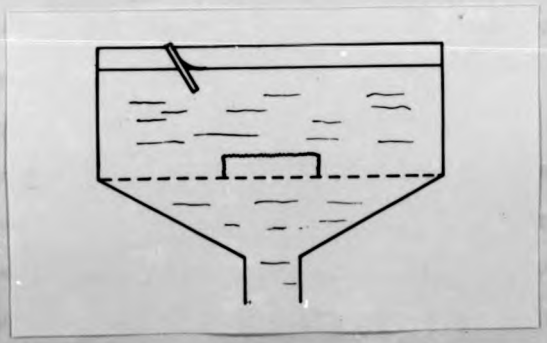

Fig. 2.9. Stripped replica film.

make a detailed study of the sizes and shapes of etch pits in etched cleavage surfaces by electron microscopy (see section 2.2.3).

Good replicas were obtained when the specimen was shadowed at an angle of 45° with an amount of gold which would give a 2000 A thick layer if evaporated with perpendicular incidence. This film was backed with a Carbon film and striped as described above.

2.2.3. Etching

It is necessary to carry on decoration and chemical etching simultaneously (section 2.2.2) in order to correlate etch pit density with the cleavage structures of the decorated crystal half (section 2.2.2). While one half of the crystal is in the coating unit, the other half is removed from the dry-box and immediately immersed in the etching solution.

Barber's solution (4) is the etchant widely used to reveal dislocations in sodium chloride crystals. It consists of 1- part of a saturated solution of ferric chloride in hydrochloric acid, -1 part distilled water, -50 parts glacial acetic acid.

The crystal is immersed in this solution for only two to five seconds, rinsed in pyridine to stop the etching and dried with filter paper.

Fig. 2.10 is an optical micrograph of the same zone that was studied in electron microscope. Very well developed pyramidal pits can be seen where the dislocation density is low but this is not so in high density regions like AA, where the size of the pits makes it impossible to get any information about individual dislocations.

Some work had to be done to decrease the size of the etch pits. Shadowed replicas (section 2.2.2) of the etched cleavage surfaces were prepared and examined in the electron microscope to make a detailed study of the shape and sizes of the smallest etch pits obtained. The base of the smallest pits obtained with Barber's

Fig. 2.10. Optical micrograph of a cleavage surface of a NaCl crystal etched with Barber's solution. Magn. x360.

solution was approximately 2,5 μ x 2,5 μ .

Extensive trials of variations of standard etchants described in references (5, 6, 7) led to negative results. For example following Argon & Padawer work, an etchant of 20 ml. glacial acetic acid containing 10 drops of a saturated solution of zinc chloride in glacial acetic acid was tried, followed by a rinse with pure glacial acetic acid and anhydrous ether. The replica showed that pits were too big to resolve individual dislocations.

These negative results led to a review of current theories of etch pit formation. There are two mechanisms to reduce the lateral size of the pits: 1) the presence of Fe^{+++}, Zn^{++}, Cd^{++}, etc ions which complex with neighbouring chloride ions and 2) the decrease in the concentration of the active agents which dissolve the crystal at a high rate; both result in a decrease of V_s (rate of dissolution of the crystal parallel to the surface).

All the above mentioned etching solutions contained different kinds and concentrations of complexing ions.
The second mechanism was borne in mind in choosing new variations of the etchant solutions.

Sodium chloride is highly hygroscopic, therefore an attempt was made to reduce the water content of the etching solutions.

A solution of -1 part of a saturated solution of ferric chloride in hydrochloric acid, -50 parts glacial acetic acid was tried.

Fig. 2.11a) and b) are electronmicrographs illustrating the well developed etch pits obtained with a) Barber's solution and b) the solution mentioned above. The pits obtained with the latter

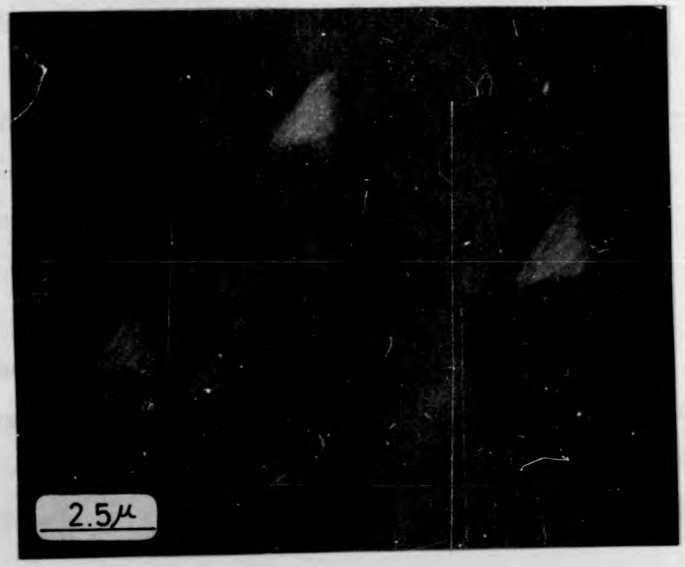

6.000

Fig. 2.11. a)

13.000

Fig. 2.11. b)

Fig. 2.11. Electron micrographs of shadowed replicas of NaCl crystals etched with: a) Barber's solution

b) Barber's solution, distilled water suppressed.

have 1μ x 1μ square bases, which are smaller than those obtained with Barber's solution but are still unsatisfactory to resolve dislocations in high density regions.

A further improvement resulted from elimination of hydrochloric acid. A saturated solution of ferric chloride in glacial acetic acid proved satisfactory, and small, but terraced, etch pits were obtained (Fig. 2.12).

It was thought that the water content of the reactives should be important in controlling the v_s obtained up to this point. Hydrated ferric chloride had been used all through the experiments as anhydrous material hydrates rapidly when exposed to Buenos Aires climate.

All further experiments were conducted using anhydrous ferric chloride and glacial acetic acid with a controlled humidity less than 3% and all the work was performed inside the dry-box, including the preparation of the solutions.
The reactive containers were sealed each time they were taken out of the dry-box to avoid any contact with humid atmosphere.

A saturated solution of anhydrous ferric chloride in glacial acetic acid hence forward called solution A was used. The crystal was immersed for two seconds in the solution, rinsed twice in pyridine to stop the etching rapidly, and dried with filter paper.

The etching is very susceptible to the concentration of the inhibitor (ferric chloride) in the solution.

A shadowed replica of a cleaved surface of sodium chloride crystal etched with solution A can be seen in Fig. 2.13.
Excellent pyramidal non terraced 0.25μ x 0.25μ square based pits were obtained with this solution. Comparison of the areas of the bases

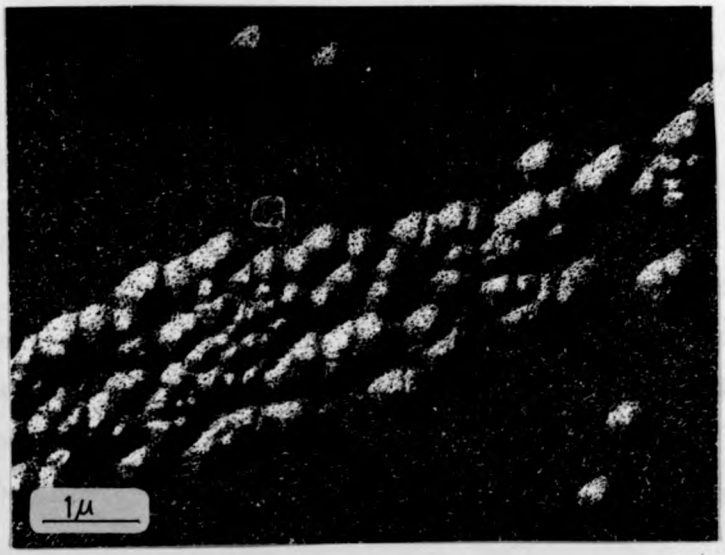

16.000

Fig. 2.12. Electron micrograph of a shadowed replica of a NaCl crystal etched with a saturated solution of ferric chloride in glacial acetic acid.

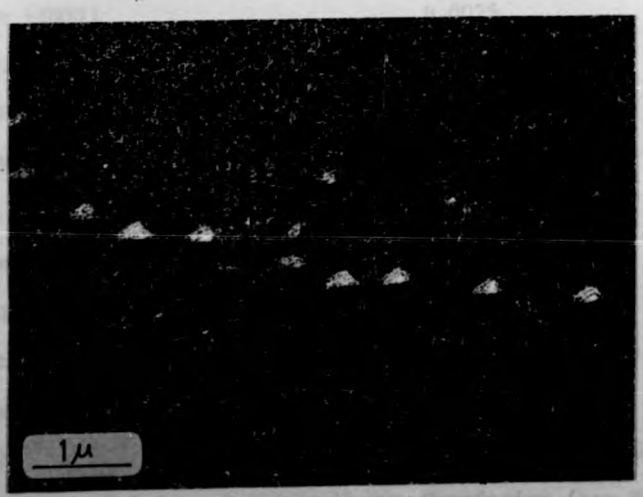

16.000

Fig. 2.13. Shadowed replica of a cleavage surface of a NaCl crystal etched with solution A.

of the pits obtained with solution A and Barber's solution shows a favourable reduction of 1/100 th.

Etch pits are now small enough for individual dislocations to be revealed even in high density dislocation zones such as that shown in Fig. 2.14. Dislocation density of approximately 6×10^9 $disl/cm^2$ can thus be resolved.

2.4 Supply of raw materials

Throughout this work "high purity"single crystals of sodium chloride and lithium fluoride supplied by Hilger & Watts were used. Three different batches were employed. Chemical analyses were required each time but obtained from the manufacturers only for batch N°2, stating the following impurity content for the sodium chloride crystals.

Table I

Sodium Chloride

Free Acid	0.05ml N/1%
Free Alkali	0.05ml N/1%
Sulphate (SO4)	0.003%
Nitrate (INO3)	0.002%
Phosphate (PO4)	0.0005%
Iron (Fe)	0.0005%
Heavy Metals (Pb)	0.001%
Barium (Ba)	0.003%
Calcium & Magnesium(Ca & Mg)	0.005%
Potassium (K)	0.01%
Ammonium (NH4)	0.001%
Arsenic (As)	0.0001%

Semiquantitative spectrographic analyses were carried out at the Analytical Division of Atomic Energy Commission (see Table II).

The high content of Cu in N°1 crystal N°1 is remarkable.

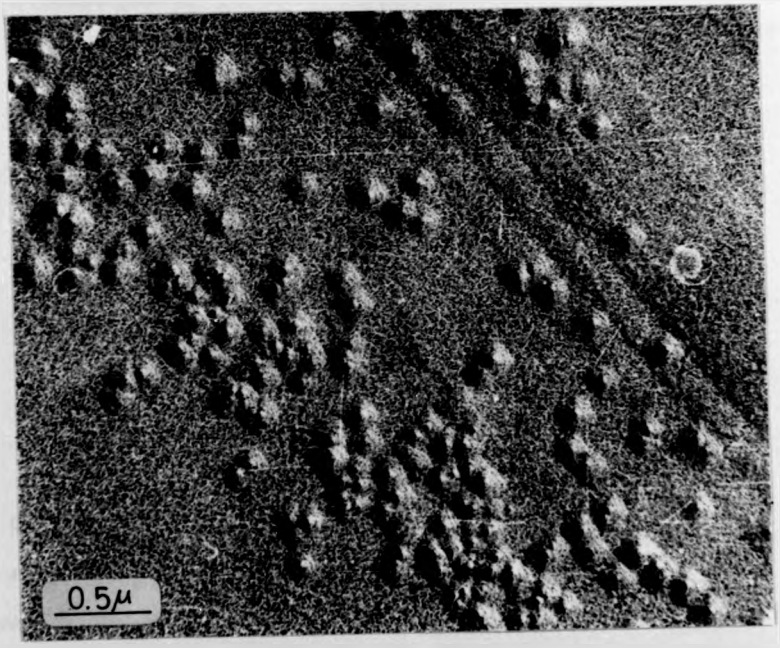

Fig. 2.14. High density dislocation zone. Shadowed replica of a NaCl crystal etched with solution A.

Table II

	First batch polished crystal	First batch blank		Second batch
		Crystal N°1	Crystal N°2	
Na	>10 gr%gr.	> 10 gr%gr	> 10 gr%gr	> 10 gr%gr
Li	N.D.	∿ 0.01%	< 0.01%	∿ 0.01%
K	N.D.	N.D.(9.1)	∿ 0.1 %	∿ 0.1 %
Rb	N.D.	N.D.(0.1)	N.D.	N.D.
Sr	N.D.	N.D.(0.1)	< 0.1 %	N.D.
Ca	N.D.	N.D.	N.D.	N.D.
Ba	N.D.	N.D.(0.01)	N.D.	N.D.
Cu	< 0.0001 %	∿ 0.001%	N.D.	N.D.

N.D. = non-detected

Semiquantitative limit of detection Sr, Rb, Ca = 0.1g%g Li = 0.01g%g.

Though the first batch proved to be quite good, successive crystal batches gave rise to various experimental difficulties; for example, for one batch the extremely high density of low angle boundaries made it impossible to obtain good cleavages and the whole batch had to be rejected and sent back to England.

The delay between the time the first faulty lot was ordered and the time the final crystals arrived was of the order of two years.

These delays hampered experimental work as most of the materials necessary for research work had to be imported; even single edge razor blades used in cleavage are not available in Buenos Aires.

Lesser difficulties were found with national materials, although the obtaining of some of them was particularly complicated;

Table II

	First batch polished crystal	First batch blank		Second batch
		Crystal N°1	Crystal N°2	
Na	>10 gr%gr.	> 10 gr%gr	> 10 gr%gr	> 10 gr%gr
Li	N.D.	∿ 0.01%	< 0.01%	∿ 0.01%
K	N.D.	N.D.(9.1)	∿ 0.1 %	∿ 0.1 %
Rb	N.D.	N.D.(0.1)	N.D.	N.D.
Sr	N.D.	N.D.(0.1)	< 0.1 %	N.D.
Ca	N.D.	N.D.	N.D.	N.D.
Ba	N.D.	N.D.(0.01)	N.D.	N.D.
Cu	< 0.0001 %	∿ 0.001%	N.D.	N.D.

N.D. = non-detected

Semiquantitative limit of detection Sr, Rb, Ca = 0.1g%g Li = 0.01g%g.

Though the first batch proved to be quite good, successive crystal batches gave rise to various experimental difficulties; for example, for one batch the extremely high density of low angle boundaries made it impossible to obtain good cleavages and the whole batch had to be rejected and sent back to England.

The delay between the time the first faulty lot was ordered and the time the final crystals arrived was of the order of two years.

These delays hampered experimental work as most of the materials necessary for research work had to be imported; even single edge razor blades used in cleavage are not available in Buenos Aires.

Lesser difficulties were found with national materials, although the obtaining of some of them was particularly complicated;

for example anhydrous ferric chloride was obtained after a long search when a private firm kindly offered a sample as the commercially available chemical is always slightly hydrated.

R.2. References

(1) Bethge, H, Phys. Stat. Sol. 2, 775 (1962)

(2) Huches, M, Oberlin A, Wyart, S.R. Acad. Sc. Paris, 6473 (1964)

(3) Wyatt, S.H, J. Elect. Mic. 19, 283 (1970)

(4) Barber, D.H., J. Appl. Phys. 33, 3141 (1962)

(5) Rozhanskii, V.N. , Parvova, E.V. et al Soviet Phys. Cryst. 6, 564 (1962)

(6) Bhagavan Raju IVK et. al J. Cryst. Growth, 11, 171 (1971)

(7) Argon , A.S., Padawer, G.E., Phil Mag. 25, 1073 (1972)

Chapter 3

SHADOW - DECORATION

3.1.0. Introduction

A knowledge of the sign of the monoatomic steps and slip lines is essential to understand the mechanism through which the observed decoration pattern develops in the cleavage surfaces of ionic crystals. It was thought that the sign of most of the monoatomic steps could be determined by combining the thin film decoration and the shadowing techniques.

3.1.1. Standard thin film decoration technique

The thin film decoration technique was first developed by Bassett (1958) (1) for the study of cleavage surfaces in ionic crystals as mentioned in section 1.2. . The original technique has been described in section 2.2.2. and consists mainly of the evaporation of a metal in a vacuum of 10^{-4} - 10^{-5} Torr, the metal atoms impinging perpendicularly on a freshly cleaved surface of the crystal maintained at about 120°C.

An extremely light deposit develops in the form of small particles predominantely nucleated on the imperfections of the surface. Details of the surface structure on an atomistic scale are thus rendered visible. The decoration mechanism depends on the mobility of the metal atoms on the substrate and on the high density of nucleation sites along the surface steps. When the sample is heated thermal agitation increases and nucleation and growth of the metal clusters are enhanced. Poor decorations are obtained on crystals kept at room

Chapter 3

SHADOW - DECORATION

3.1.0. Introduction

A knowledge of the sign of the monoatomic steps and slip lines is essential to understand the mechanism through which the observed decoration pattern develops in the cleavage surfaces of ionic crystals. It was thought that the sign of most of the monoatomic steps could be determined by combining the thin film decoration and the shadowing techniques.

3.1.1. Standard thin film decoration technique

The thin film decoration technique was first developed by Bassett (1958) (1) for the study of cleavage surfaces in ionic crystals as mentioned in section 1.2. . The original technique has been described in section 2.2.2. and consists mainly of the evaporation of a metal in a vacuum of 10^{-4} - 10^{-5} Torr, the metal atoms impinging perpendicularly on a freshly cleaved surface of the crystal maintained at about 120°C.

An extremely light deposit develops in the form of small particles predominantely nucleated on the imperfections of the surface. Details of the surface structure on an atomistic scale are thus rendered visible. The decoration mechanism depends on the mobility of the metal atoms on the substrate and on the high density of nucleation sites along the surface steps. When the sample is heated thermal agitation increases and nucleation and growth of the metal clusters are enhanced. Poor decorations are obtained on crystals kept at room

Chapter 3

SHADOW - DECORATION

3.1.0. Introduction

A knowledge of the sign of the monoatomic steps and slip lines is essential to understand the mechanism through which the observed decoration pattern develops in the cleavage surfaces of ionic crystals. It was thought that the sign of most of the monoatomic steps could be determined by combining the thin film decoration and the shadowing techniques.

3.1.1. Standard thin film decoration technique

The thin film decoration technique was first developed by Bassett (1958) (1) for the study of cleavage surfaces in ionic crystals as mentioned in section 1.2. . The original technique has been described in section 2.2.2. and consists mainly of the evaporation of a metal in a vacuum of 10^{-4} - 10^{-5} Torr, the metal atoms impinging perpendicularly on a freshly cleaved surface of the crystal maintained at about 120°C.

An extremely light deposit develops in the form of small particles predominantely nucleated on the imperfections of the surface. Details of the surface structure on an atomistic scale are thus rendered visible. The decoration mechanism depends on the mobility of the metal atoms on the substrate and on the high density of nucleation sites along the surface steps. When the sample is heated thermal agitation increases and nucleation and growth of the metal clusters are enhanced. Poor decorations are obtained on crystals kept at room

temperature. This is a draw-back because cleavage structures can be modified by the heat activated motion of dislocations and by other thermal processes such as evaporation.

One of the most important advantages of this technique is the very high resolution that can be achieved: even steps of unit lattice height can be rendered visible, so that the vertical resolution is of the dimension of the unit cell of the crystal; horizontal resolution is limited by the size of the decorating nuclei.

It is possible to calculate the height of a cleavage step in sodium chloride-like crystals by measuring the displacement of the surface traces of slip steps intersecting it.
This can be clearly seen in Fig. 3.1. The cleavage step AA is intersected at B by a slip line [010] , which is the trace of dislocations gliding on (101) or ($\bar{1}$01) planes; as has been mentioned in section 1.3.1 in sodium chloride crystals these planes make an angle of 45° with the (001) cleavage plane.

A cleavage step is the boundary between two different levels of the cleavage surface. The deflection of the trace of a (101) slip plane when it intersects the cleavage step is shown in Fig. 3.2. and it is equal to the height of the step.
For the particular case of Fig. 3.1 the height of step A is approximately 80 Å or about 14 unit cell distances.

The measurement of this deflection gets increasingly difficult as the height of the steps diminishes. It is limited by the diameter and the perfection of alignment of the decorating gold nuclei. The sign of large cleavage steps can be obtained from shadowed replicas (see section 2.2.2.)and it is possible to determine the height of steps down from the shadow-casting geometry (Williams and

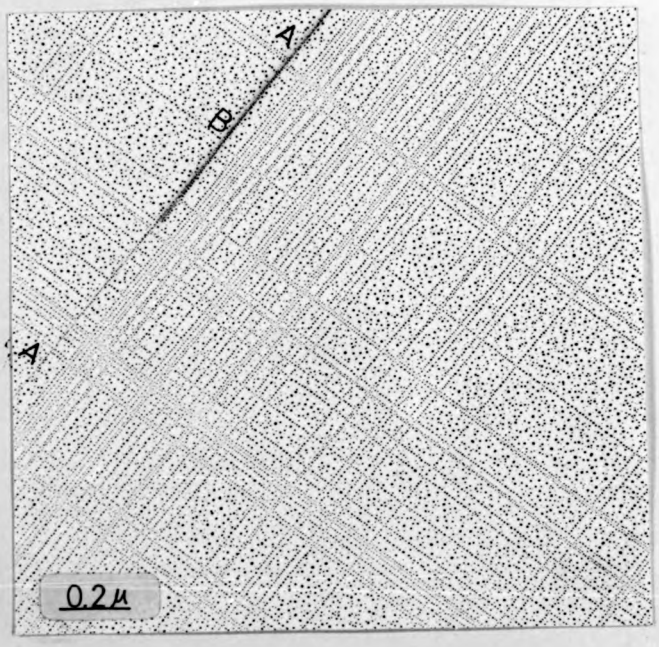

Fig. 3.1. Displacement of surface traces of slip steps when they intersect a cleavage step.

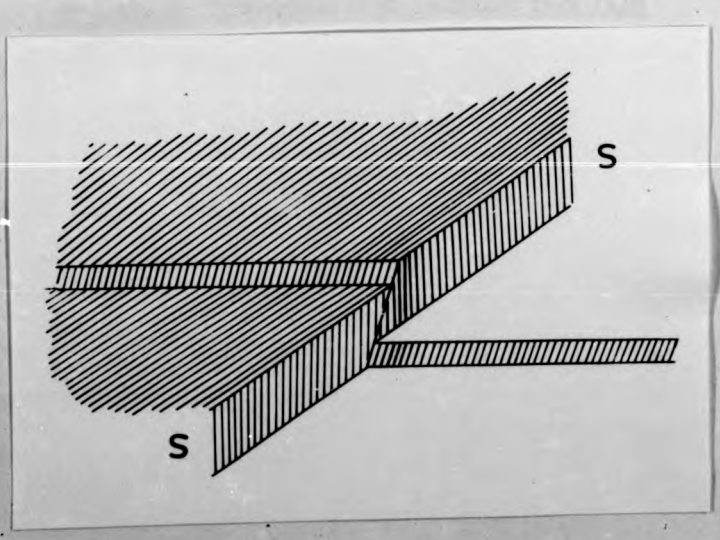

Fig. 3.2. Diagram showing the displacement of the trace of a (101) slip plane when it intersects a cleavage step 55.

Wyckoff, 1946 (2) as seen in Fig. 3.3.

But the thickness of the continuous metal layer impairs the resolution of the replica and therefore it becomes completely impossible to observe monoatomic steps.

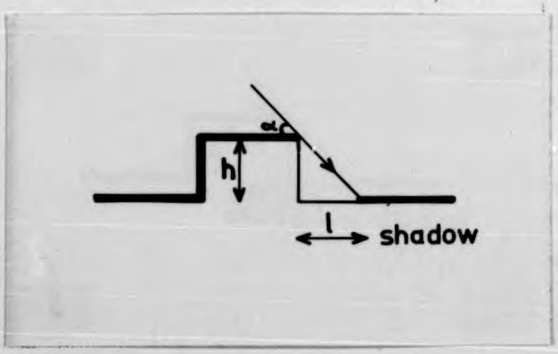

Fig. 3.3. Shadow casting geometry

3.2.1. Shadow decoration: comparison with standard thin film decoration technique

It was thought a combination of these two techniques might give very effective decoration at room temperature, if the metal atoms strike the crystal surface at near grazing incidence, say 2°-3°, as described in the published note (Wainer L.S. (3)) included at the end of this thesis. Under such conditions the principal component of the kinetic energy of the arriving atoms will lie in the plane of the surface and a larger proportion of them collects at steps-up (Fig. 3.4).

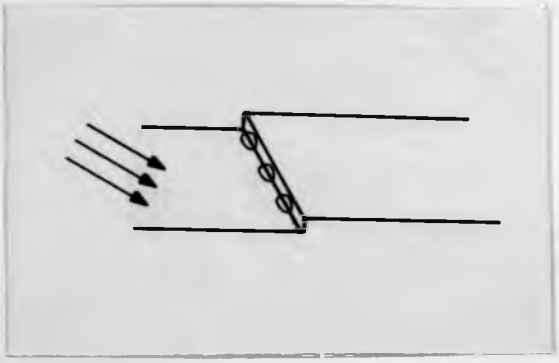

Fig. 3.4. Collection of gold nuclei at step-up

Since nucleation occurs almost exclusively on preferential sites, such as kinks along the edges of steps, a very low density of nuclei is obtained on the flat areas and resolution is improved.

The "shadow-decorated" replicas were prepared as follows: a crystal of sodium chloride was cleaved inside the dry-box and without further exposure to the air a small amount of gold was then evaporated onto the freshly cleaved surface kept at room temperature, so that the incident atoms arrived with a glancing angle 2°-3° to the surface.

Several attemps were made until the appropriate geometry and amount of gold were found.

For the gecmetry adopted (see Fig. 3,5 crystal b) very good decoration was obtained with a quantity of gold which would give a mean thickness of 50 Å if spread uniformly over the surface with perpendicular incidence.

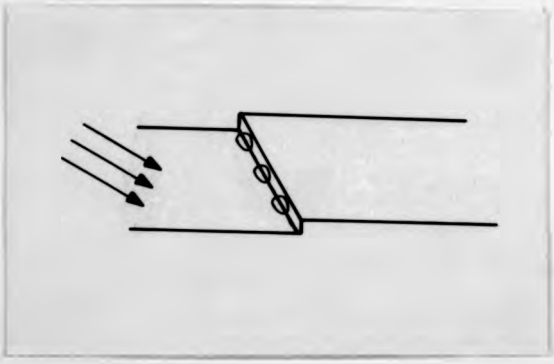

Fig. 3.4. Collection of gold nuclei at step-up

Since nucleation occurs almost exclusively on preferential sites, such as kinks along the edges of steps, a very low density of nuclei is obtained on the flat areas and resolution is improved.

The "shadow-decorated" replicas were prepared as follows: a crystal of sodium chloride was cleaved inside the dry-box and without further exposure to the air a small amount of gold was then evaporated onto the freshly cleaved surface kept at room temperature, so that the incident atoms arrived with a glancing angle 2°-3° to the surface.

Several attemps were made until the appropriate geometry and amount of gold were found.

For the geometry adopted (see Fig. 3,5 crystal b) very good decoration was obtained with a quantity of gold which would give a mean thickness of 50 Å if spread uniformly over the surface with perpendicular incidence.

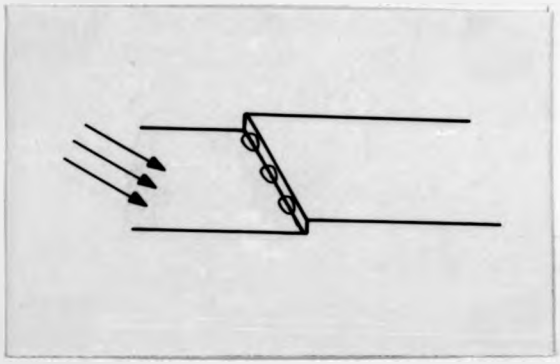

Fig. 3.4. Collection of gold nuclei at step-up

Since nucleation occurs almost exclusively on preferential sites, such as kinks along the edges of steps, a very low density of nuclei is obtained on the flat areas and resolution is improved.

The "shadow-decorated" replicas were prepared as follows: a crystal of sodium chloride was cleaved inside the dry-box and without further exposure to the air a small amount of gold was then evaporated onto the freshly cleaved surface kept at room temperature, so that the incident atoms arrived with a glancing angle 2°-3° to the surface.

Several attemps were made until the appropriate geometry and amount of gold were found.

For the geometry adopted (see Fig. 3.5 crystal b) very good decoration was obtained with a quantity of gold which would give a mean thickness of 50 Å if spread uniformly over the surface with perpendicular incidence.

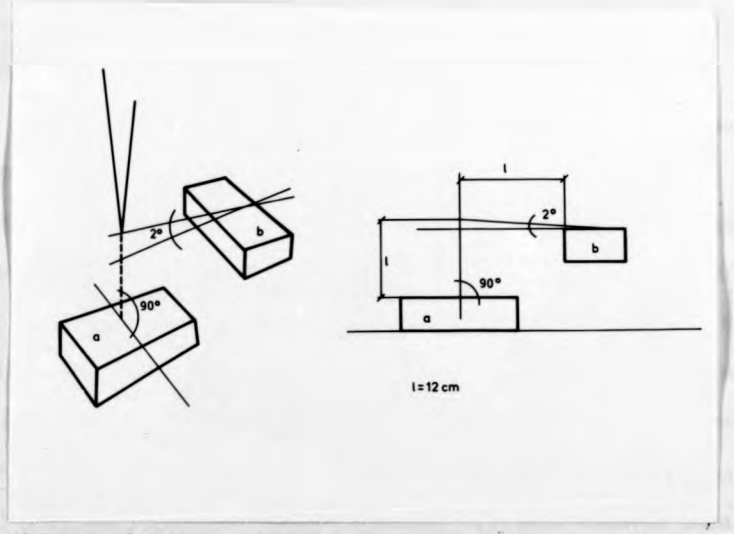

Fig. 3.5. Geometry for gold evaporation for

a - normal incidence decoration

b - shadow-decoration

An attempt was made to compare results for perpendicular and oblique incidence decoration. It was not possible to make the comparison for replicas prepared at the same time with experimental arrangement shown in Fig. 3.5 because the amount of gold appropriate for the shadow-decoration was found to be far too much for the perpendicular decoration.

From the density of gold nuclei condensed on the flat areas of the surface, a mean distance between nuclei was calculated. It was found that the ratio between that distance and the mean distance between muclei condensed on the monoatomic steps was of the order of six for good shadow-decorated samples, while it was of the order of two for

specimens decorated with normal incidence at room-temperature (Fig. 3.6a and b).

The collecting area for gold nuclei depends of the migration distance of the gold atoms. Bassett (1) estimated a migration distance of 150-200 Å for air cleaved rocksalt decorated near 100°C. Stirland (4) estimated that this distance is 250-300 Å for vacuum cleaved rocksalt decorated at 150°C. These migration distances were estimated from measurements of the distance between gold decorated steps separated by a flat area completely free from random gold nuclei. Following the same criterion a migration distance of 500 Å was found for sodium chloride crystals cleaved in a dry nitrogen atmosphere and shadow decorated at room temperature. It is then possible to have flat areas of 500x 1200 Å completely free from random nuclei.

This constitutes an important advance in technique since possible modification of cleavage structures due to the heat activated motion of dislocations is avoided by shadow-decorating the crystals at room temperature.

3.2.2. Feasibility of sign determination of steps by shadow-decoration technique

It is possible from the observation of shadow-decorated replicas to determine the sense of most of the steps running perpendicularly to the propagation direction of the arriving gold atoms. While the size of nuclei condensed along one and the same step is approximately constant, there are mainly two sizes of nuclei that condense on different monoatomic parallel steps.

It is believed that this difference in size may be related

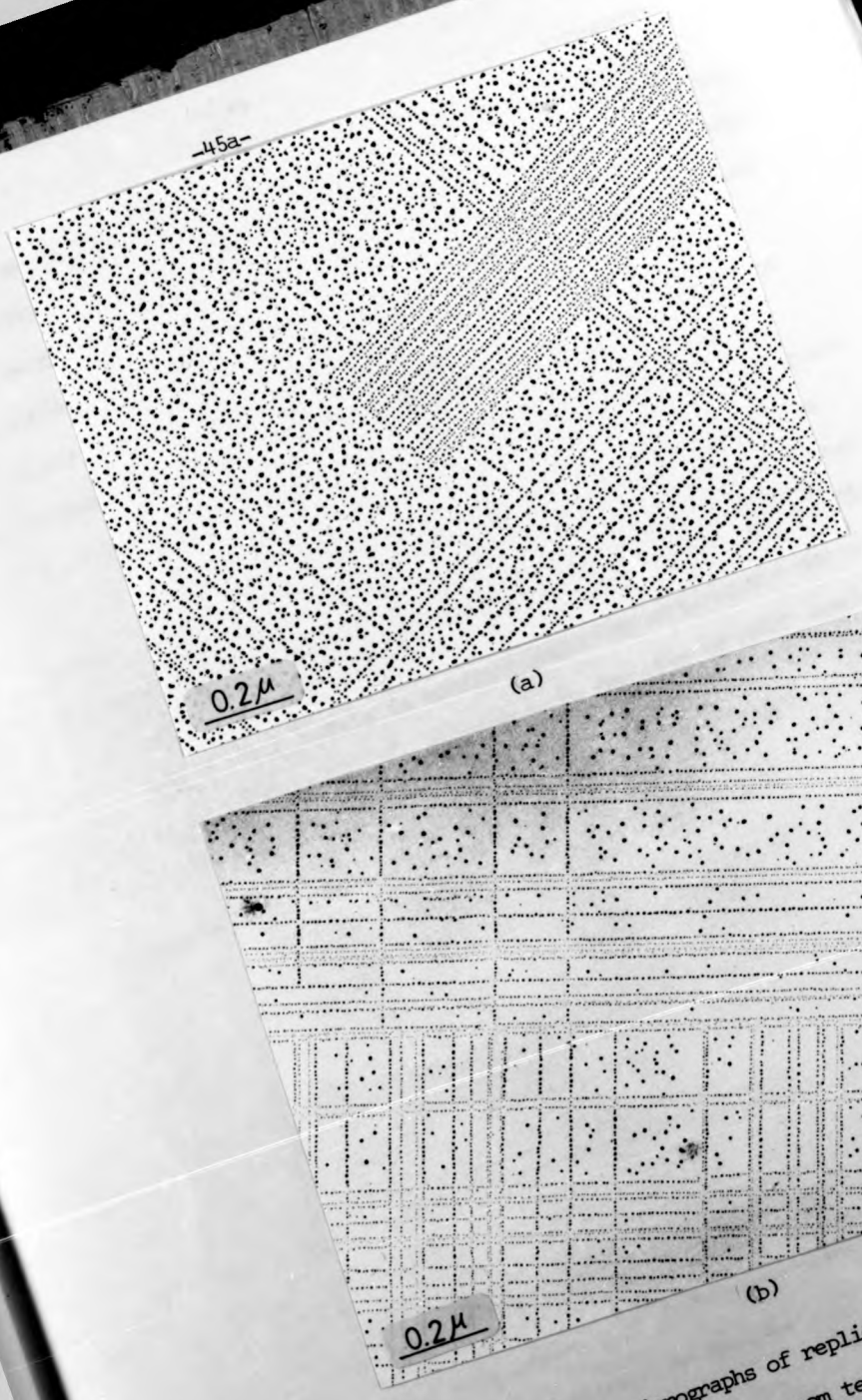

Fig. 3.6. Electron micrographs of replicas of NaCl cleavage surfaces prepared at room temperature.
a) perpendicular incidence
b) near grazing incidence

to the sense of the steps; on what will be called a positive monoatomic step or a step-up, the atoms arrive at a re-entrant angle and large nuclei are condensed; although no shadow can be observed on monoatomic negative steps or steps-down, diffusing atoms render them visible through the condensation of small nuclei. An interpretation of the relief corresponding to steps AA and BB of Fig. 3.7a according to this idea is sketched in Fig. 3.7b.

Thermal evaporation spirals are an ideal system to check whether the difference in size of the condensed gold nuclei is related to the sense "up" or "down" of the monoatomic steps. It has long been established (5, 6, 7, 8, 9) that the pitch of the growth and evaporation spirals is constant and it usually equals one or two Burgers' vectors. Any difference in the size of gold nuclei condensed on the steps can only be assigned to a difference in the sign of the steps (see Fig. 3.8).

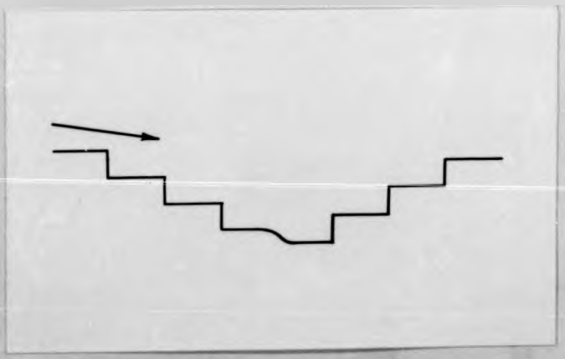

Fig. 3.8. Geometry of shadow-decoration for an evaporation spiral.

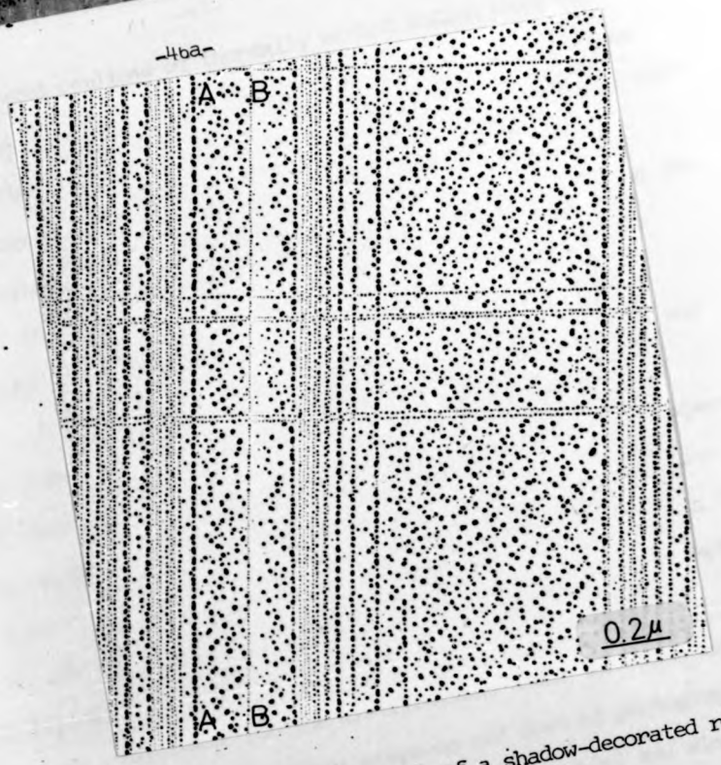

Fig. 3.7a. Electron micrograph of a shadow-decorated replica of a NaCl cleavage surface.

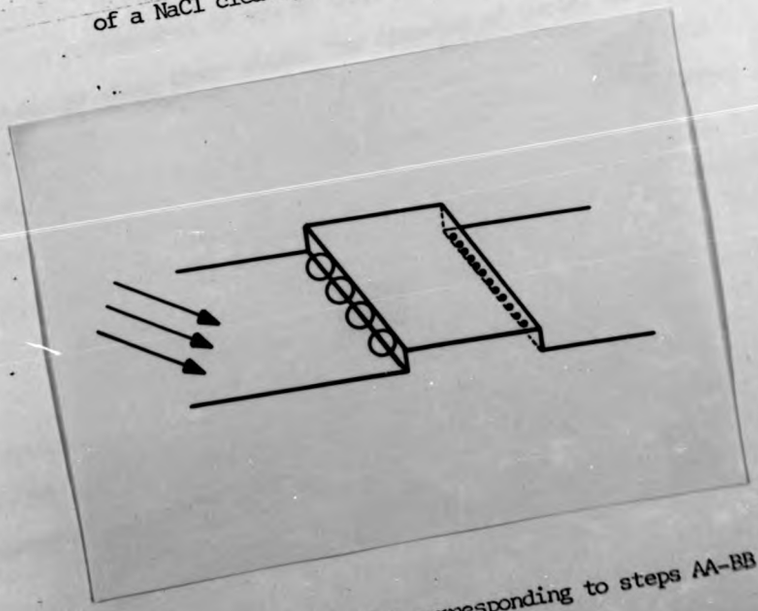

Fgi. 3.7b. Surface relief corresponding to steps AA-BB.

Shadow decorated replicas of thermally etched sodium chloride crystals were prepared. Fig. 3.9a and b are electron micrographs of evaporation spirals from a sodium chloride crystals kept at 500°C during 30 minutes.

The difference in size between nuclei condensed on steps-up (at the bottom of the photograph) and steps-down (at the top of the photograph) is evident.

A statistical analysis of the sizes of these nuclei was made in order to have a quantitative proof of this statement. The "t" or Student test (10) was used to decide whether the expected values of the sizes of nuclei condensed on positive and negative monoatomic steps were equal or not. Two assumptions are made in the use of the "t" test: that the two parent populations considered are normally distributed and that their variances are the same. Both seem reasonable for the distributions under consideration. The sizes of gold nuclei along steps-up and down of photograph 3.9a) were measured in a Quantimet* microscope. As nuclei are elongated and a partial coalescence of two of them sometimes occurs, they were always measured along their width. The diameter of nuclei decorating steps-up ranges from 18 Å to 50 Å, with a mean value of 35 Å and a standard deviation of 6.4. No nuclei smaller that 14 Å were observed for these positive steps. For steps-down nuclei between 9 Å and 42 Å were measured, with a mean value of 26 Å and a standard deviation of 9.

*Quantimet
Metals Research LTD
Cambridge, England

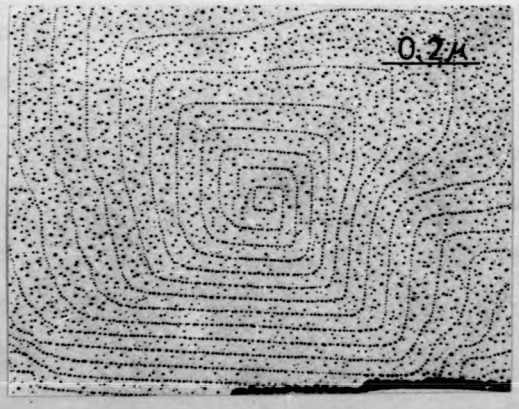

Fig. 3.9. Electron micrographs of evaporation spirals. Shadow-decorated replica of a NaCl crystal kept at 500°C during 30 minutes.

It is to be noted that measurements of the smaller nuclei are all affected by larger errors due to the fact that they are in the limit of resolution of the electron microscope and do not have good contrast or well resolved shapes; some of them are not even registered by the Quantimet.

A value of

$$t = \frac{(\bar{x}-\bar{y})\sqrt{n_x n_y (n_x+n_y-2)}}{\sqrt{(n_x+n_y)(n_x s_x^2 + n_y s_y^2)}} = 7.85$$

was found for n= 204, where

x= size of nuclei along steps-up

y= size of nuclei along steps-down

$\bar{x}$= mean value for x

$\bar{y}$= mean value for y

n_x= number of observations of x

n_y= number of observations of y

s_x= standard deviation of x

s_y= standard deviation of y

$n = n_x+n_y - 2$ =

= degrees of freedom.

It can be seen from tables (11) that this t value exceeds even the 0.1% value. It is then possible to conclude, with a probability of error of at most 0.1%, that the mean for the size of nuclei condensed on monoatomic steps-up and that for the size of nuclei condensed on monoatomic steps-down are different.

3.3. Sign determination by the shadow-decoration technique:
Application to sodium chloride cleavage structures

The analysis of the sign of the stepped cleavage structures is not as straightforward as in the case of evaporations spirals. Some of the factors which complicate sign determination analysis are:

1) Decoration effects are probably not the same for cleavage as for

It is to be noted that measurements of the smaller nuclei are all affected by larger errors due to the fact that they are in the limit of resolution of the electron microscope and do not have good contrast or well resolved shapes; some of them are not even registered by the Quantimet.

A value of

$$t = \frac{(\bar{x}-\bar{y})\sqrt{n_x n_y (n_x+n_y-2)}}{\sqrt{(n_x+n_y)(n_x s_x^2 + n_y s_y^2)}} = 7.85$$

was found for n= 204, where

x= size of nuclei along steps-up

y= size of nuclei along steps-down

$\bar{x}$= mean value for x

$\bar{y}$= mean value for y

n_x= number of observations of x

n_y= number of observations of y

s_x= standard deviation of x

s_y= standard deviation of y

$n = n_x+n_y - 2$ =

= degrees of freedom.

It can be seen from tables (11) that this t value exceeds even the 0.1% value. It is then possible to conclude, with a probability of error of at most 0.1%, that the mean for the size of nuclei condensed on monoatomic steps-up and that for the size of nuclei condensed on monoatomic steps-down are different.

3.3. Sign determination by the shadow-decoration technique:
Application to sodium chloride cleavage structures

The analysis of the sign of the stepped cleavage structures is not as straightforward as in the case of evaporations spirals. Some of the factors which complicate sign determination analysis are:

1) Decoration effects are probably not the same for cleavage as for

slip steps. Included angle is 90°for cleavage steps while it is 135° for slip steps. Sholl et al (12) have theoretically studied the effectiveness of the decoration process as a function of the included angles of the steps and have found that for a given supersaturation, steps of small reentrant angle η are more effectively decorated than are steps of larger η.

2) Small cleavage and slip steps of different height are usually present. Nuclei condensed on steps-up increase their size with the height of the steps. For example an up-slip step which is four Burgers' vectors high is decorated by larger nuclei than an up-slip step one Burgers' vector high. This consideration must be specially borne in mind when analysing the sign of stepped cleavage structures.

3) The separation between neighbouring steps in a cleavage structure can be very small, as can be seen in very dense bands. Collecting area for the nuclei condensed on the closely spaced monoatomic steps is small and smaller nuclei are formed.

Notwithstanding these difficulties, the sense of most of the steps of the cleavage structures can be inferred from a detailed analysis of shadow-decorated replicas.

An example of sign determination analysis will be given below. Fig. 3.10 is an electron micrograph of a shadow-decorated replica, with shadowing direction perpendicular to the longitudinal steps, in which some groups of very closely spaced steps can be seen. The sign of the steps will be studied from left to right starting by step AA. The size of condensed nuclei indicates that step AA is a step-up. It is followed by a faintly decorated step which is assumed to be a step-down.Two different interpretations can be made on the sign of the third step according to the actual

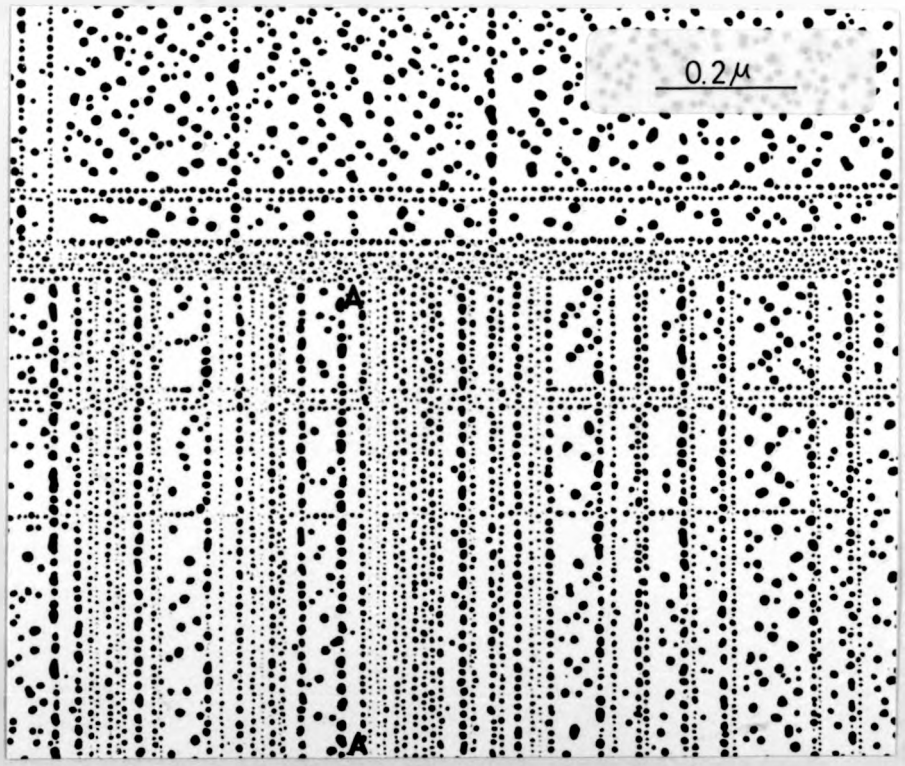

Fig. 3.10. Electron micrograph of a shadow-decorated replica of a NaCl crystal. Shadowing direction perpendicular to the longitudinal steps.

height of the second one. Were it monoatomic in height, the third step, also faintly decorated, should be a step-down. But if the second step were a few units high, the third could well be a monoatomic step-up lying in its shadow. Both possibilities are sketched in Fig. 3.11.a) and b).

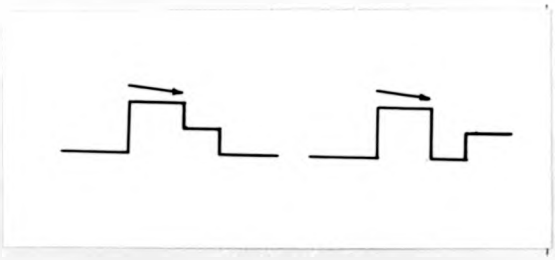

Fig. 3.11. Schematic diagrams of possible sign for the third step to the right of step AA in Fig. 3.10.

The fourth line corresponds to a monoatomic (or only a few units high) step-up. The following six lines are decorated by gold nuclei of approximately the same size. The distance between any two neighbouring lines from this group of six is of the same order as the distance between the first and the second lines that are evidently of different sign. There is no reason to suppose that the six steps could be decorated by gold nuclei of the same size if they were of different signs.

It is possible to identify in the shadow decorated replicas pairs of consecutive longitudinal lines alternate in sign. Many of these pairs are found as in Fig. 3.10. But from observation of photographs similar to Fig. 3.10 it can be ascertained that most of the parallel longitudinal lines grouped together do not alternate in sign although there is about the same number of lines of both signs in average.

That is to conclude that groups of closely spaced small steps or monoatomic steps in general have same sign; overall level is maintained by groups alternating in sign.

3.4. Comment on a long range decoration effect.

It is to be noted that cleavage steps and slip lines are still effectively decorated even if they lay in the shadow cast by large steps, as can be seen in Fig. 3.12. This is an electron micrograph of a shadow-decorated replica of a sodium chloride crystal in which two large cleavage steps AA, FF can be observed. AA is a cleavage step 160 Å high, as measured from the displacement of transverse slip lines HH, II. It casts a shadow approximately 1900 Å long. Cleavage step FF is approximately 130 Å high and its shadow is 1500 Å. At the shadow of step AA two groups of steps BB, CC and DD, EE can be observed.

Some mechanisms must be found to explain the long range decoration of steps such as BB, CC, DD, EE, which lie in the shadow cast by large steps. As was explained in paragraph 3.2.1 the migration distance of the gold atoms in shadow-decorated replicas is at least 500 Å. It is not likely that gold atoms and small gold clusters could migrate 2000 Å in a backward direction. Some other mechanisms must be operative at the same time. It is believed that the most likely are the following;

a) Although the mean free path of the evaporated gold atoms at 10^{-5} Torr is longer than the diameter of the bell-jar, collision with residual gas molecules over the otherwise depleted region can account for some of the nuclei condensed in the shadow region.

b) Due to the near grazing incidence, the gold beam is everywhere very close to the surface. As gold clusters start growing, some of

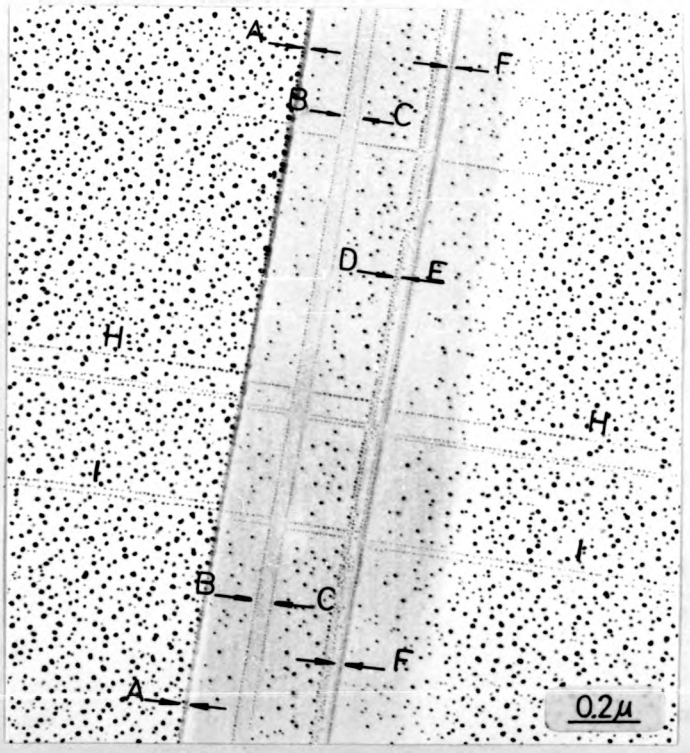

Fig. 3.12. Decoration of slip and cleavage steps lying in the shadow of large steps.

the arriving gold atoms may collide with the bigger nuclei, as well as with the adsorbed gas molecules, and be reflected backwards. If operative, this mechanism should be particularly efficient near the edge of the shadow, where the arriving atoms are particularly close to the surface.

c) Stirland (4) assumes that a step-down is a barrier to the migration of the gold atoms. This is a convincing assumption for the normal incidence decoration technique. But, in the shadow-decoration technique the principal component of the kinetic energy of the arriving gold atoms is in the plane of the surface; therefore, it is possible for the atoms impinging near the edge of a large step down, to reach the lower surface by dropping over the riser of the step.

3.5. Conclusions

A new replica technique for the electron microscopy observation of cleavage structures in sodium chloride crystals has been described in this chapter.

The main advantages of the shadow-decoration technique over the standard thin film decoration technique are the following:

1) Resolution of surface structures, as measured by the ratio between the mean distance between nuclei condensed on flat areas of the surface and the mean distance between nuclei condensed on the monoatomic steps, is improved with the use of shadow-decorated replicas.

2) Thermal activated motion of dislocations and evaporation of cleavage structures due to heating of the specimen during the preparation stage, are both avoided. Shadow-decorated replicas are prepared at room temperature; as a consequence no cross-slip due to

the arriving gold atoms may collide with the bigger nuclei, as well as with the adsorbed gas molecules, and be reflected backwards. If operative, this mechanism should be particularly efficient near the edge of the shadow, where the arriving atoms are particularly close to the surface.

c) Stirland (4) assumes that a step-down is a barrier to the migration of the gold atoms. This is a convincing assumption for the normal incidence decoration technique. But, in the shadow-decoration technique the principal component of the kinetic energy of the arriving gold atoms is in the plane of the surface; therefore, it is possible for the atoms impinging near the edge of a large step down, to reach the lower surface by dropping over the riser of the step.

3.5. Conclusions

A new replica technique for the electron microscopy observation of cleavage structures in sodium chloride crystals has been described in this chapter.

The main advantages of the shadow-decoration technique over the standard thin film decoration technique are the following:

1) Resolution of surface structures, as measured by the ratio between the mean distance between nuclei condensed on flat areas of the surface and the mean distance between nuclei condensed on the monoatomic steps, is improved with the use of shadow-decorated replicas.

2) Thermal activated motion of dislocations and evaporation of cleavage structures due to heating of the specimen during the preparation stage, are both avoided. Shadow-decorated replicas are prepared at room temperature; as a consequence no cross-slip due to

thermal activation of dislocations occurs: cross-slip structures observed are typical of cleavage surfaces (see section 4.3.3).

3) It is possible to determine the sense of most of the cleavage and slip steps if appropriate shadowing conditions are selected. This possibility has been checked by shadow-decorating evaporation spirals in sodium chloride crystals.

Sign determination analysis has been used in this research (chapters 4.3. and 6) to identify the slip systems activated by cleavage as well as to study their distribution in different regions of the crystals and to interpret other cleavage structures observed in the electron microscope.

The shadow-decoration technique has also been tested in lithium fluoride crystals, though no extensive studies have been performed on replicas of this material. The fact that excellent shadow-decorated replicas of lithium fluoride cleavage surfaces were also obtained, suggests that this technique could be widely used for the study of surface structures of ionic crystals at room temperature.

R.3. References

(1) Bassett, G.A., Phil. Mag. 3, 1042 (1958)

(2) William, R.G., Wyckoff, R.W.G., J. Appl. Phys. 15, 712 (1944)

(3) Wainer, L.S., Thin Sol. Films 21, 531 (1974)

(4) Stirland, D.J., Phil. Pag. 25, 1181 (1966)

(5) Burton, W.D., Cabrera, N., Frank, F.C., Phil. Trans. Roy. Soc. A243, 299 (1951)

(6) Forty, A.J., Frank, F.C.., Proc. Roy. Soc. A217, 262 (1953)

(7) Cabrera, N. Levine, M.M., Phil. Mag. 1, 450 (1956)

(8) Hirth, J.P., Ponund, G.M., Acta Met. 5, 649 (1957)

(9) Bethge, H., Phys. Stat. Sol. 2, 3 (1962)

(10) Cramer, H., The Elements of Probability Theory and some of its applications, John Wiley & Sons, New York (1955)

(11) Cramer, H., ibid, page. 276

(12) Sholl, C.A., Fletcher, N.H., Acta Met. 18, 1083 (1970)

Chapter 4

RESULTS

4.1. Introduction

It has long been recognized that plastic deformation accompanies the propagation of cleavage cracks in alkali halide crystals. A crack propagating with unsteady velocity leaves, in the newly created cleavage surfaces, narrow bands of intense plastic deformation, particularly at the zones where it halted, as has been described in detail in Chapter 1.

The purpose of this Chapter is to describe the results of different complementary experiments, performed to study the dislocation processes involved in the plastic deformation associated with the unsteady propagation of cleavage cracks in sodium chloride single crystals, for a wide range of crack velocities. The study of surface features characteristic of crack propagation at different velocities can be most suitably performed on one and the same crystal, by stopping a cleavage crack several times and observing the zones between two successive stopped fronts (section 2.2).

A detailed description will be given of the optical and electron microscopy observations of fresh cleavage surfaces and of chemically etched cleavage surfaces for cracks propagating in different crystallographic directions. The interpretation and discussion of these observations will be given in Chapter 6.

The stepped structures of a cleavage surface associated with different velocities of crack propagation were studied over a wide range of magnification. Special emphasis was placed on the

Chapter 4

RESULTS

4.1. Introduction

It has long been recognized that plastic deformation accompanies the propagation of cleavage cracks in alkali halide crystals. A crack propagating with unsteady velocity leaves, in the newly created cleavage surfaces, narrow bands of intense plastic deformation, particularly at the zones where it halted, as has been described in detail in Chapter 1.

The purpose of this Chapter is to describe the results of different complementary experiments, performed to study the dislocation processes involved in the plastic deformation associated with the unsteady propagation of cleavage cracks in sodium chloride single crystals, for a wide range of crack velocities. The study of surface features characteristic of crack propagation at different velocities can be most suitably performed on one and the same crystal, by stopping a cleavage crack several times and observing the zones between two successive stopped fronts (section 2.2).

A detailed description will be given of the optical and electron microscopy observations of fresh cleavage surfaces and of chemically etched cleavage surfaces for cracks propagating in different crystallographic directions. The interpretation and discussion of these observations will be given in Chapter 6.

The stepped structures of a cleavage surface associated with different velocities of crack propagation were studied over a wide range of magnification. Special emphasis was placed on the

constant comparison between the micro (electron microscopy) and macro (optical microscopy) scale of observations.

It has often been assumed that semi-brittle fracture behaviour is similar for many ionic crystals with sodium chloride-like structures (section 1.1.2. An electron microscopy study of cleavage surfaces of lithium fluoride crystals was carried out to compare results for both alkali halides.

4.2. Optical microscopy

4.2.1. Introduction

The discontinuous propagation of cleavage cracks in alkali halide crystals has been studied by optical microscopy by several authors (1) (2) (3); the surface structures originated in the plastic deformation introduced by cleavage cracks has also been extensively studied by optical microscopy (4) (5) (6) as has been summarized in section 1.1.2.

The purpose of this section is to present a comprehensive description of the relevant characteristic features observed in different regions of cleavage surfaces of sodium chloride crystals which correspond to different velocities of crack propagation. This macro description of the cleavage features as observed in the optical microscope complements the electron microscopy observations; in this way an integral picture of the phenomena accompanying unsteady crack propagation can be envisaged.

4.2.2. Observations

The propagation of cleavage cracks in sodium chloride single crystals was studied under the optical microscope through the interference pattern between the light reflected from the two surfaces

created by the crack as described in section 2.1.

The sharpness on the crack front and the regular spacing of the fringes that can be observed in Fig. 4.1 are an indication that the crack is wedge shaped.

Observation of a large number of specimens shows several features that can be considered as typical of propagation of cleavage cracks in sodium chloride single crystals under the experimental conditions described in section 2.1. The mode in which the cleavage crack propagated is sketched in Fig. 4.2. The crack usually started at a corner and propagated radially until reaching the two opposite <100> crystal edges where it began to straighten up. Bulging of the crack front at the crystal edges as a consequence of the drag exerted on the propagating crack front is evident in Fig. 4.3.
Once the crack has been stopped, it nucleates, when restarting, near the center of the crack front, provided no large cleavage steps are present; it then propagates forwards and sideways at high velocity as depicted in Fig. 4.2 until it is able to run almost freely and straightens up again.

If the cleavage tool is withdrawn, the crack front retreats slightly; Fig. 4.3 shows the crack finally at rest. It shows a noticeable ragging everywhere except in the zones where the crack front is exactly parallel to [010] direction.

Cleavage steps follow the general direction of crack propagation and are almost always perpendicular to the instantaneous positions of the crack front. When the crack is propagating in the [100] general direction and the velocity is not high, they have a tendency to run in the crystallographically preferred [100] direction.

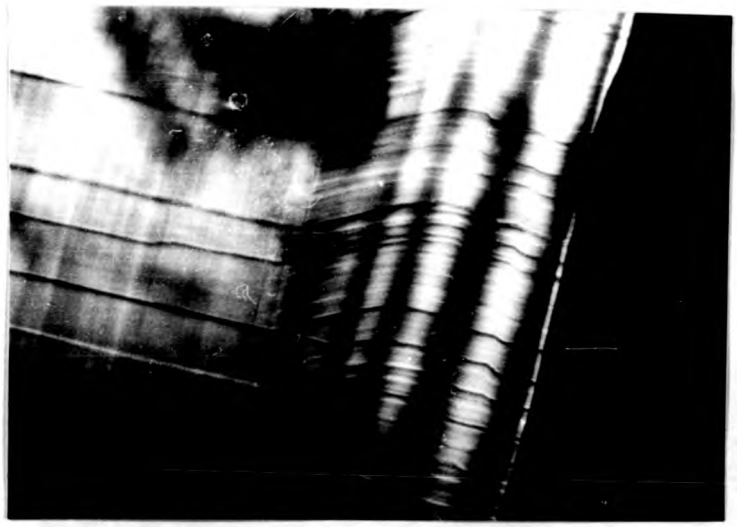

Fig. 4.1. Optical micrograph of a stopped cleavage crack front in a NaCl crystal. Magn. x 110.

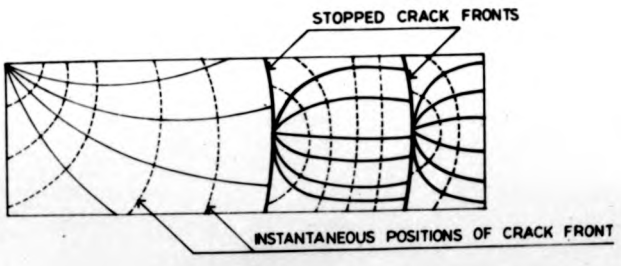

Fig. 4.2. Schematic diagram of the mode in which a cleavage crack propagates.

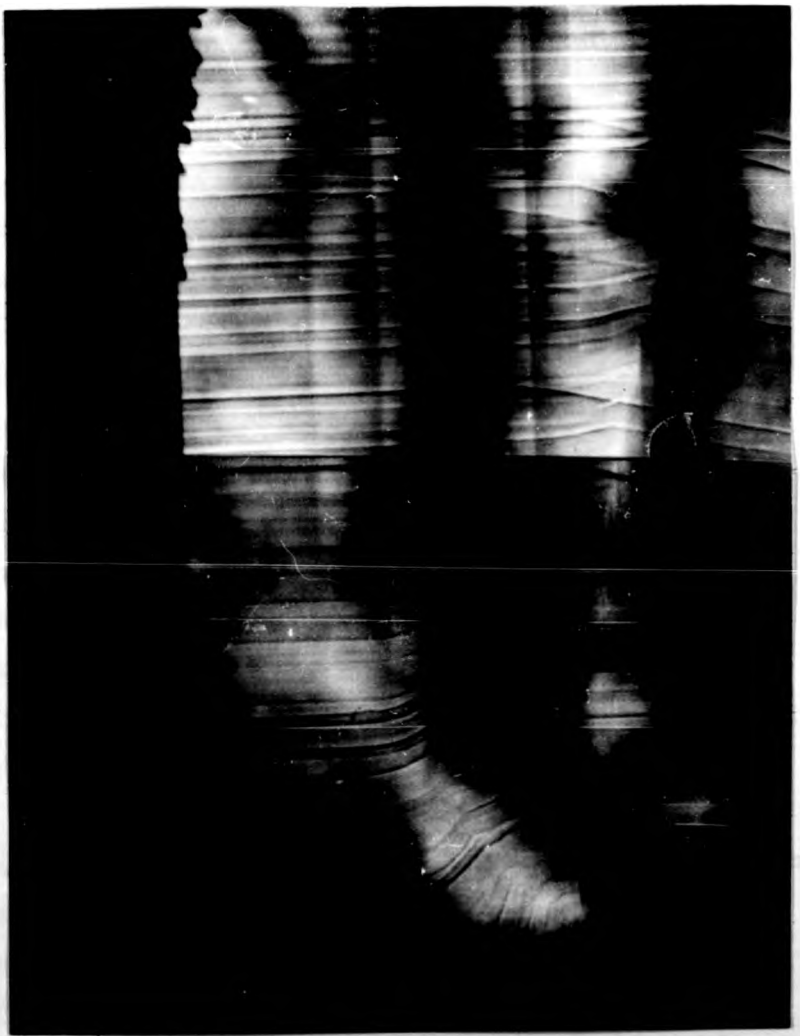

Fig. 4.3. Optical micrograph of a partially cleaved sodium chloride crystal showing the stopped front after removing the cleavage chisel. Magn. 110x

Where the crack front bulges, particularly when restarting, they do not follow the [100] direction but run along non-crystallographic curved paths, following again the local crack propagation direction. Arrow in Fig. 4.4 points out to a zone where local bulging of the crack front can be recognized by the opposite slopes of neighbouring cleavage steps at a particular stopped front. This highly localized bulge in the crack front must be related to a perturbation in the stress field of the crack tip.

The crack front is distorted by the presence of cleavage steps. This distortion increases with the height of the step. For high cleavage steps the crack front can make a turn of approximately 90°as can be seen in Fig. 4.4.

Overlapping of the crack front, preceeding the formation of a cleavage step can also be observed in micrograph 4.4 through the interference fringes. Perturbation in the propagation direction of small cleavage steps occurs near the riser of high cleavage steps. As can be seen in Fig. 4.4 small steps at both levels of high step AA are deviated towards its riser.

Cleavage steps may sometimes, at a stopped front, change direction abruptly and develop a short [010] segment before following again the local direction of crack propagation. Fig. 4.5 is a micrograph from an etched cleavage surface in which steps PQRT, P'Q'R'T' illustrate this phenomenon. This perturbation in the propagation of cleavage steps can sometimes be observed even at their intersection with slip bands as very short segments.

Fig. 4.6 shows a lateral (010) cross-section (see section 2.2) of a sodium chloride crystal with a stopped (001) cleavage crack in which a peculiar effect exhibited by several cracks is observed.

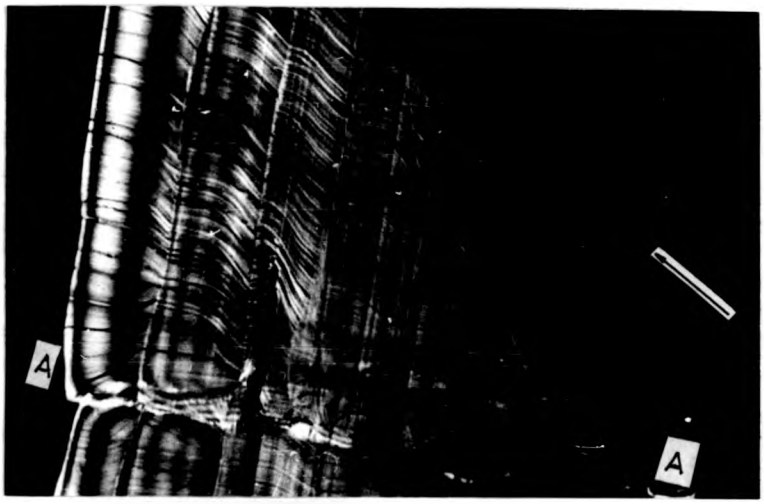

Fig. 4.4. Distortion of crack front by the presence of a high cleavage step. Arrow shows localized bulging of a stopped crack front as revealed by opposite slope of neighbouring cleavage steps. Magn. 110x.

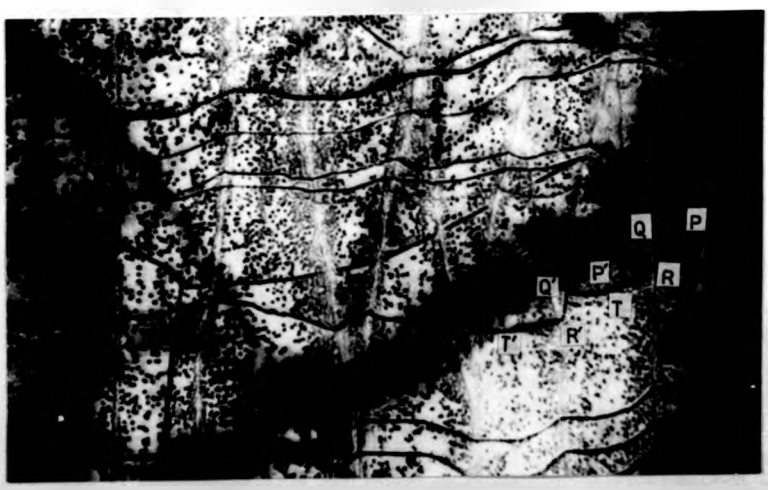

Fig. 4.5. Optical micrograph from an etched cleavage surface of a NaCl crystal . Magn. 110x .

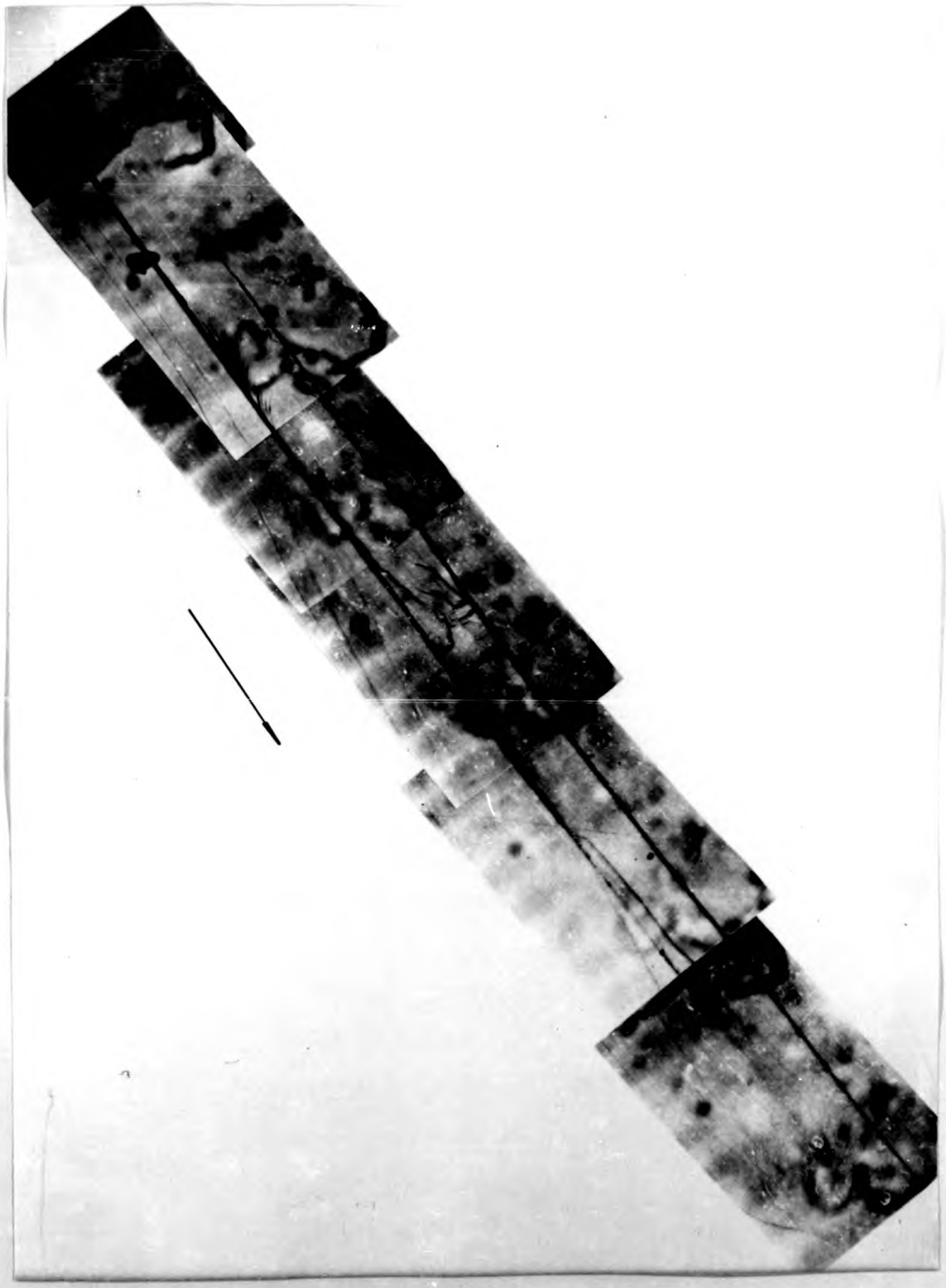

Fig. 4.6. Composite optical micrograph from a lateral (001) cross section of a NaCl crystal with a stopped (001) cleavage crack. Magn. 130x .

The crack was propagating as indicated by the arrow. A few microns before it stopped a secondary parallel cleavage appeared. The original cleavage gradually ceased to propagate and the secondary cleavage was the one that cut through the crystal. Fig. 4.6 is a composite micrograph from the crystal in which the distance between primary and secondary cleavage was a maximum among the twenty crystals studied.

Optical microscopy studies of chemically etched cleavage surfaces of sodium chloride crystals showed that there is a high density of dislocations at the stopped fronts.

Fig. 4.5 is an example of the resolution that was obtained at an optical microscope scale. As already described in section 2.2.3 it was not possible to resolve individual dislocations in the stopped fronts and the investigation was continued at an electron microscopy level.

4.3. Electron microscopy

The individual surfaces of a sodium chloride single crystal revealed after the completion of cleavage, have different features depending on the velocity and direction of cleavage propagation (as already described in section 1.1.2).

Partial electron microscopy studies of decorated replicas of sodium chloride cleavage surfaces were reported for example by Bassett (11), Bethge (12), Forwood (13,14), Stirland (15), Robins et al. (16), Appel et al. (17), Levi (18), but no comprehensive investigation has been published on the different features associated with different crack propagation velocities and directions.

This section will deal with a detailed description of these different features on an atomic level, as rendered visible by

decorated and shadow-decorated replicas (see sections 2.2.2 and 3.2.1) observed in the electron microscope. A discussion and interpretation of these features is deferred to Chapter 6.

The zone between two stopped crack fronts has been studied in the electron microscope for a large number of crystals and a schematic tracing of the main characteristic features observed is shown in Fig. 4.7. Five different zones have been considered:

1) "Tartan pattern" zone

2) "Stop band" zone

3) Restarting zone with inclined steps

4) V or "lightning" zone

5) Transition zone from V pattern to tartan pattern

Three of these zones, the tartan pattern, the stop band, and the restarting are shown in the composite electron micrograph, Fig.4.8.

These five zones appear always in the same sequence. When a cleavage crack is decelerating prior to stopping the electron micrographs show numerous transverse slip lines as well as longitudinal lines, forming a "tartan pattern". The transverse slip lines become more and more frequent as the velocity decreases and form slip bands that are closer and closer together. They become so crowded that they can seldom be resolved into individual lines: this zone is a few tenth of a micron wide and henceforth will be called "stop band" (zone 2, Fig. 4.7). It is believed that this zone is where the crack came to rest after a healing process, even if very slight, is completed. The healing process cannot proceed in the presence of transverse deformation. Very numerous short straight lines parallel to the [100] direction start at the the "stop band". Some of these lines end at transverse slip steps, others end at small

Fig. 4.7. Schematic tracing of main characteristic features observed between two stopped crack fronts - 1) Tartan pattern zone - 2) Stop band zone - 3) Restarting zone with inclined steps - 4) V or lightning pattern zone - 5) Transition zone from V pattern to tartan pattern.


5
4
3
2
1

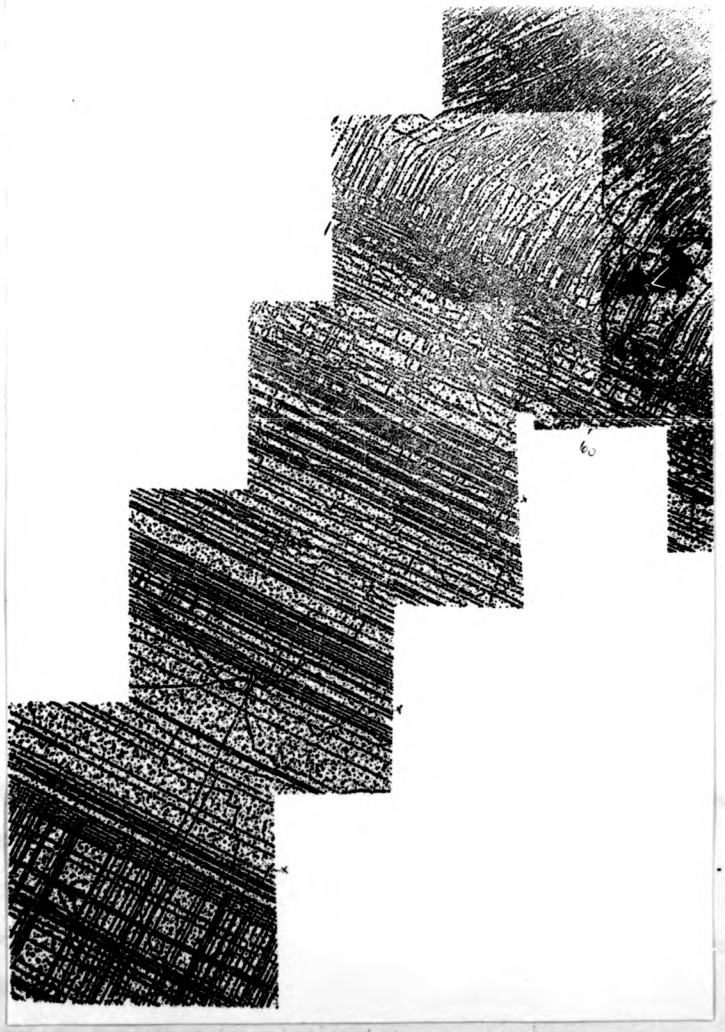

Fig. 4.8. Composite electron micrograph of a decorated replica of a sodium chloride crystal showing tartan pattern, stop band and restarting zones.

cleavage steps that follow the local direction of crack propagation, and others depending on the direction of crack propagation, change direction. This region is followed by a very intricate pattern of inclined cleavage steps, generally similar to a lightning pattern. The inclination of these steps is related to the local direction of crack propagation. These steps become straighter until they form a well developed lightning pattern (zone 4, Fig. 4.7). Part of the lines, following the local crack propagation direction become parallel to [100] , some transverse slip lines appear and both types of lines tend to form the tartan pattern.

The analysis of these zones will begin with a brief mention of the already well-known lightning pattern and the transition zone and it will be followed by a detailed description of the other three zones.

4.3.1. V or lightning zone

The lightning pattern is composed of straight and well formed Vs and is always present when a cleavage crack is running freely at high velocities in a direction different from [100] . It has already been studied in detail by electron microscopy by several authors (3) (13) (18).

The relatively high steps present in this zone are inclined with respect to the [100] direction as a result of the local crack propagation direction (originated in the bowing of the crack front as already described in section 4.2)

4.3.2. Transition zone from V-pattern to tartan pattern

When the crack is running at slower velocities, the atomic steps forming the Vs tend to align parallel to the crystallographically

preferred [100] direction as can be observed in Fig. 4.34. Transverse slip lines and the [100] longitudinal lines form a tartan pattern.

4.3.3. TARTAN PATTERN ZONE

As the crack decelerates, the transverse slip systems are activated and as a consequence numerous transverse slip lines appear (Fig. 4.9 lines AA, BB, etc).

These transverse slip lines and the longitudinal lines parallel to the [100] direction accompanying the propagating crack are arranged in a way quite similar to a tartan pattern. This zone, related to a decrease in the velocity of crack propagation, will be called the tartan pattern zone.

The length of this tartan pattern zone is dependent on the spacing between two consecutive stop bands; it extends over one fourth to one half of the distance between these bands. Under the present working conditions, zone lengths between 50μ-100μ to 400μ-500μ have been observed.

4.3.3.a) Observations of normal decorated replicas

All along the tartan pattern zone, atomic cleavage steps run parallel to the crystallographically preferred [100] direction. Under these conditions it is not possible to distinguish between the elementary cleavage steps and the longitudinal slip lines appearing in this region. Fig. 4.10 is a composite electron micrograph of the beginning of a tartan pattern zone.

No displacement is observed at the intersection of these perpendicular lines, although displacement of transverse slip lines can be seen at their intersection with high cleavage steps.

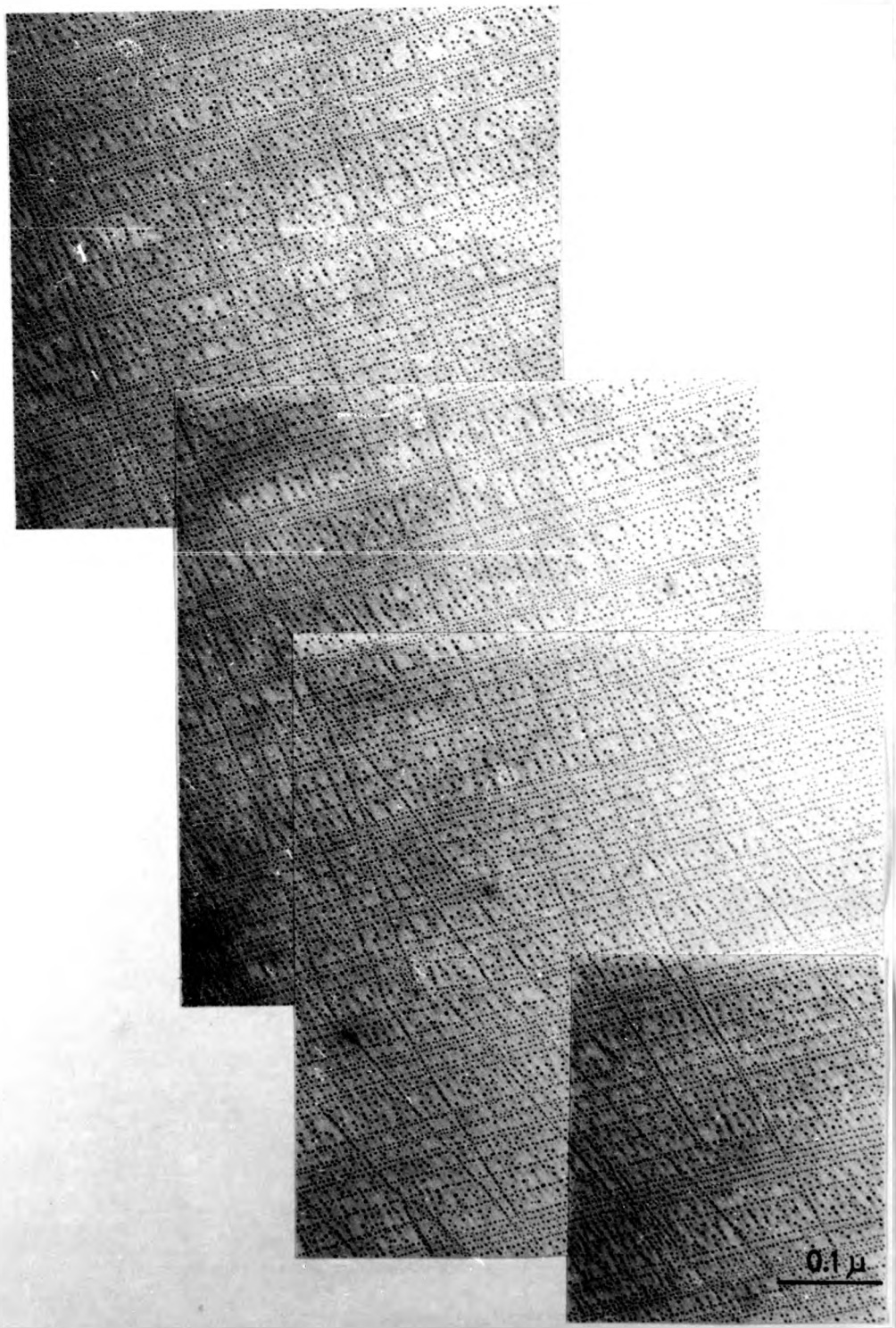

Fig. 4.34. Transition zone from V-pattern to tartan pattern.

Standard decorated replica of a NaCl crystal.

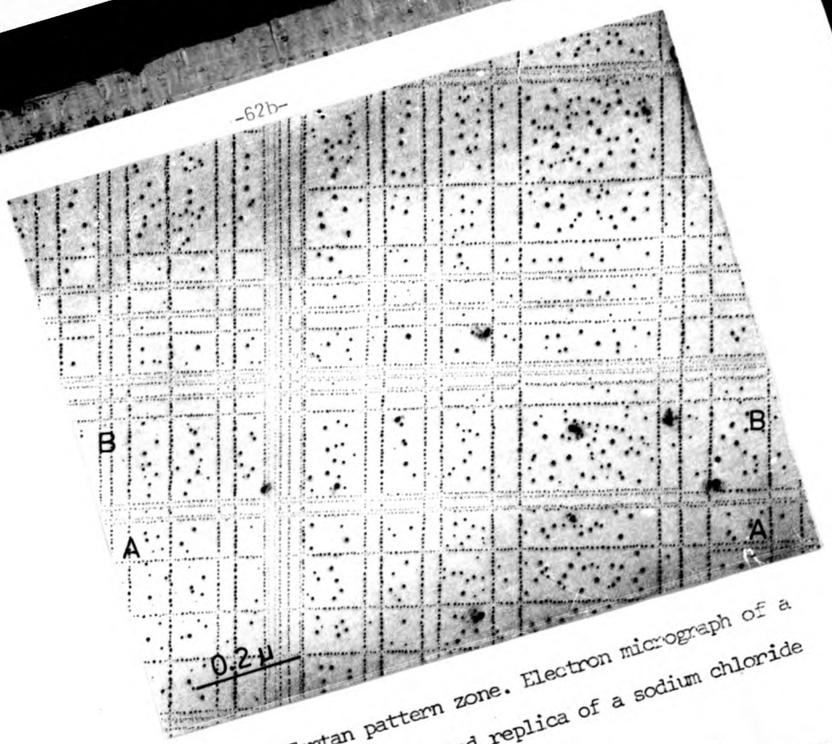

Fig. 4.9. Tartan pattern zone. Electron micrograph of a shadow-decorated replica of a sodium chloride crystal.

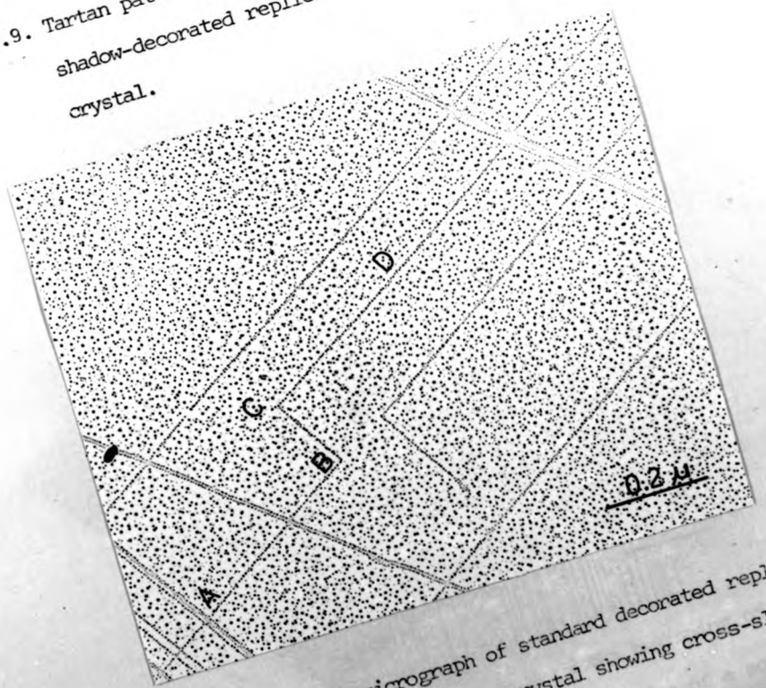

Fig. 4.11. Electron micrograph of standard decorated replica of a sodium chloride crystal showing cross-slip structures.

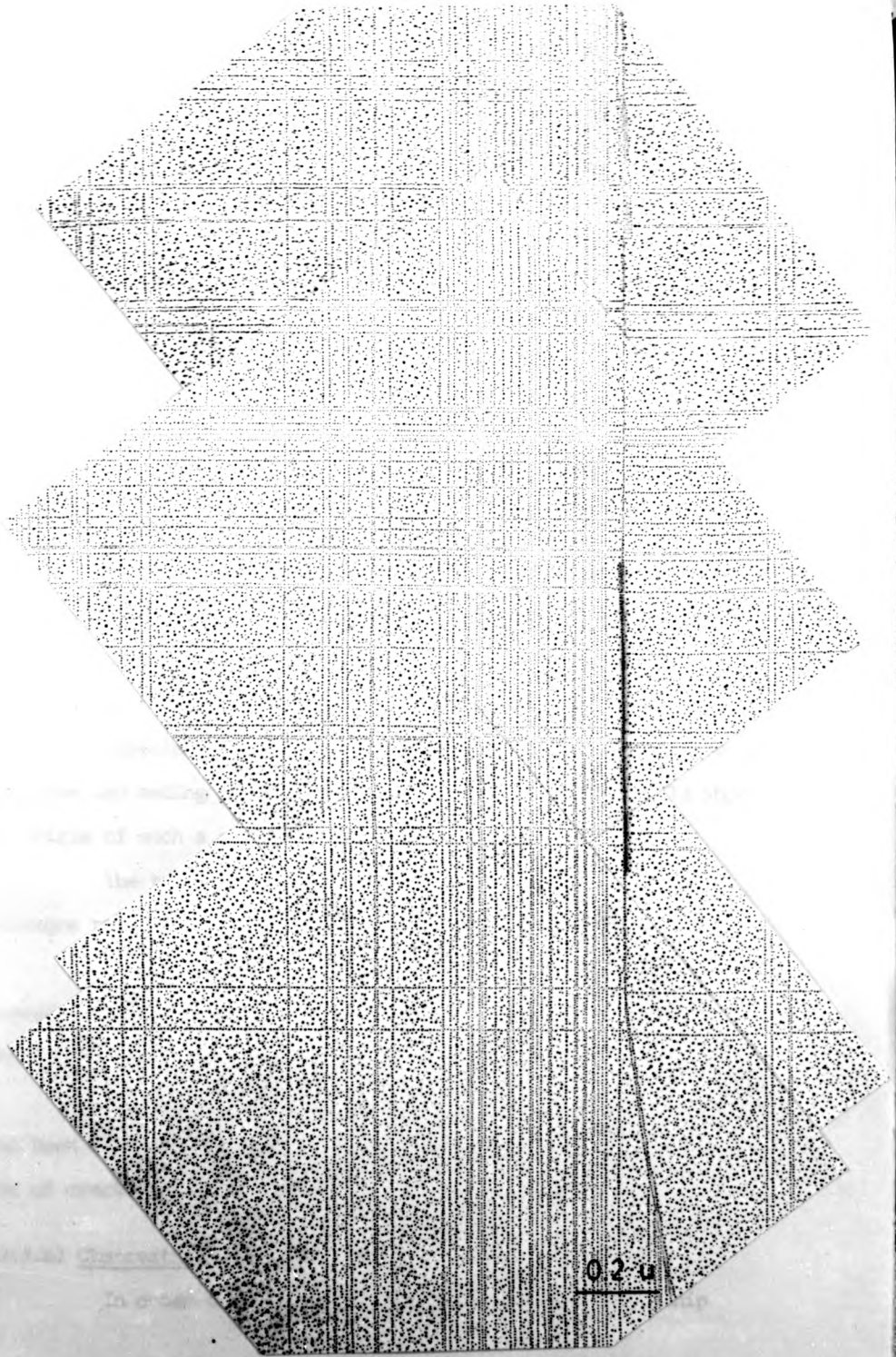

Fig. 4.10. Composite electron micrograph of the beginning of a tartan pattern zone. Standard decorated replica of a sodium chloride crystal.

At the beginning of the tartan pattern zone there are few transverse slip lines. The density of transverse slip lines increases as the velocity of the crack decreases; very frequently they are grouped in bands of variable width. The longitudinal lines are not homogeneously distributed (see Fig. 4.10).

It is not uncommon to observe a transverse line deflected from its [010] direction into an oblique or perpendicular line and back to a line parallel to the original [010] direction. This is interpreted as a cross-slip of a (101) [$\bar{1}$01] dislocation from its original (101) plane to a neighbouring (101) plane (Fig. 4.11) (line ABCD). More often the cross-slip segment follows a curved path (Fig. 4.12 line ABC). As was seen in the introduction, it was sometimes assumed that this cross-slip was related to the heating of the specimen during preparation of the decorated replicas.
Another characteristic of this zone is the presence of well localized bundles of parallel longitudinal lines, starting from a transverse slip line and ending in another transverse slip line. Fig. 4.13 shows the origin of such a structure.

The tartan pattern structures were also studied for cleavages propagating in a direction different from [100].

No new features were observed except for the presence of cleavage steps running in directions other than [100] following the local direction of crack propagation.

The presence of bundles of parallel longitudinal lines has also been observed, but their length is noticeably shorter than in the case of cracks running parallel to [100] .

4.3.3.b) Observations of the shadow-decorated replicas

In order to have a better insight of the relationship

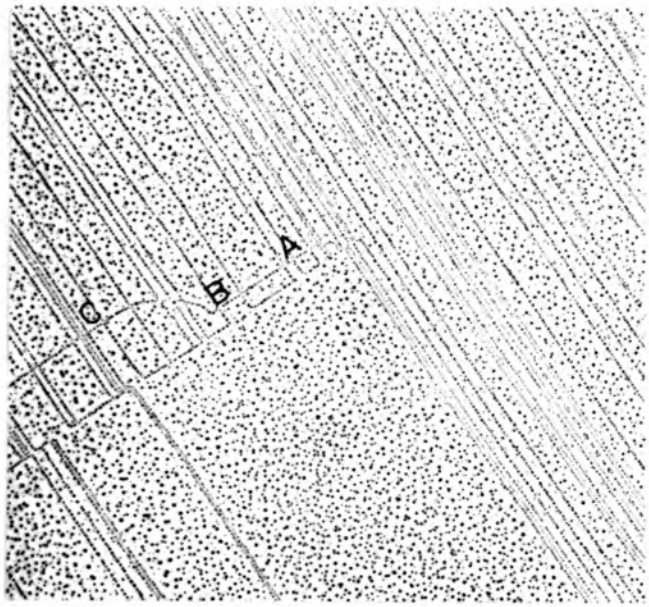

Fig. 4.12. Electron micrograph of standard decorated replica of a NaCl crystal showing a cross-slip structure with a curved path.

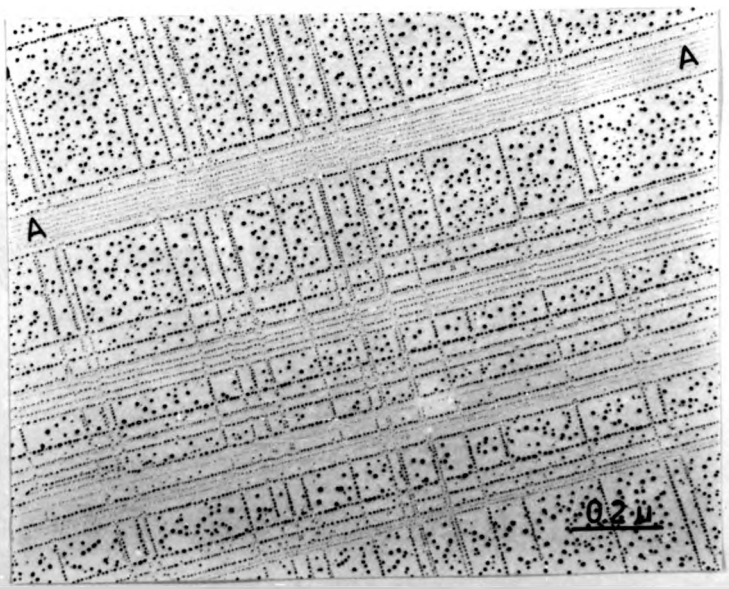

Fig. 4.15. Electron micrograph of a shadow-decorated replica of a NaCl crystal. Shadowing direction perpendicular to the transverse lines.

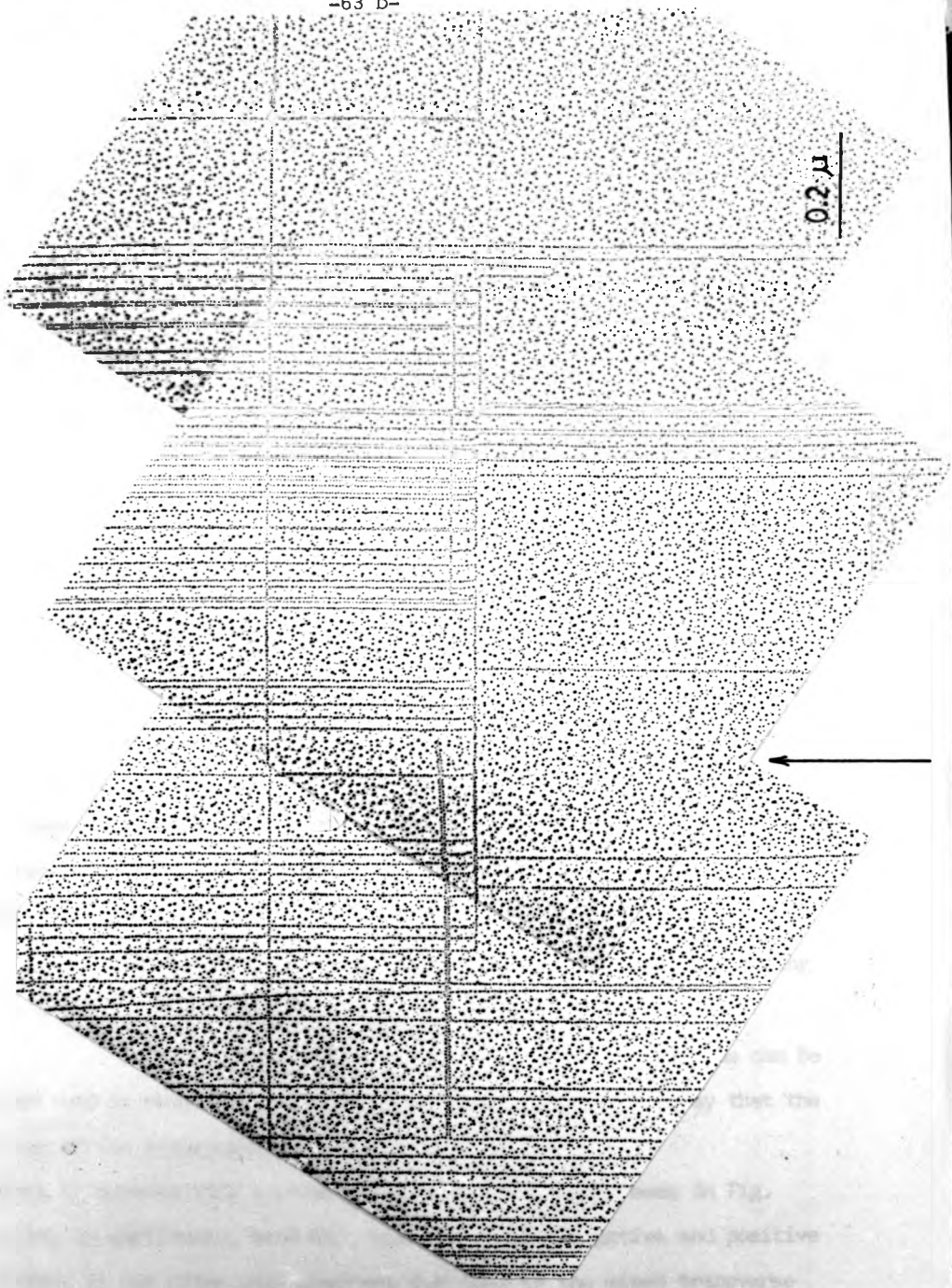

Fig. 4.13. Composite electron micrograph of a standard decorated replica of a NaCl crystal.

between these surface structures and the activated slip planes, shadow-decorated specimens were studied. As described in Chapter (3), in shadow - decorated replicas positive steps or steps-up are characterized by the condensation of large nuclei; negative steps or steps-down are rendered visible through the condensation of small nuclei.

Two kinds of experiments were performed as described in section 3.2.2 so that the sense of the longitudinal lines or the sense of the transverse lines could be determined by shadowing in different directions.

Fig. 4.14 is a composite electron micrograph of a replica with the shadow-decoration performed so that the up or down longitudinal steps can be distinguished. It is evident that longitudinal lines of both signs are present. An important observation from a large number of photographs is that there is about the same number of lines of both signs in average. Although steps do not alternate in sign regularly the presence of pairs of up and down steps was fairly frequently observed. As has been stated in section 3.3 groups of closely spaced small monoatomic steps, have in general the same sign. The overall level is maintained by groups alternating in sign.

Several interesting features of the transverse bands can be observed in shadow-decorated replicas prepared in such a way that the sign of the transverse steps can be determined.
Both transverse slip systems are activated as can be seen in Fig. 4.15. In particular, band AA , consists of both negative and positive steps. It has often been observed that many of the mixed transverse slip bands, like AA (Fig. 4.15), consist mostly of lines of one sign,

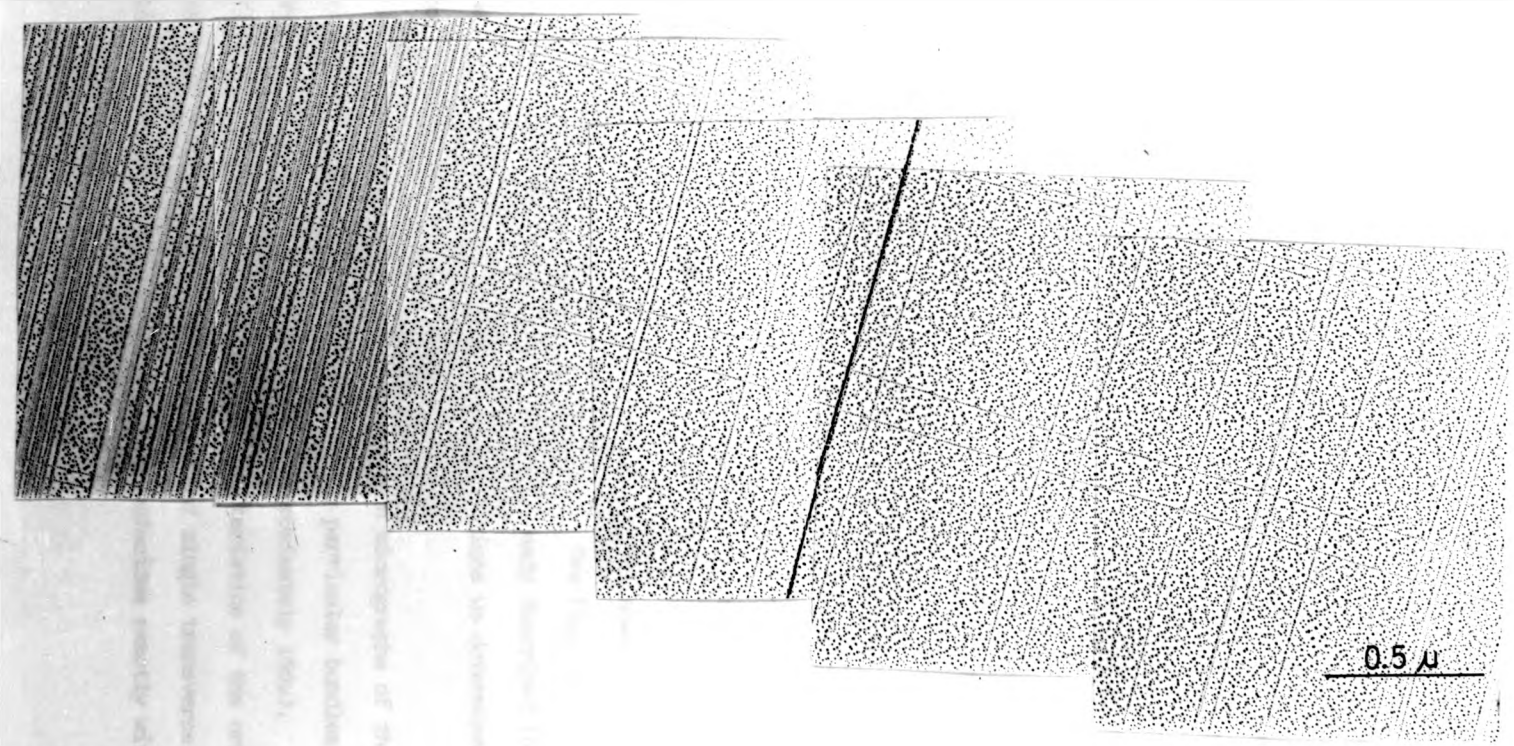

Fig. 4.14. Composite electron micrograph of a shadow-decorated replica of a NaCl crystal. Shadowing direction perpendicular to the longitudinal lines.

bounded by two lines of the opposite sign.

Fig. 4.16 shows a wide band consisting mostly of slip steps of the same sign (originated as a consequence of the activation of only one slip system).

Although many of the transverse lines are of monoatomic height, some of the slip lines of the transverse bands are several units high.

Another interesting feature is the interaction of many small cleavage steps with dense transverse slip bands. Cleavage step PQR, Fig. 4.17, shows a peculiar effect exhibited by many small cleavage steps: the step follows the general direction of crack propagation until it developes a jog in the [010] direction at a particular step of the slip band; the cleavage step develops another jog when it resumes the general direction of crack propagation. Distances of interaction between 0.5μ and 5μ have been observed. This same effect on a macro scale has been described in section 4.2.2.

The fact that the lines of the transverse band increase (or decrease) their height discontinuously over short distances by the interaction with very small cleavage steps was strikingly shown through the observation of shadow decorated specimens. See Fig. 4.17.

Bundles of parallel longitudinal lines already described in section 4.3.3.a have been studied in shadow-decorated replicas to determine, when possible, the sign of the observed steps.

Fig. 4.18a) and b) are composite electron micrographs of the origin and end of three of these bundles. These particular bundles were photographed all along their lenght (approximately 150μ).

Fig. 4.18a illustrates the typical characteristics of the origin of these bundles: they stem from a region of single transverse slip lines; one end of the transverse lines coincides exactly with the

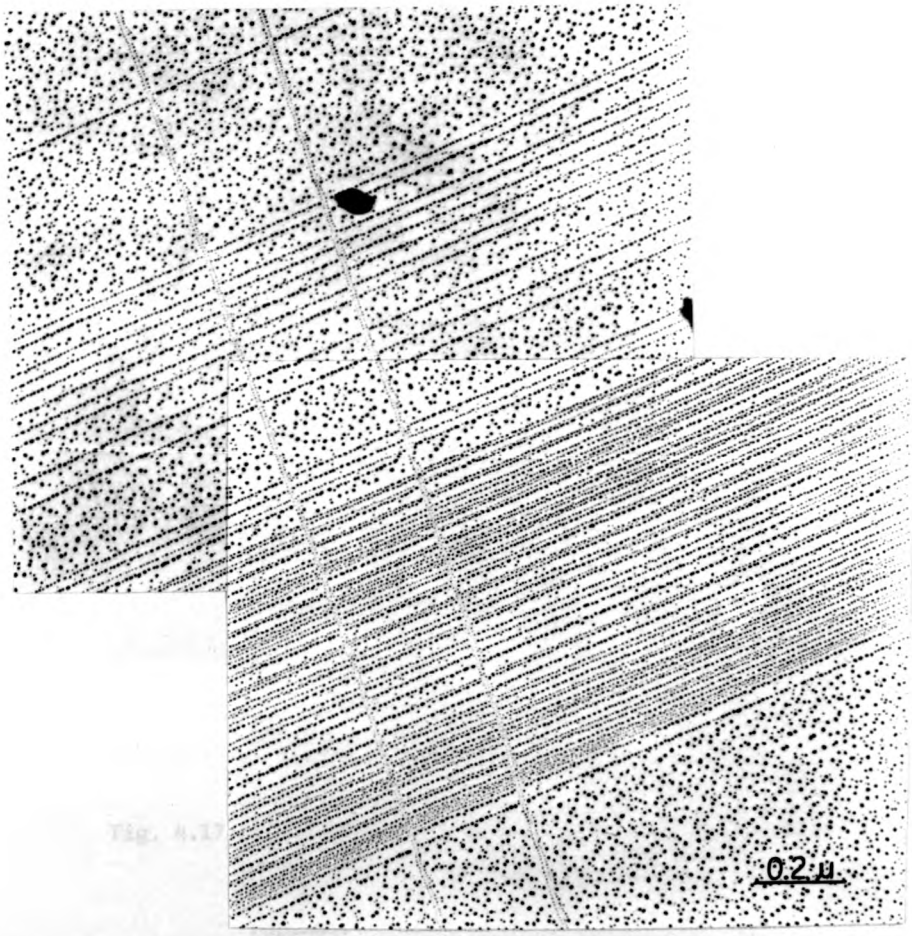

Fig. 4.16. Wide transverse slip band consisting mostly of slip steps of the same sign. Shadow decorated replica.

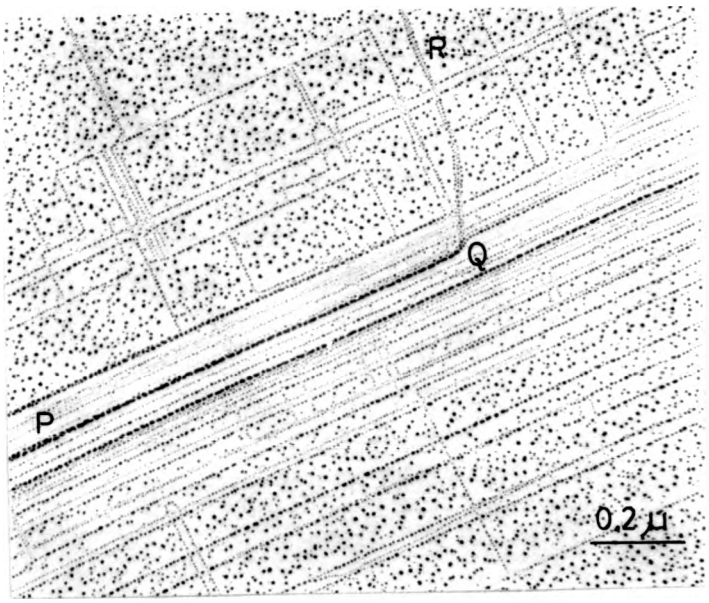

Fig. 4.17. Interaction of a small cleavage step with a dense transverse slip band. Shadow-decorated replica.

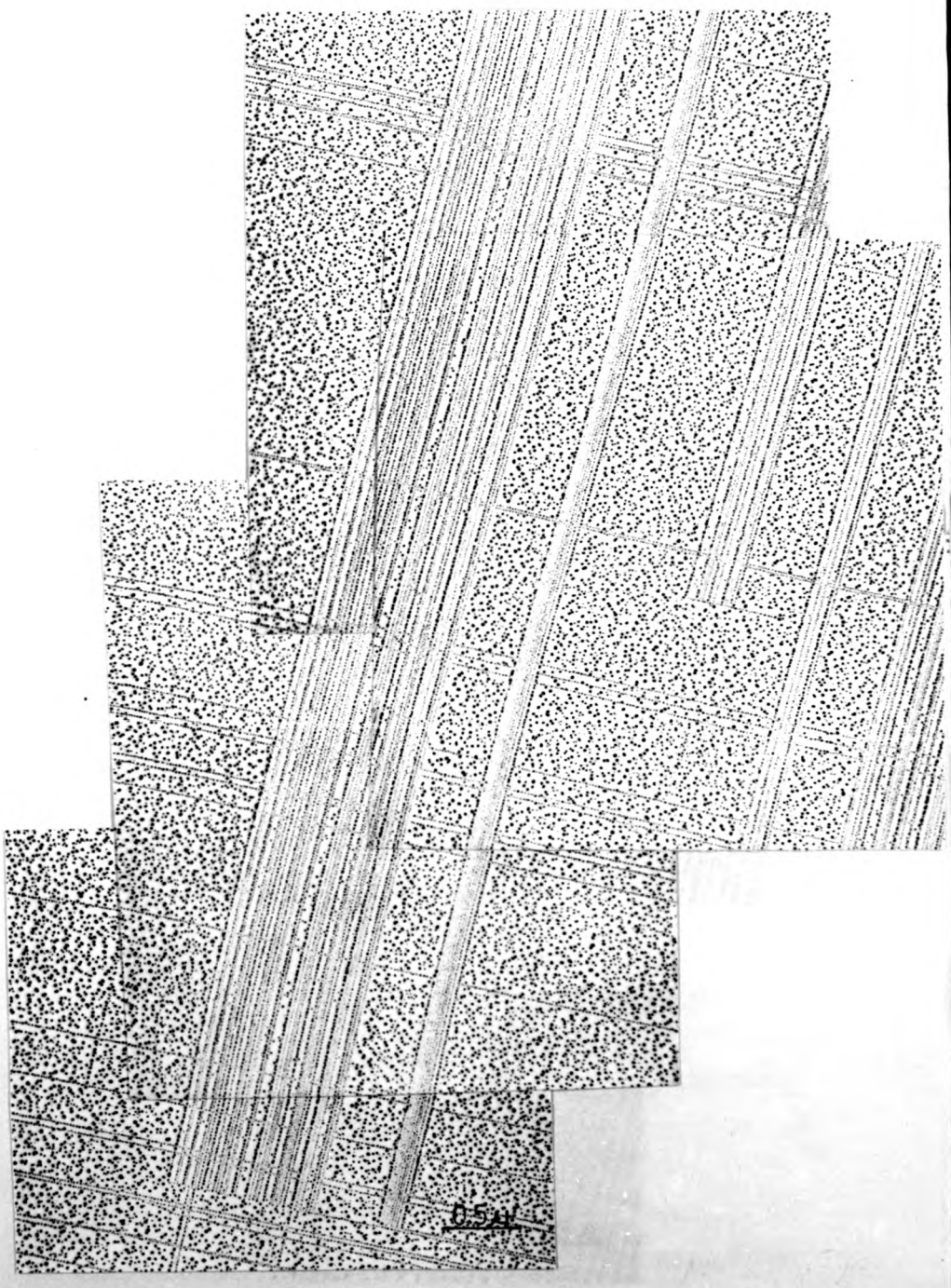

Fig. 4.18. Composite electron micrograph of a shadow-decorated replica of a NaCl crystal.
a) Origin of a bundle of parallel longitudinal lines.

Fig. 4. 18.b) End of bundle of Fig. a)

first longitudinal step. No remarkable feature is observed on the transverse slip lines at the other end of the bundles. There is no noticeable change in the bundles all along their length, even when they intersect single or grouped transverse slip lines (see for example groups AA, BB in Fig. 4.18 and CC in Fig. 4.19).

No systematic distribution of signs of neighbouring longitudinal lines has been observed. In particular, as stated above, they do not alternate their signs.

A peculiar effect has been observed, concerning the origin of one of the bundles (Fig. 4.20): the slip line which gives origin to this extended bundle has a cross-slip segment and the left section of the bundle stems from this cross-slip segment.

Another feature of this micrograph is worth mentioning: the relatively high cleavage step SS (180 Å high) is clearly deflected at its intersection with the slip line which is the origin of the bundle being described. This is particularly noteworthy as this slip line does not look different from the previous slip lines which the step intersects. The fact that the deviation of the high cleavage step as well as the beginning of the bundle, both occur at this particular transverse slip line, distinguish it as different from its neighbours.

There is one more feature worth mentioning in this micrograph: slip lines are deflected by the cleavage step SS; pairs AA, BB, CC, DD in the same sense, but pairs EE, FF are deviated in the opposite sense. This strongly suggests that both transverse slip systems have been activated.

In electron micrograph N°4.21 the typical cross-slip structure already described in section 4.3.1.a can be observed for

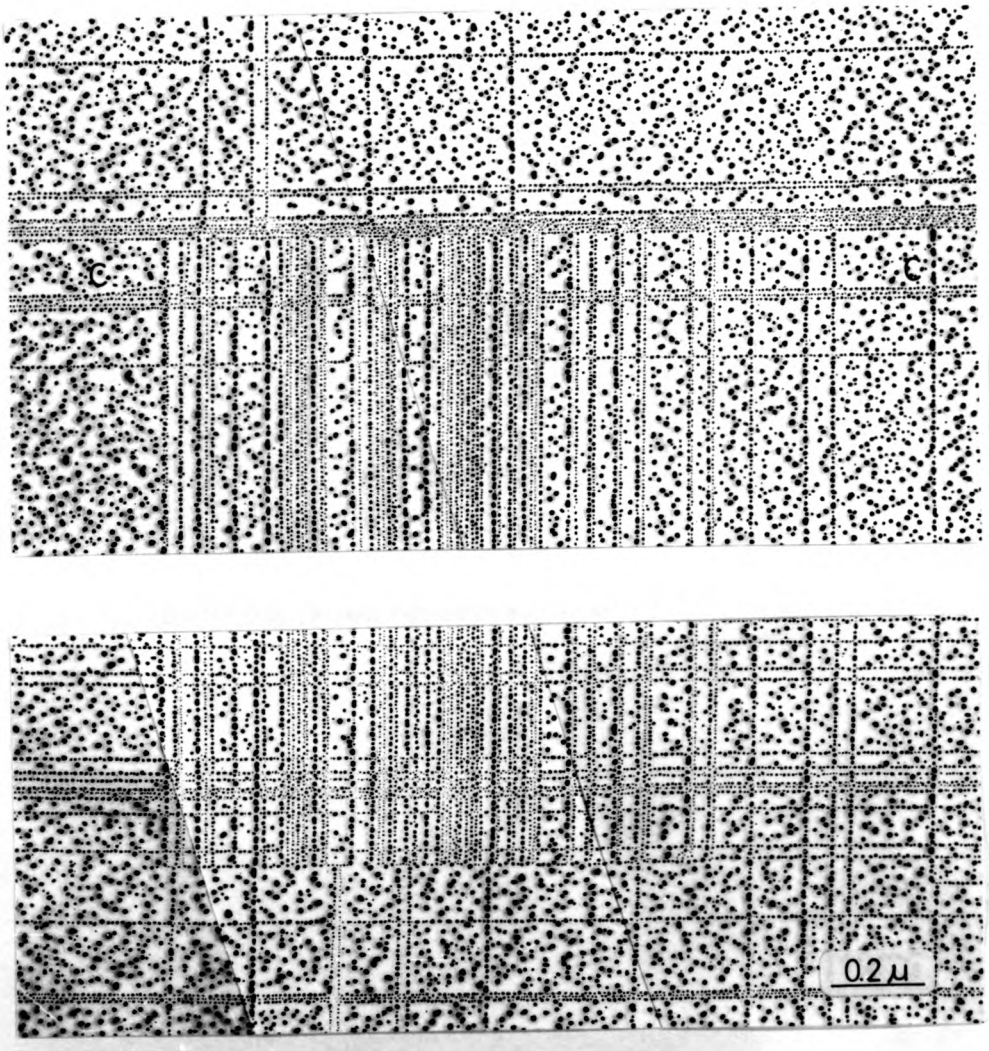

Fig. 4.19. Composite electron micrograph of a shadow-decorated replica of a NaCl crystal. Origin and end of a bunch of parallel longitudinal lines.

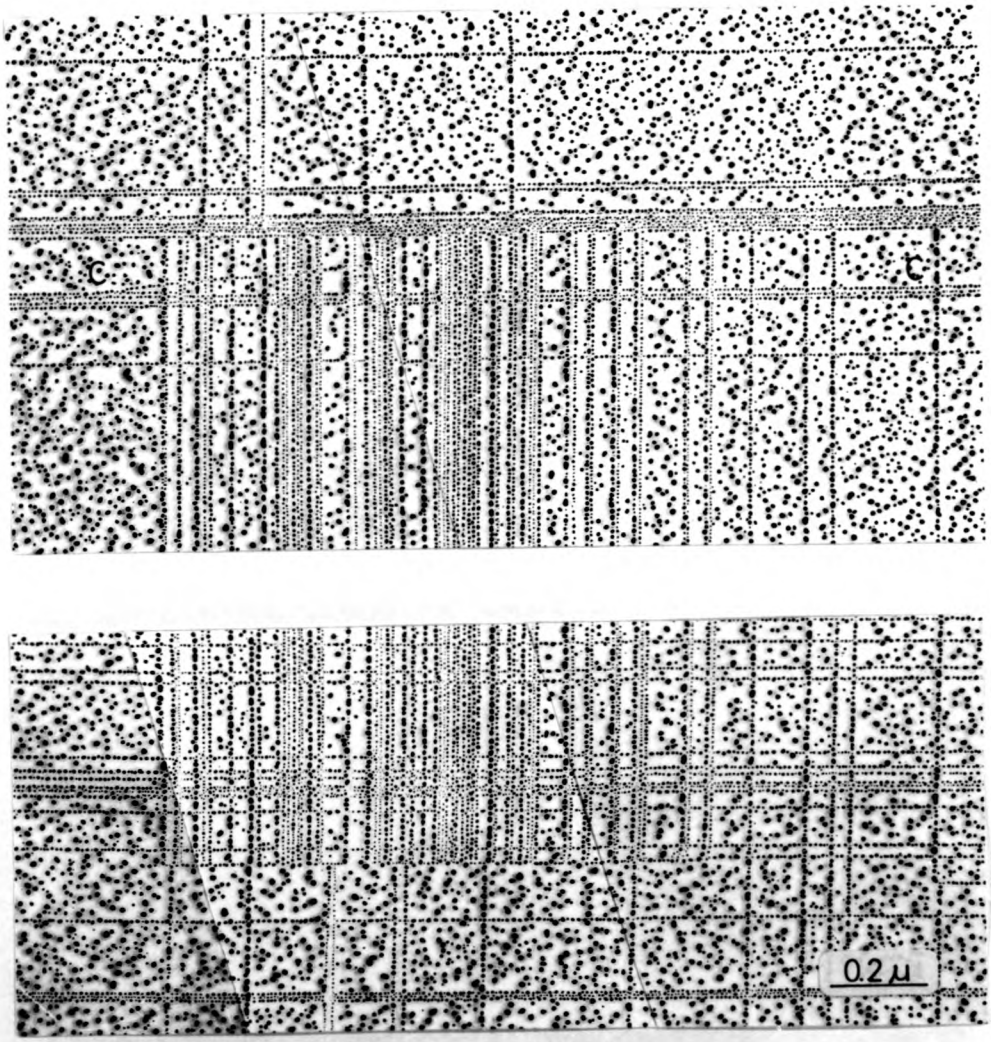

Fig. 4.19. Composite electron micrograph of a shadow-decorated replica of a NaCl crystal. Origin and end of a bunch of parallel longitudinal lines.

Fig. 4.20. Cross-slip of the line giving origin to an extended bunch. Shadow-decorated replica.

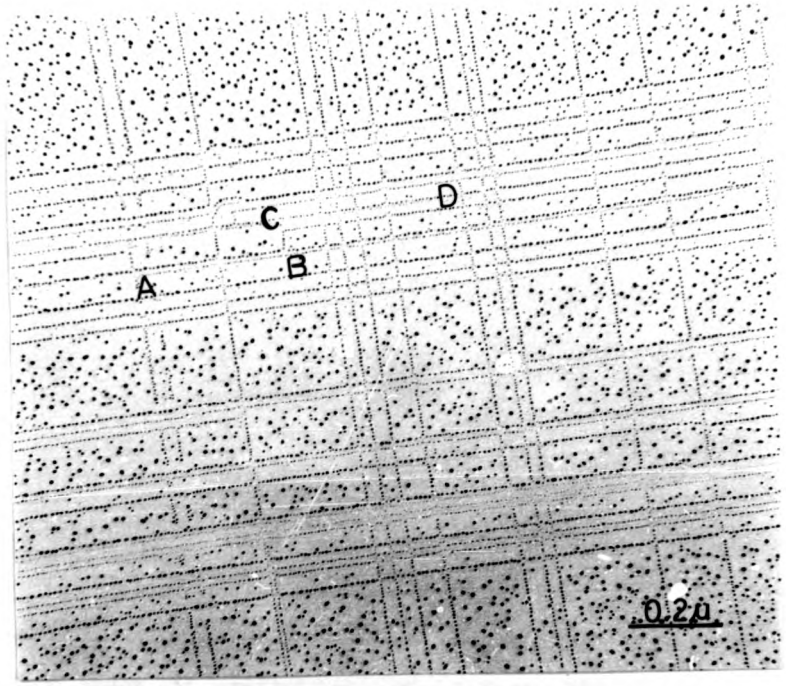

Fig. 4.21. Typical cross-slip structure. Shadow-decorated replica. Arrow indicates crack propagation and shadowing directions.

slip step ABCD.

The density of these cross-slip structures decreases for shadow-decorated replicas as compared to the replicas prepared with the standard decoration technique.

For shadow-decorated specimens most of the cross-slip structures are along low index crystallographic directions.

4.3.4. "Stop Bands"

4.3.4a) Observations in standard decorated replicas.

As the deceleration of the crack proceeds, the width and density of the transverse bands increases. These bands are closer and closer together as they approach the "stop band". Longitudinal unit lines are stopped or deviated by different transverse bands, and their density decreases noticeably.

The "stop bands" can seldom be resolved into individual slip lines. In the few light bands where this is possible, densities of the order of 10^6 lines/cm have been measured for the transverse slip lines. These stop bands form walls that only cleavage steps higher than 100 Å can transverse with a minor deviation; atomic cleavage steps and longitudinal slip lines are completely stopped at these bands (see Fig. 4.8).

Very numerous short straight lines parallel to the [100] direction start at the stop bands, in the zones where the local direction of the crack front is roughly parallel to the [010] direction(the crack is propagatingin the general [100] direction, see Fig. 4.22) The length of these short lines ranges from 0.2μ to about 1μ.

Their density varies from approximately 4×10^5/cm to 7×10^5/cm and their distribution is not uniform. Some of these lines end at transverse slip lines, others end at small cleavage steps that follow

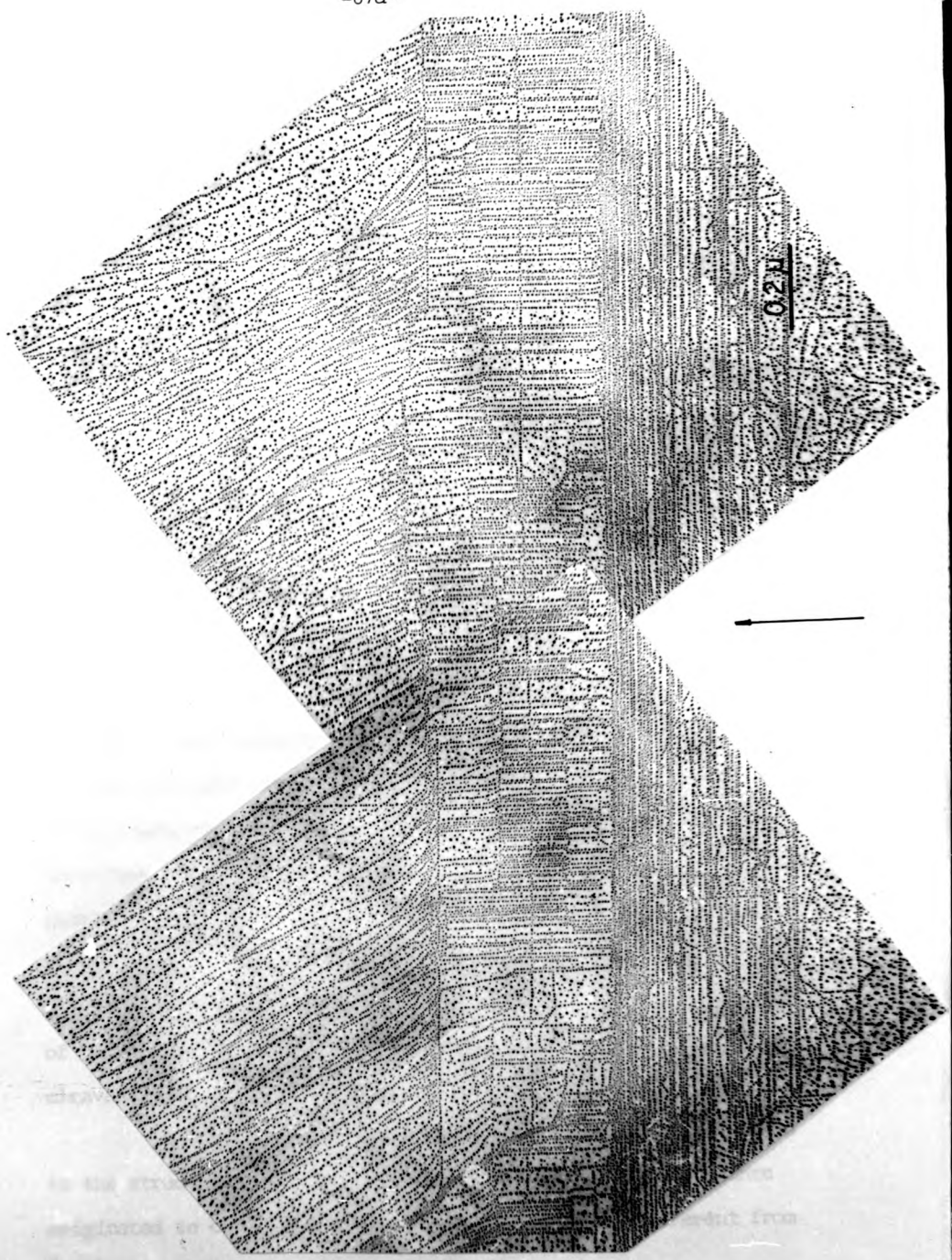

Fig. 4.22. Stop band. Standard decorated replica of a NaCl crystal.

the local direction of crack propagation. Many change direction following the local direction of crack propagation.

A crack front that is roughly parallel to the [010] direction, is not strictly straight: a slight curvature, only visible on the scale of the electron microscope is always present, apart from the large bulges observed at high cleavage steps, crystal edges, etc.. In these slightly curved zones, the short straight lines have their origins at different transverse slip lines, starting always strictly in the [100] direction, as can be seen in Fig. 4.23.

The behaviour of the short straight lines originating at the stop bands is altered by the presence of a high step, and it is not the same for both levels of the step. This effect can be seen in the composite electron micrograph, Fig. 4.24. On the left side of the high step, the short straight lines starting at the stop band are parallel to the [100] direction up to a certain distance from the step where they suddenly start running parallel to the [010] direction. No short straight lines can be seen in an intermediate position. On the right side of the step they have the behaviour already described for a crack front in a [010] direction. This last photograph illustrates the different behaviour of unit steps at both levels of a high cleavage step, as observed in decorated replicas. The stresses originated at the high cleavage step disturb the shape of the crack front and unit steps running at one level of the cleavage step are deflected into the [010] direction.

For a better understanding of the processes giving rise to the structure observed at the stop bands, curved crack fronts originated in cleavages propagating in a direction different from [100] were studied.

the local direction of crack propagation. Many change direction following the local direction of crack propagation.

A crack front that is roughly parallel to the [010] direction, is not strictly straight: a slight curvature, only visible on the scale of the electron microscope is always present, apart from the large bulges observed at high cleavage steps, crystal edges, etc.. In these slightly curved zones, the short straight lines have their origins at different transverse slip lines, starting always strictly in the [100] direction, as can be seen in Fig. 4.23.

The behaviour of the short straight lines originating at the stop bands is altered by the presence of a high step, and it is not the same for both levels of the step. This effect can be seen in the composite electron micrograph, Fig. 4.24. On the left side of the high step, the short straight lines starting at the stop band are parallel to the [100] direction up to a certain distance from the step where they suddenly start running parallel to the [010] direction. No short straight lines can be seen in an intermediate position. On the right side of the step they have the behaviour already described for a crack front in a [010] direction. This last photograph illustrates the different behaviour of unit steps at both levels of a high cleavage step, as observed in decorated replicas. The stresses originated at the high cleavage step disturb the shape of the crack front and unit steps running at one level of the cleavage step are deflected into the [010] direction.

For a better understanding of the processes giving rise to the structure observed at the stop bands, curved crack fronts originated in cleavages propagating in a direction different from [100] were studied.

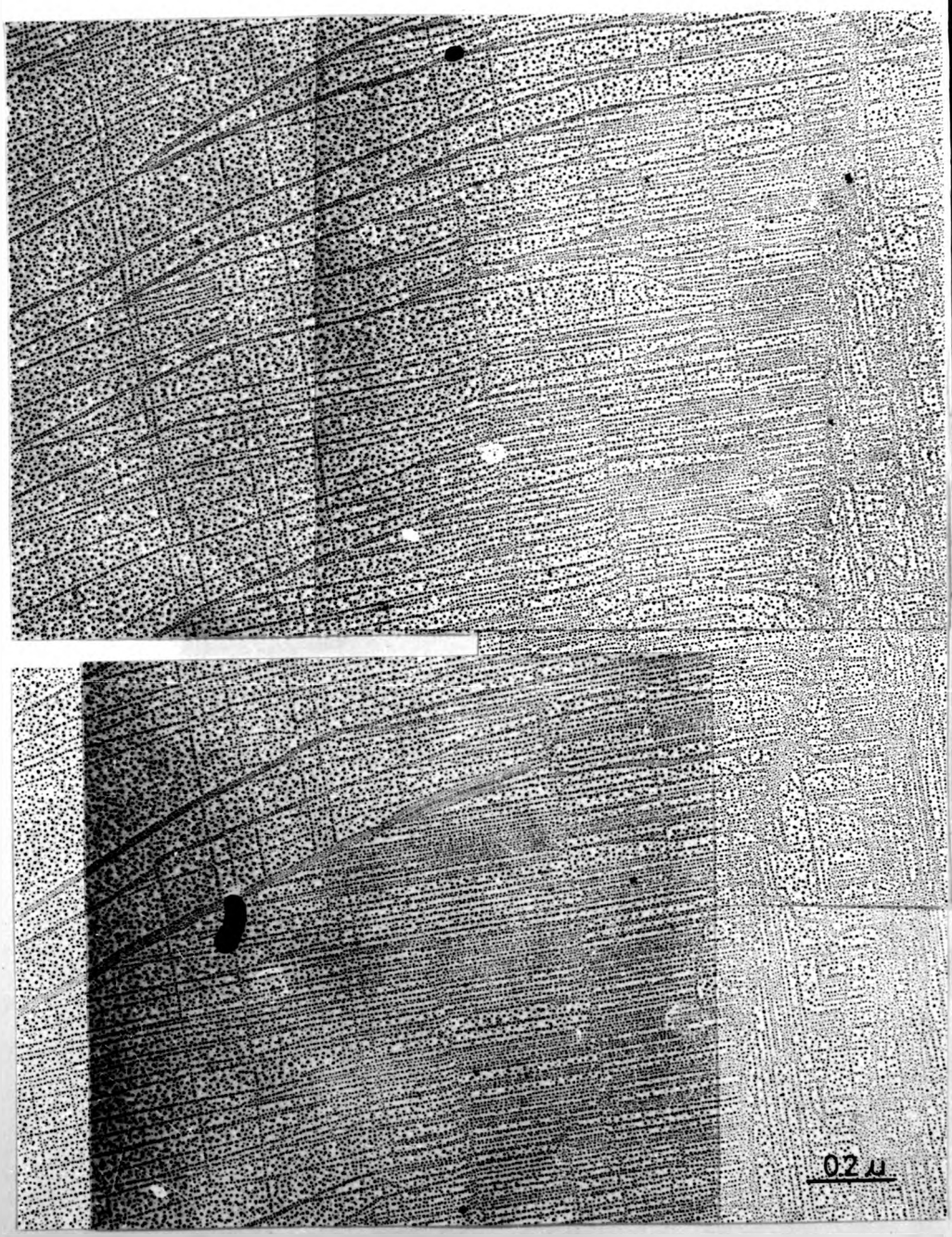

Fig. 4.23. Slightly curved stop band. Standard decorated replica of a NaCl crystal.

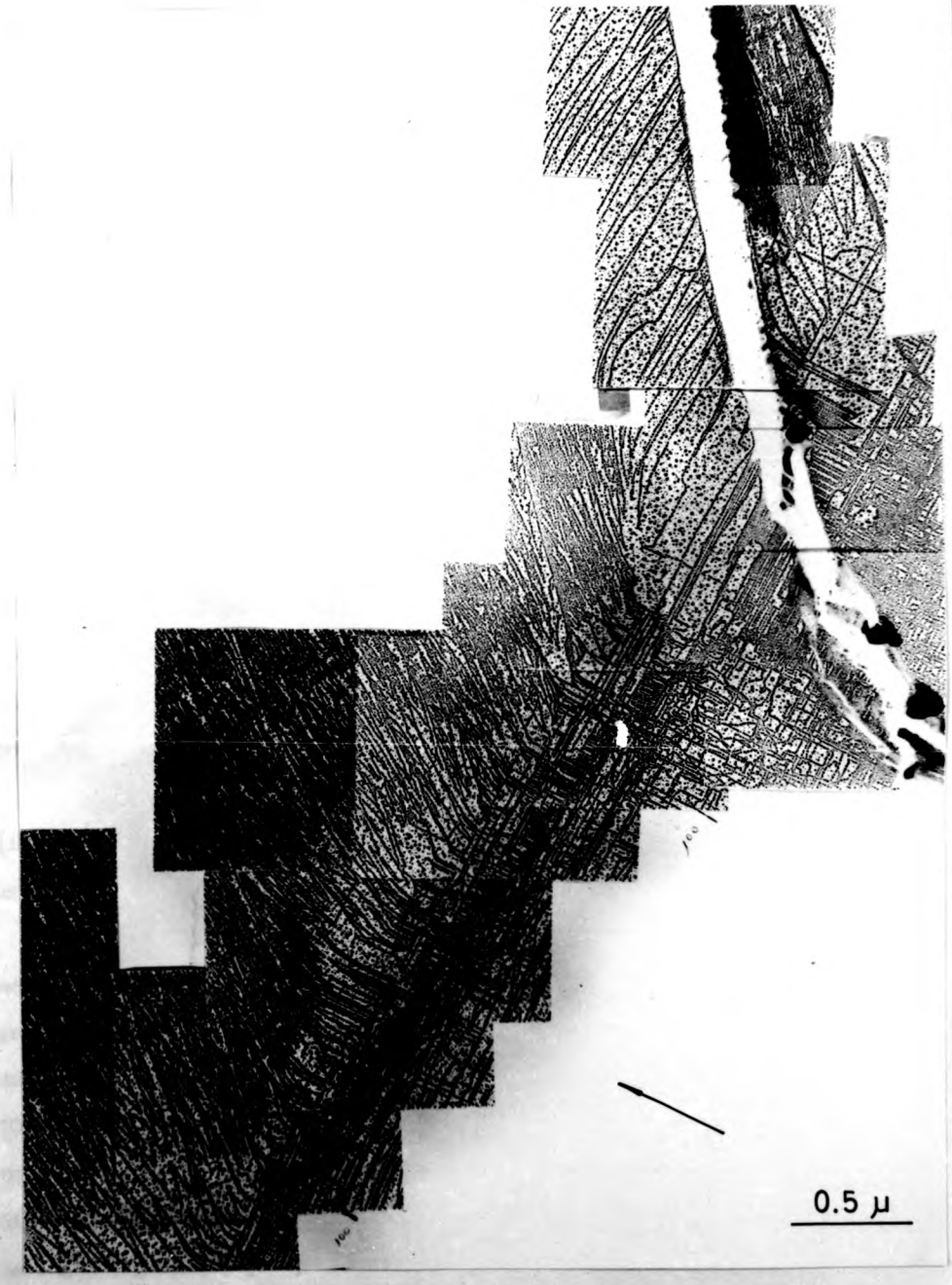

Fig. 4.24. Interaction of a high cleavage step with a stop band. Composite electron micrograph of a standard decorated replica of a NaCl crystal.

The composite electron micrograph (Fig. 4.25) shows a stopped crack front, laying roughly in a [110]direction. Numerous transverse lines parallel to [010] change direction where the crack came to rest after a brief healing process.

The peculiar effect exhibited by many small cleavage steps at dense slip bands, described in section 4.3.3.b is shown by step PQRT in this last figure: the step follows the general direction of crack propagation and develops a jog in the [010] direction at the stop band. When cleavage is restarted, the step follows the new direction of crack propagation.

Many atomic steps have a similar behaviour as can be seen in Fig. 4.25 for steps LMN and FGH, for example. These steps, running nearly parallel to [010] can be identified as cleavage steps because: a) of their intersection with slip steps running exactly parallel to [010] and b) of their curvature following the local direction of crack propagation when the crack is restarted.

Steps starting at the end of slip lines run parallel to [100] and afterwards change to the local crack propagation direction as can be clearly seen in lines SS and XX, Fig. 4.25.

Fig. 4.26 is a composite electron micrograph of another section of same stop band shown in Fig. 4.25. In this electron micrograph, probably due to a local distorsion, the crack front changes direction and is, for a short while, only slightly inclined to the [010] direction. The main features are in this case quite similar to those observed for stop bands parallel to [010] . It is very difficult to distinguish whether there are some unit cleavage steps having a jog in the [010] direction, similar to LMN, FGH, in Fig. 4.25.

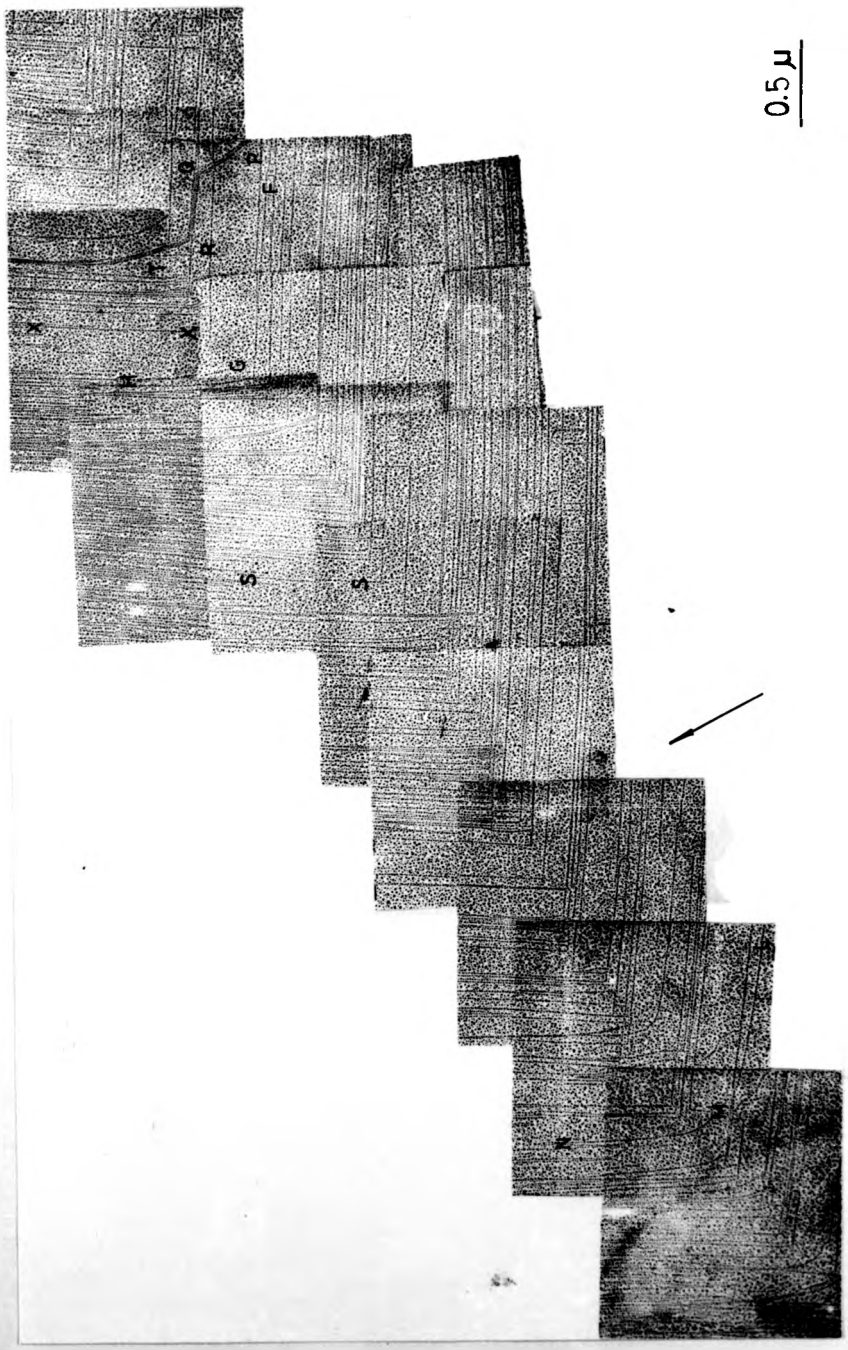

Fig. 4.25. Stop band of a cleavage propagating in a [110] direction. Composite electron micrograph of a standard decorated replica.

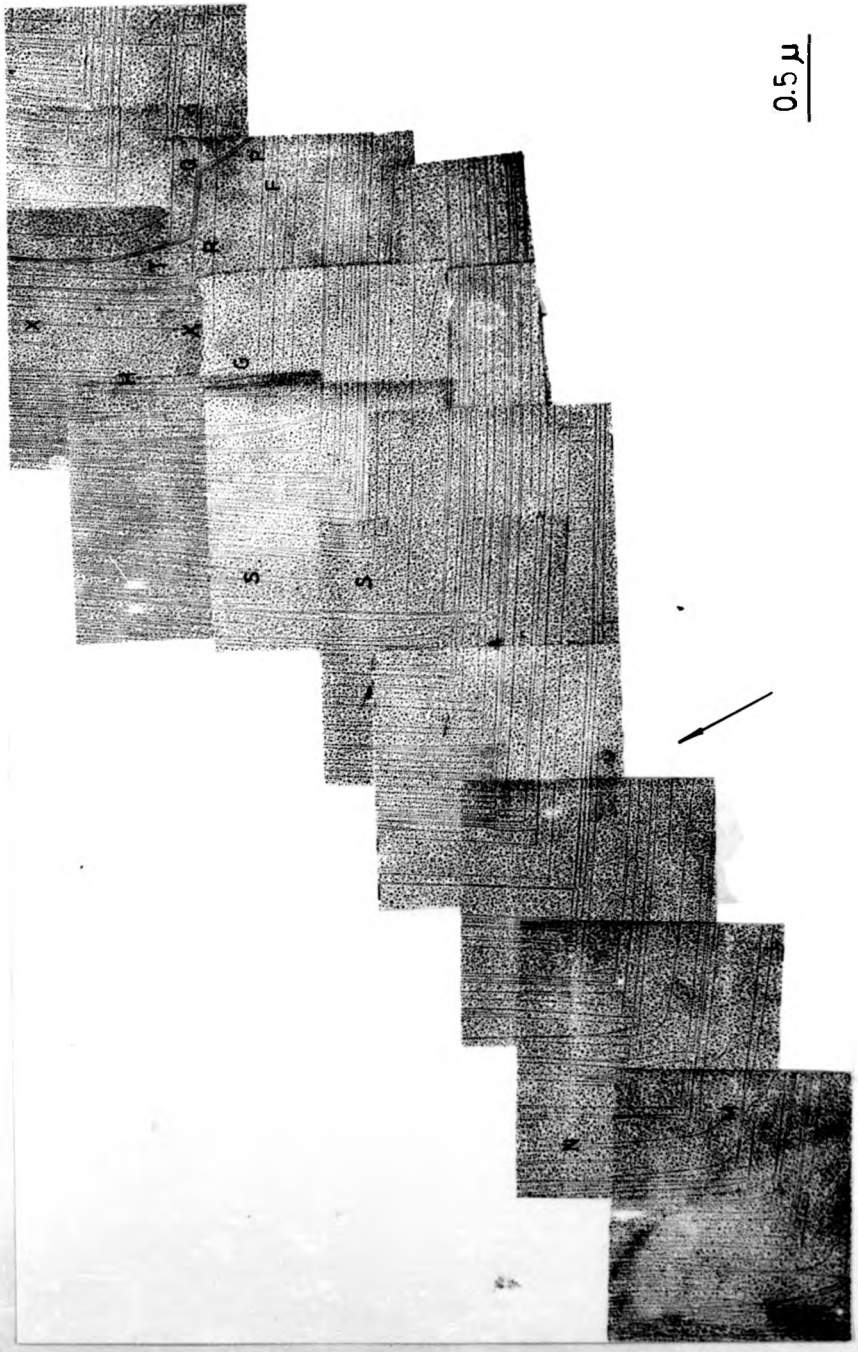

Fig. 4.25. Stop band of a cleavage propagating in a [110] direction. Composite electron micrograph of a standard decorated replica.

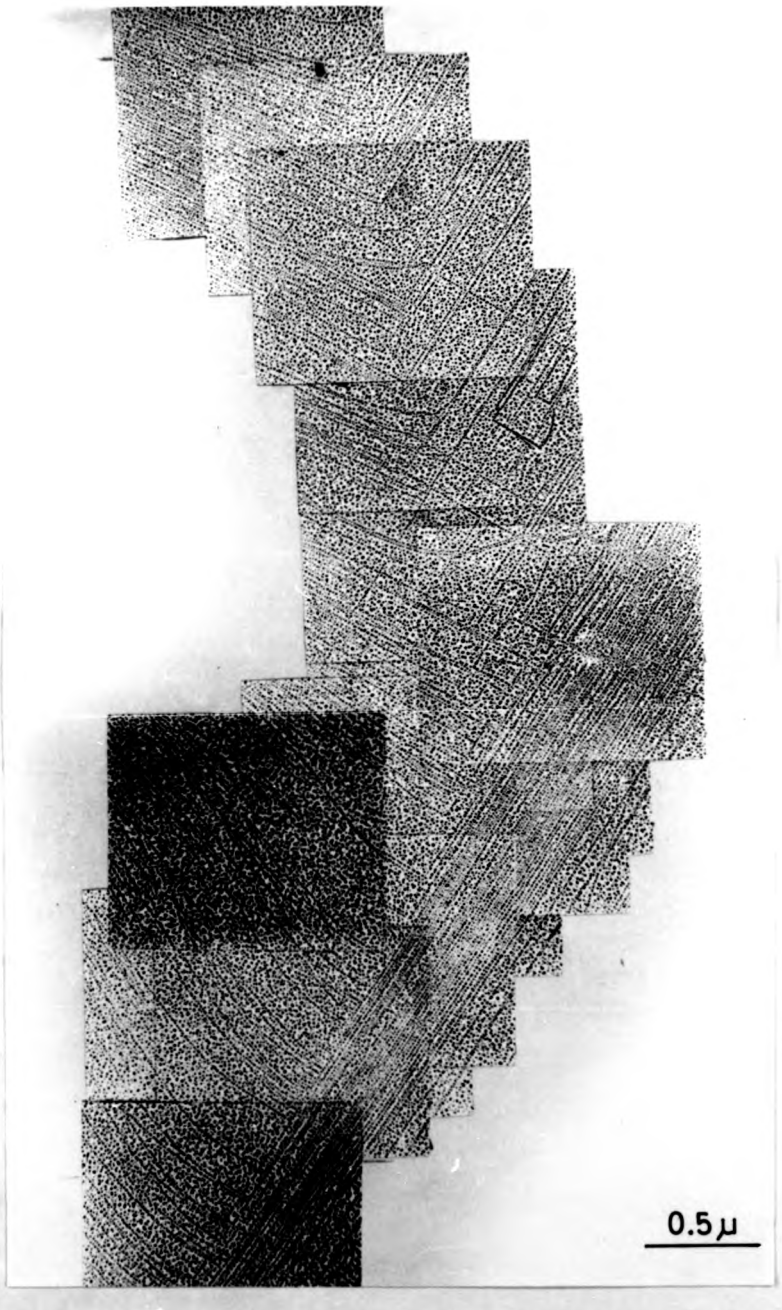

Fig. 4.26. Another section of the stop band of Fig. 4.25, with a segment almost parallel to [010] .

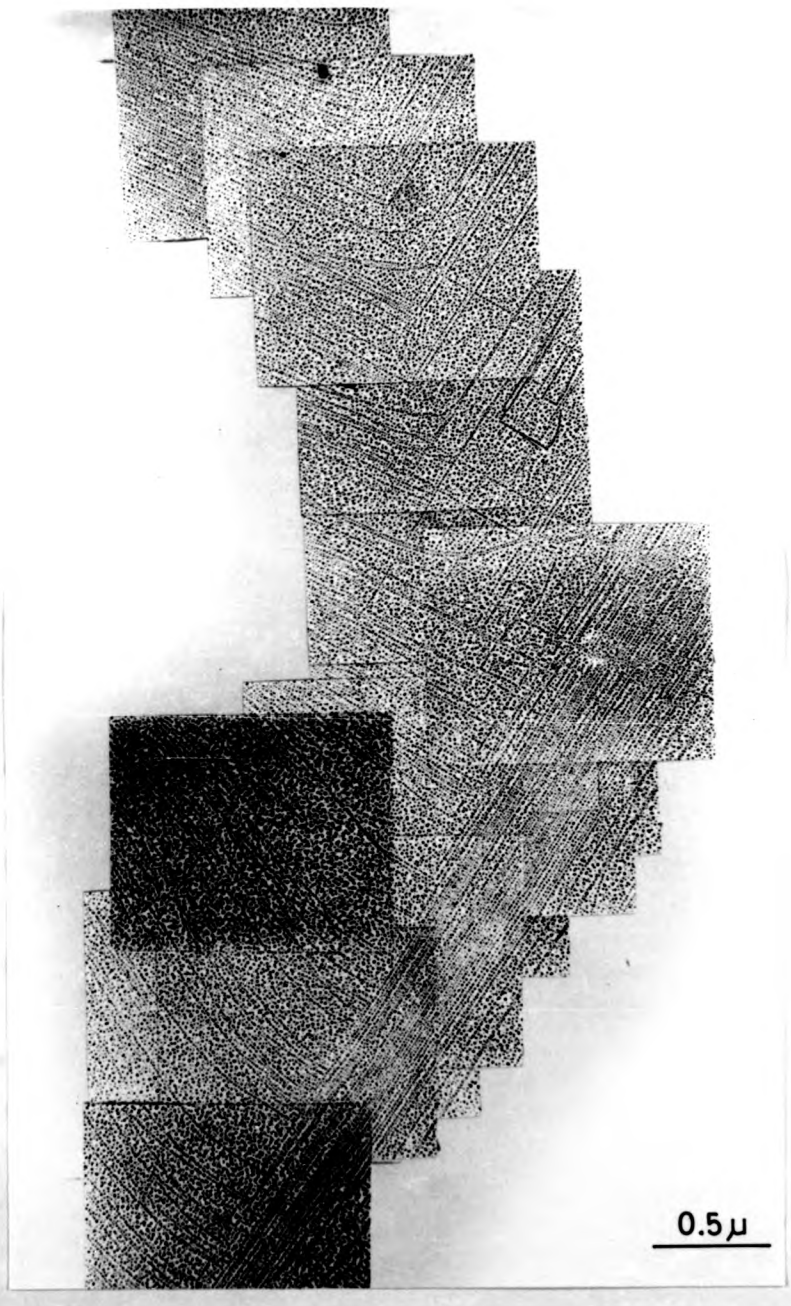

Fig. 4.26. Another section of the stop band of Fig. 4.25, with a segment almost parallel to [010] .

1.9cm 0.5μ

4.3.4.b) Observations of shadow-decorated replicas

Cleavage structures at a stop band were further investigated in shadow-decorated replicas, prepared with the shadowing direction perpendicular or parallel to the crystal length (section 3.2.2.).

Surface relief related to longitudinal steps is evident in Fig. 4.27, which is typical of replicas prepared with shadowing direction perpendicular to the crystal length. Even surface structures lying in the shadow of the relatively high steps (approximately 50 Å high) are effectively decorated by very small gold nuclei, as described in section 3.3. The collection of many of the short straight steps by a high cleavage step, as well as the ending of some of them at a transverse line (see section 4.3.3.a) are also illustrated in this figure.

It can also be inferred from the different sizes of the condensed nuclei that the sign of neighbouring short straight steps do not necessarily alternate (see for example lines ABC, DEC, FGH,LMH, in Fig. 4.27). Some of the short straight lines starting at the stop band are evidently pairs, as those indicated by the arrow in Fig. 4.27.

A zone of a stop band containing a larger than usual proportion of these pairs is shown in Fig. 4.28. It is to be noted that not all the pairs have the same orientation (the up step of each pair, marked by the larger size of the condensed nuclei, is not always on the same side of a pair, i.e. pairs A, B, C, have their up step to the left of the photograph while pairs M, N, have their up step to the right).

Another distinctive feature observed in this micrograph

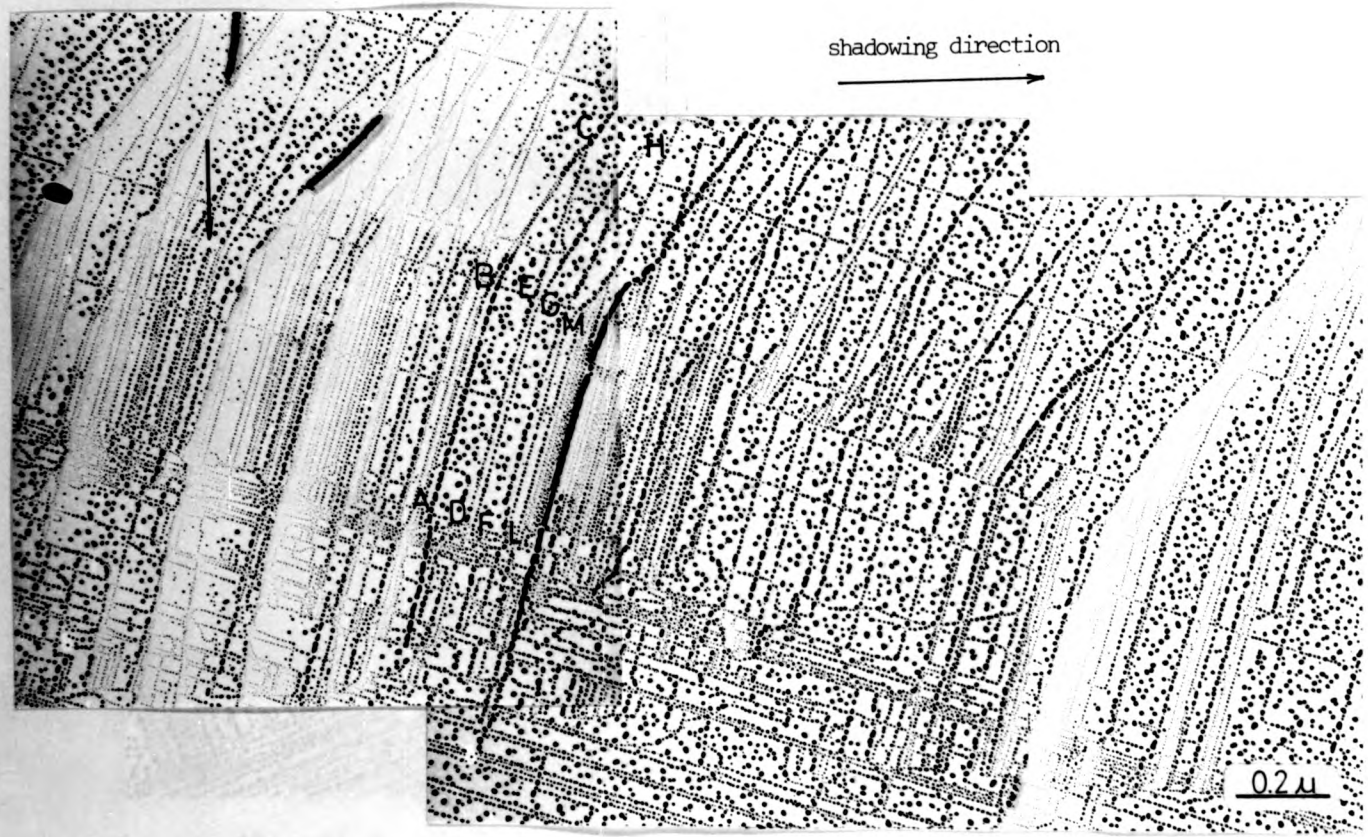

Fig. 4.27. Stop band zone. Electron micrographs of shadow-decorated replica. Shadowing direction perpendicular to the longitudinal steps.

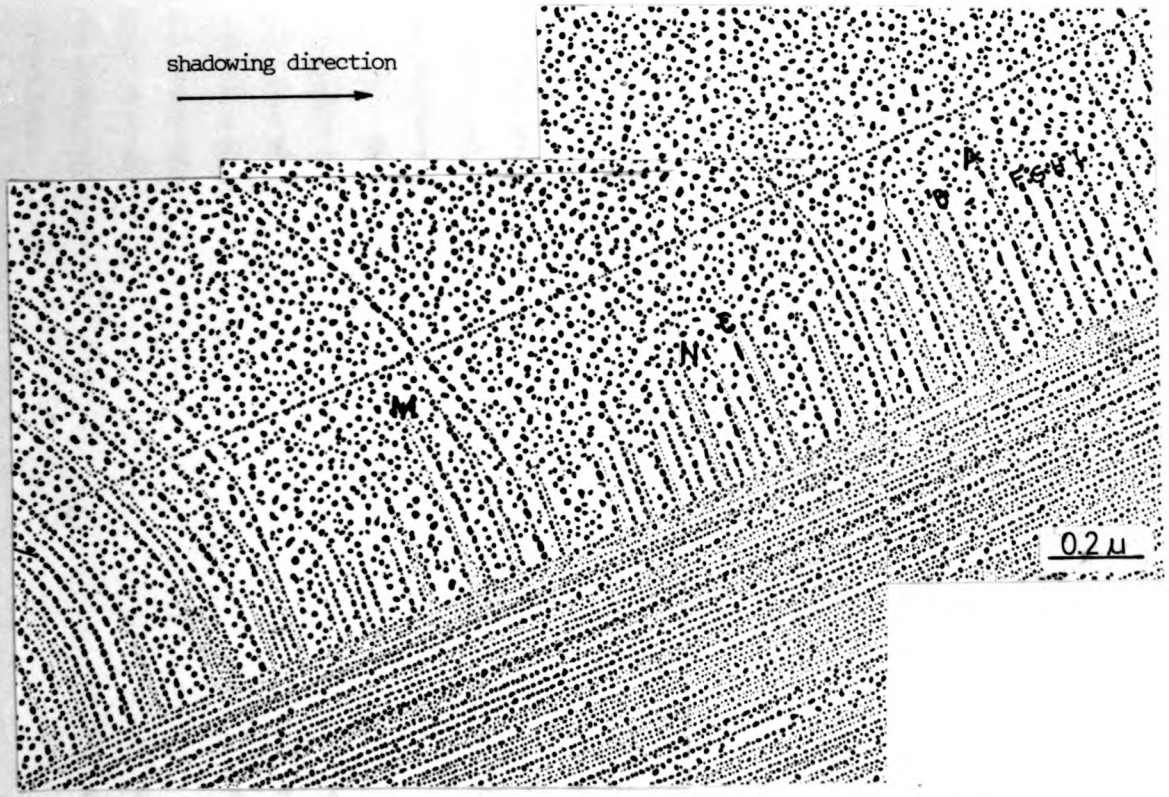

Fig. 4.28. Stop band zone. Electron micrographs of shadow-decorated replica.

Shadowing direction perpendicular to the longitudinal steps.

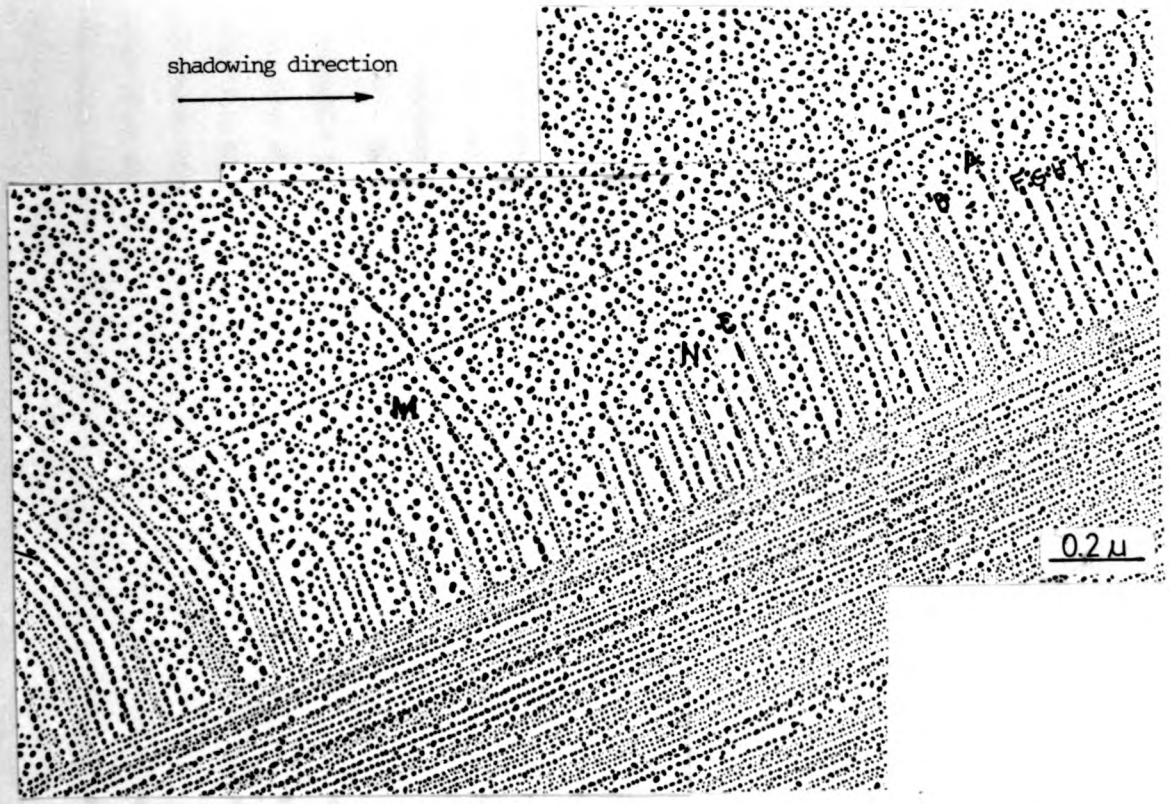

Fig. 4.28. Stop band zone. Electron micrographs of shadow-decorated replica.

Shadowing direction perpendicular to the longitudinal steps.

is the large number of isolated short straight lines. It is not possible to ascertain whether some of these are pairs of lines unresolved due to the large size of the nuclei as compared to the distance between neighbouring steps (lines F, G. H, I).

As already described in section 4.3.3.b), shadow-decoration technique makes more evident the jogged path of a cleavage step traversing a stop band (see Fig. 4.29, step SS). The unexpected observation of short segments of apparently isolated relatively high cleavage steps in the stop bands is illustrated in Fig. 4.29.

Replicas prepared with shadowing direction perpendicular to the transverse bands showed (as in Fig. 4.30) a sudden increase (or decrease) in the height of some transverse steps for short segments, not related to the presence of arriving cleavage steps, but connected to outgoing steps.

It can be inferred from both kinds of shadow-decoration experiments that the stop band is far from being only a collection of transverse monoatomic slip steps; it is a zone of marked and variable relief. In dense stop bands, even entire crystal blocks are displaced upwards or downwards.

Composite electron micrograph (Fig. 4.31) shows strikingly that a step is originated at the end of each transverse slip line when the crack cuts through the screw component at one side of a transverse dislocation loop. This micrograph suggests that all these unit steps starting from the extreme right of each transverse slip line are of the same sign. The slight curvature of the crack can be deduced from the staircase-like ending of transverse slip lines.

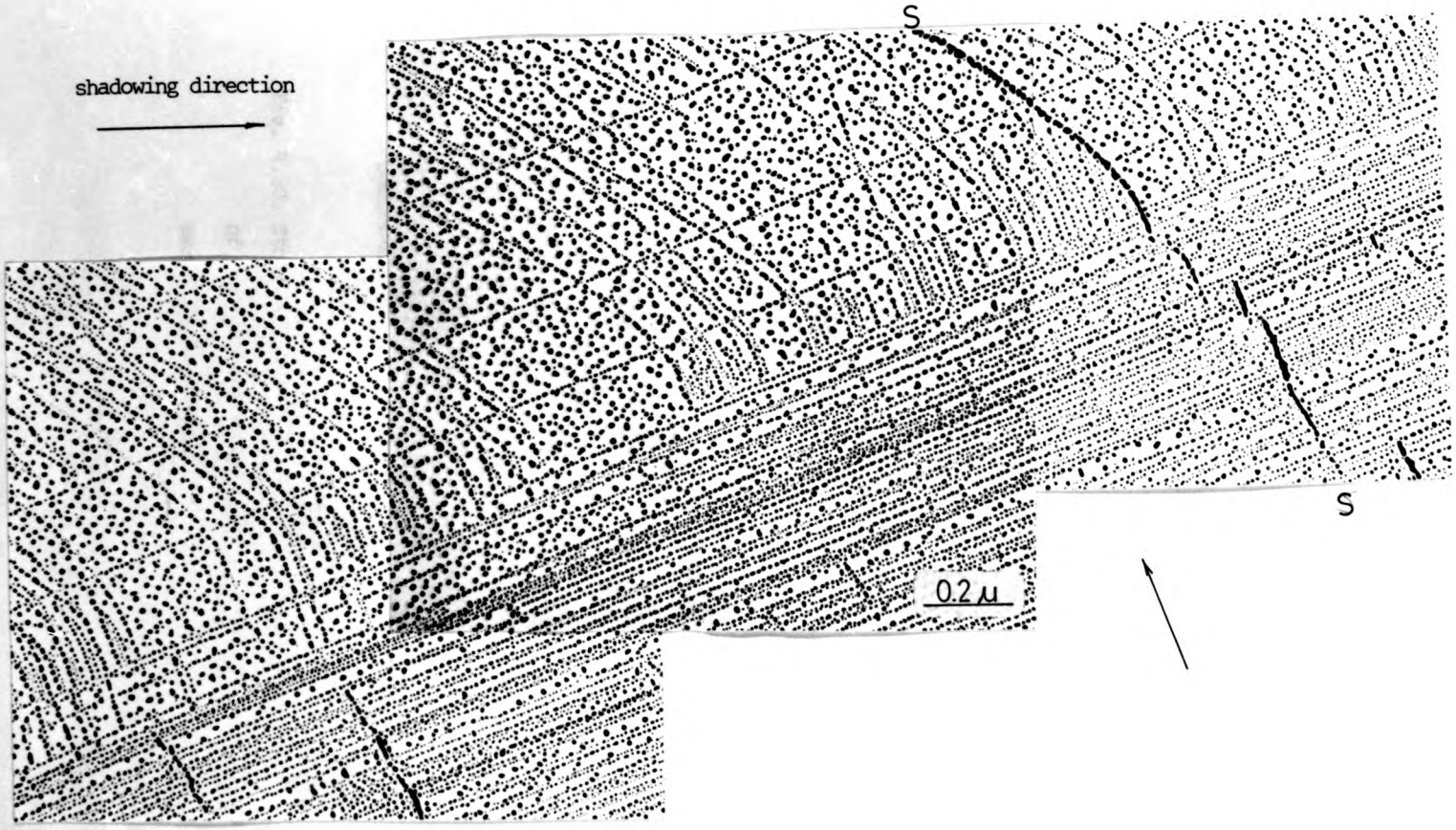

Fig. 4.29. Interaction of a small cleavage step with a stop band. Composite electron micrograph of a shadow-decorated replica. Shadowing direction perpendicular to longitudinal steps.

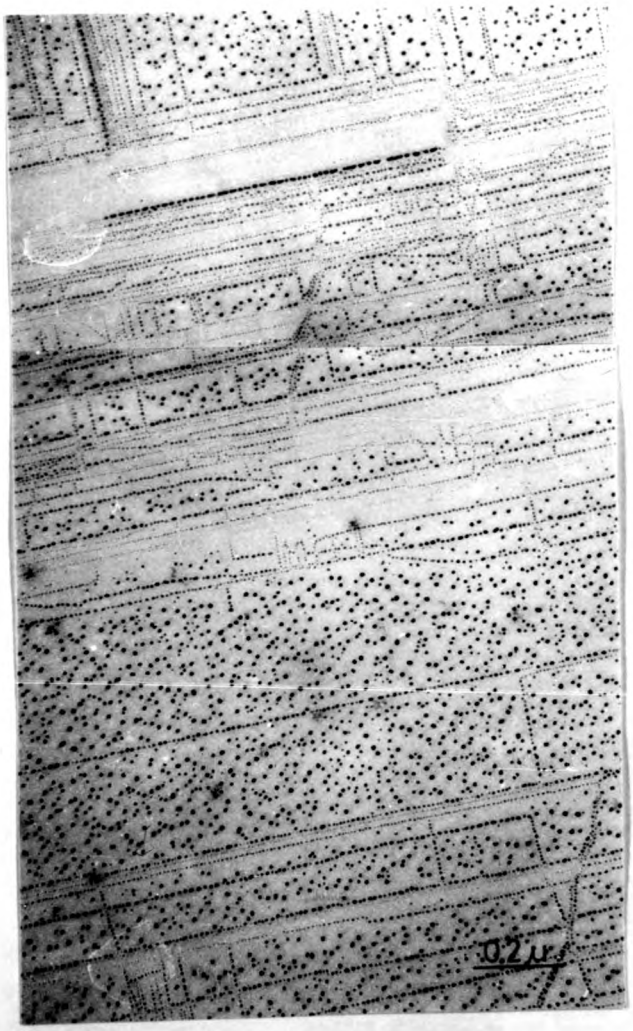

Fig. 4.30. Stop band zone. Composite electron micrograph of a shadow-decorated replica. Shadowing direction perpendicular to the transverse bands.

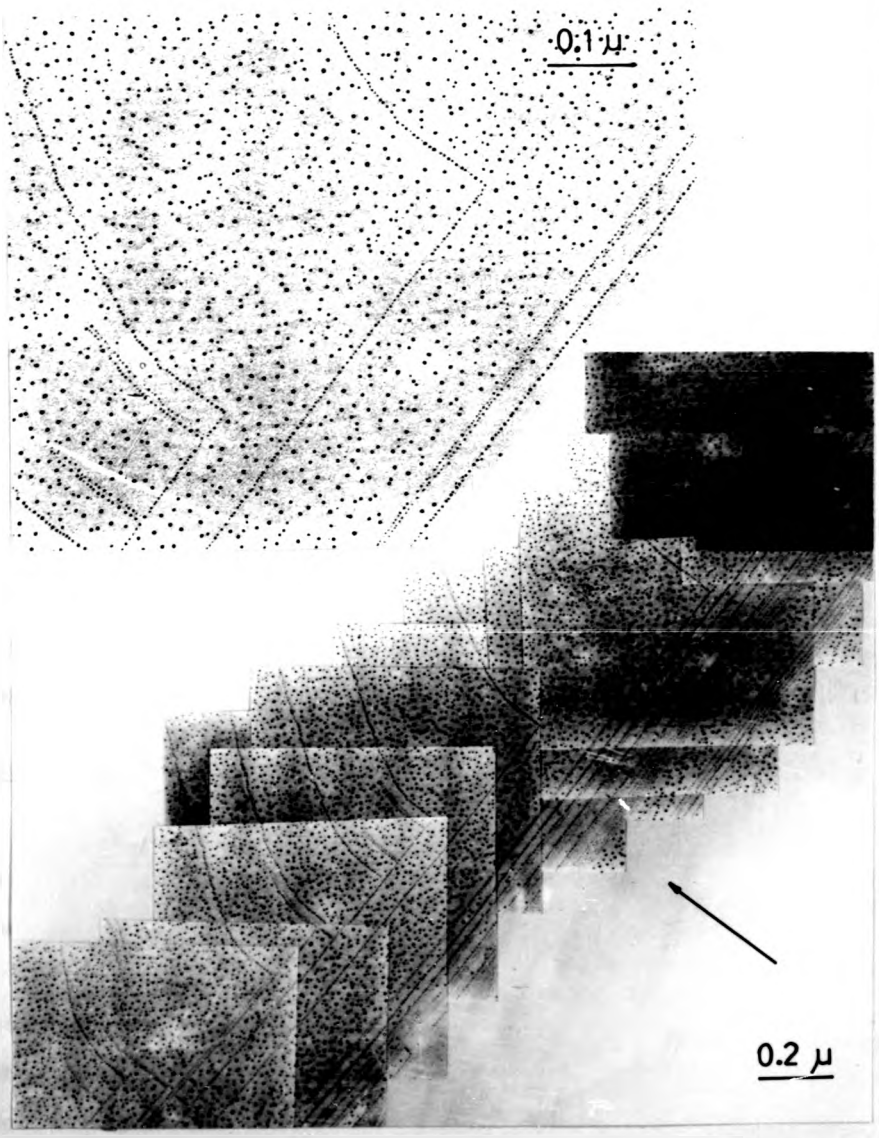

Fig. 4.31. Stop band zone. Composite electron micrograph of shadow-decorated replica of a NaCl crystal. Shadowing direction perpendicular to the long steps. Inset: high magnification of part of composite micrograph

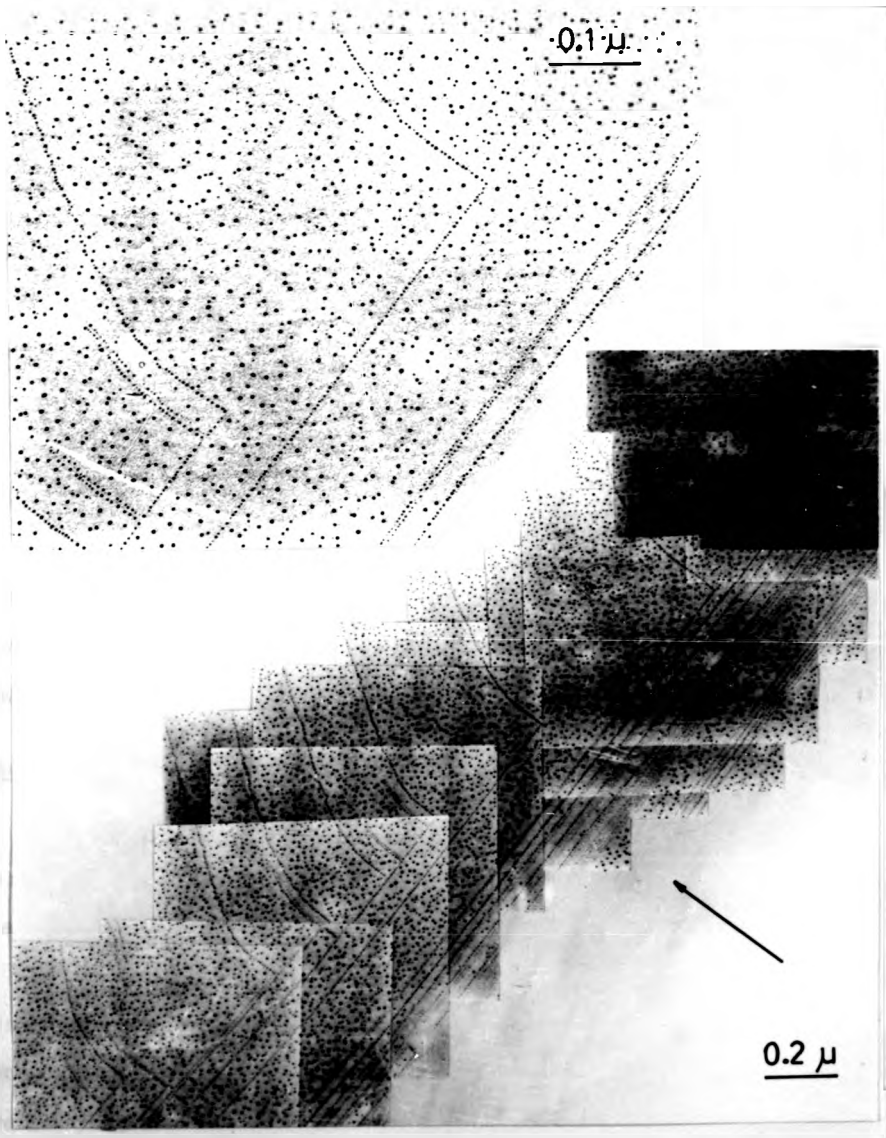

Fig. 4.31. Stop band zone. Composite electron micrograph of shadow-decorated replica of a NaCl crystal. Shadowing direction perpendicular to the long steps. Inset: high magnification of part of composite micrograph

4.3.5. Restarting zone with inclined steps

This zone is the first one immediately ahead of the short straight steps steming from a stop band.

Two types of structures can be observed simultaneously in this zone: a river pattern and something similar to a lightning pattern. The multitude of unit cleavage steps originating in the healed region form short, low angled V-shaped figures which combine to form short irregular lightning patterns. The steps in these patterns deviate to form many deltas in the river pattern. Fig. 4.32 is an enlarged photograph of a region of Fig. 4.24, illustrating these structures.

The unit steps, originating at the stop band, are inclined afterwards to follow the local crack propagation direction, added to these steps result in a very intricate pattern.

When the crack accelerates and runs again in a (001) cleavage plane, the structure clarifies: cleavage steps coalesce in a river pattern, only a few relatively high steps remain and the normal lightning structure developes (Fig. 4.33).

4.3.6. Study of a lateral cross-section of a stopped cleavage crack

Shadow-decorated replicas of a lateral (010) cross-section of sodium chloride crystals with a stopped (001) cleavage crack were prepared as described in section 2.2.2.

Same effect described in section 4.2.2 can be observed in Fig. 4.35: a secondary crack starts at a plane less than 10μ below the primary cleavage plane. The secondary crack begins approximately 50μ before the original crack end. The secondary crack is stopped some 200μ ahead of its origin.

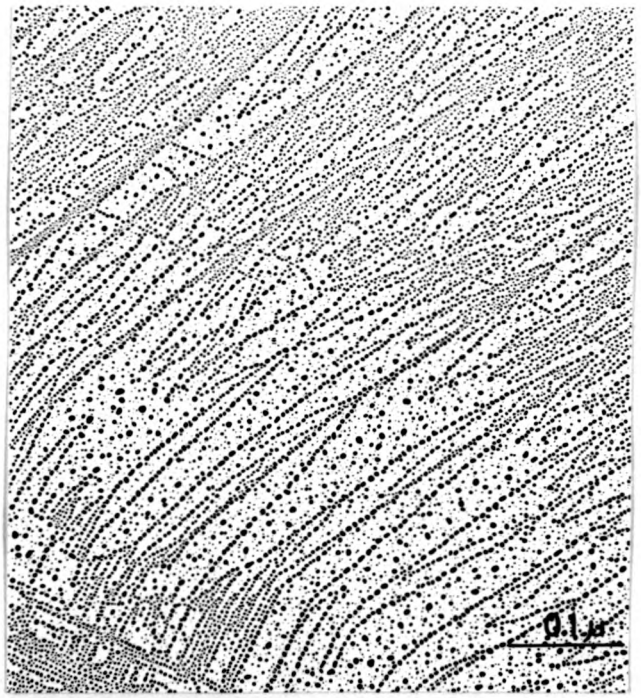

Fig. 4.32. Enlarged micrograph from a region of fig. 4.24.

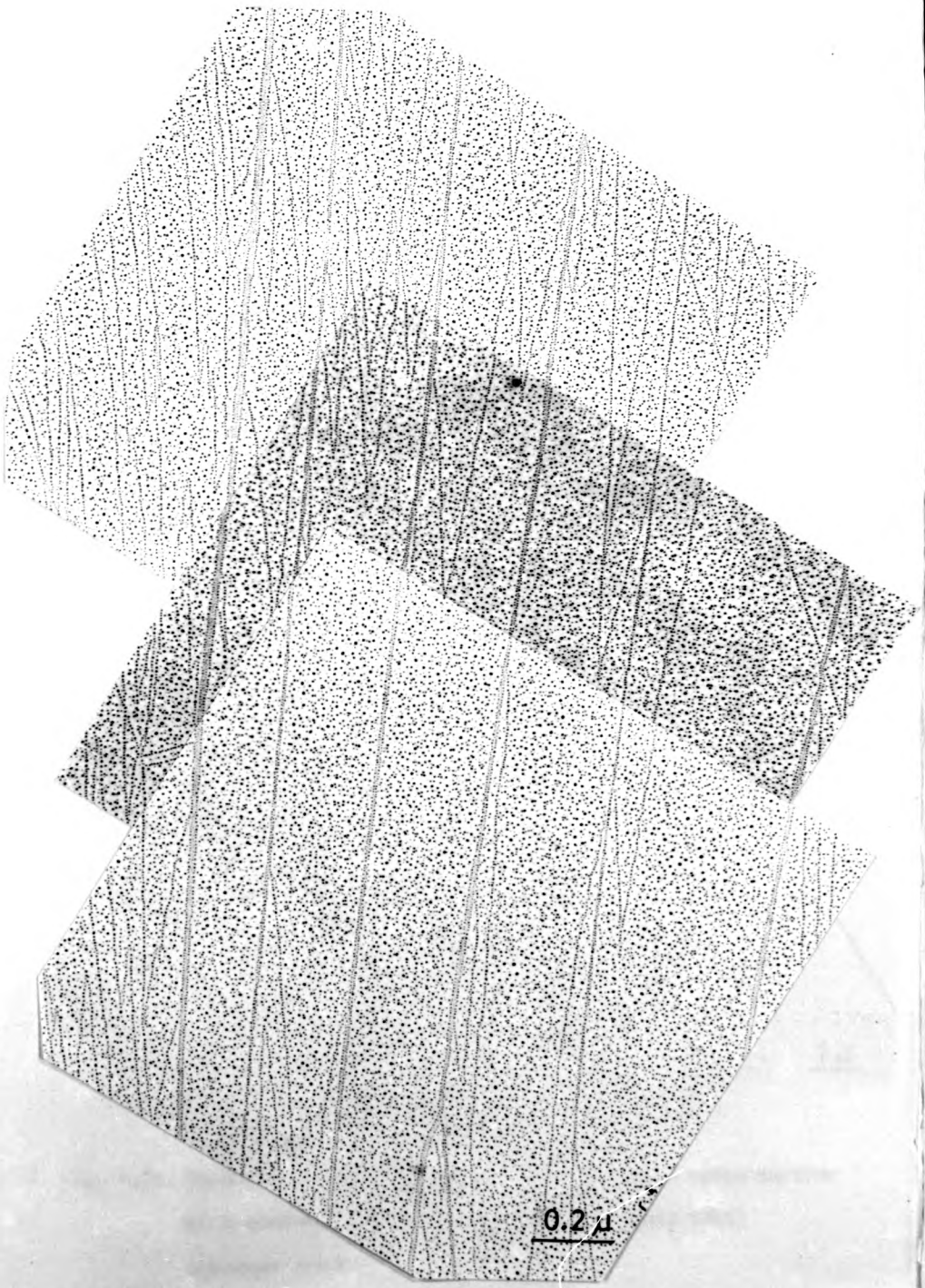

Fig. 4.33. Beginnning of lightning structure. Standard decorated replica of a NaCl crystal.

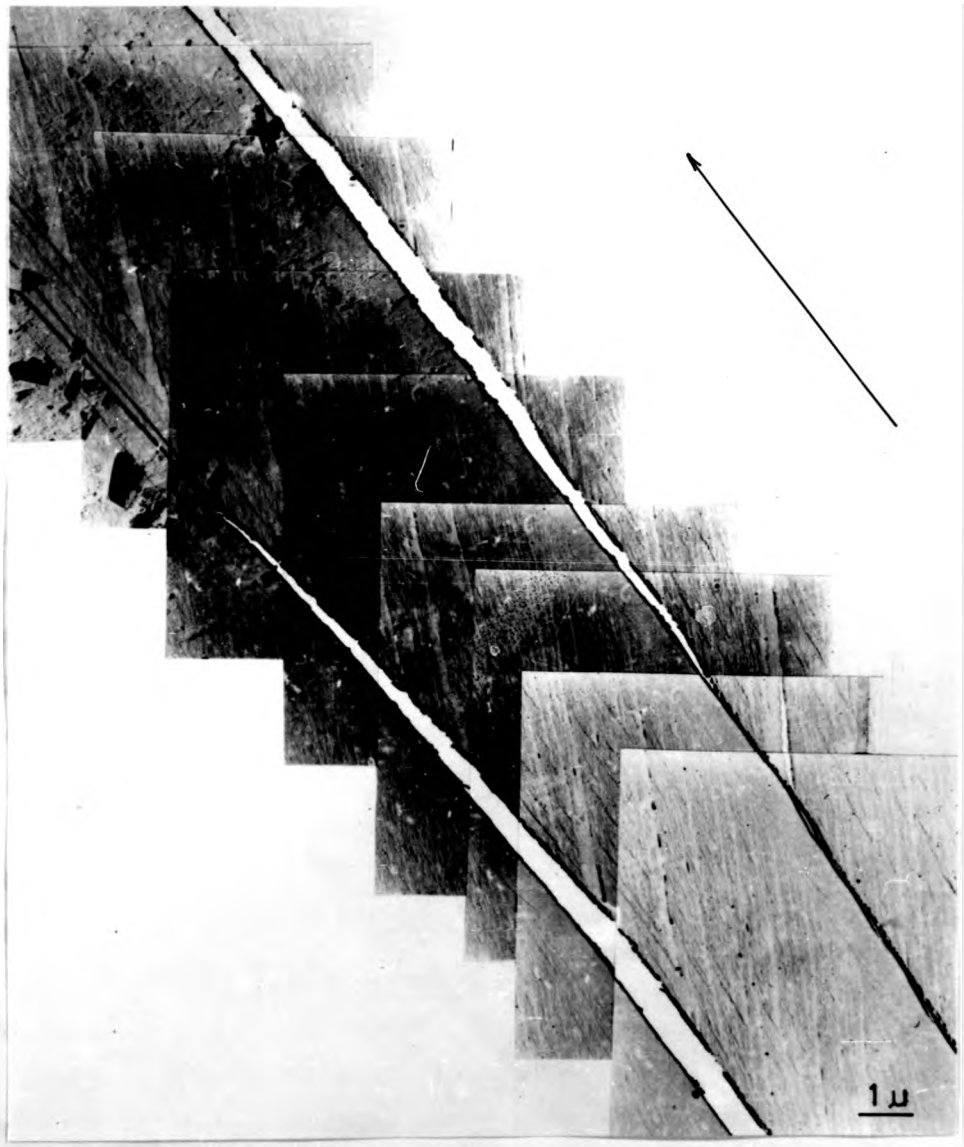

Fig. 4.35. Shadow-decorated replica of a lateral (010) cross-section of a sodium chloride crystal with a stopped (001) cleavage crack.

4.4. Etching

An electron microscopy study of shadowed replicas (see section 2.2.2) of chemically etched sodium chloride cleavage surfaces obtained as described in section 2.3 was performed.

Fig. 4.36 is a composite electron micrograph from a region of an etched cleavage surface including a stop band. There are a number of features about dislocation distribution which may be noted from this micrograph. For example, the crack front at stationary position is marked by the high density dislocation band. It deviates slightly from the [010] direction, indicated by the weak traces left by the slip bands. The weak trace of cleavage step SS provides some confirmation to the hypotesis that the stopped crack front coincides with the high density dislocation band: just before reaching this band the step propagation direction makes a small angle to the [100] direction and is perpendicular to it; the cleavage step changes direction abruptly after the dislocation band. This is the behaviour expected from a cleavage step at a stop band as already described in section 4.2.2.

Most of the etch pits at the stop band seem to be distributed at random; no preferential alignment along [100] or [010] directions could be observed.

Density of etch pits along a stop band is not homogeneous, but a typical value is approximately 10^9 disl/cm^2.

It is to be noted the low density of etch pits along the traces of slip bands. There is a low density of etch pits all along the tartan-pattern zone and no preferential alignment along any crystallographic direction was observed.

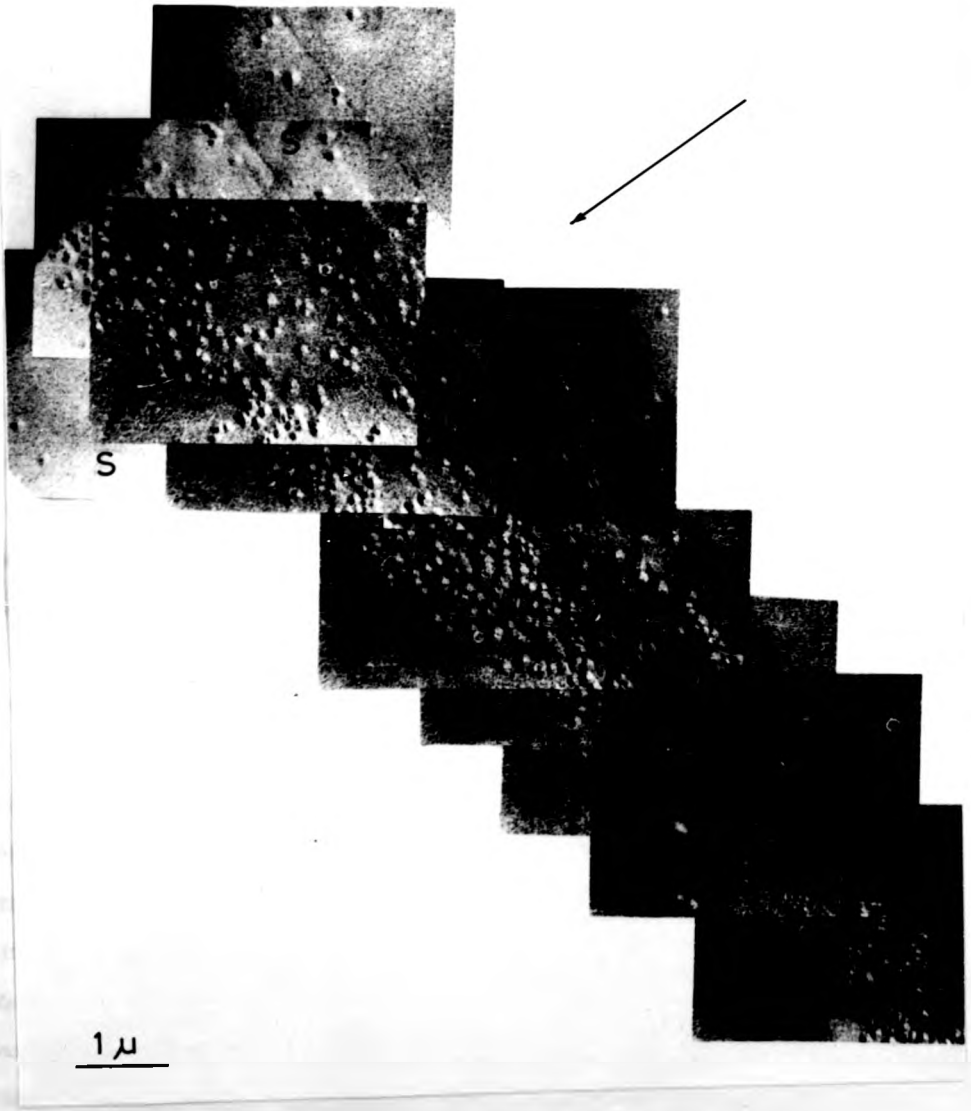

Fig. 4.36. Stop band zone. Etched cleavage surface of a NaCl crystal. Shadowed replica.

Only few rounded, shallow and large etch pits were observed at the restarting zone.

4.5. Electron microscopy study of cleavage surfaces of lithium fluoride single crystals

Standard decorated and shadow-decorated replicas of lithium fluoride crystals were prepared and studied in the electron microscope to compare the resulting cleavage structures left by unsteady crack propagation with those already studied for sodium chloride crystals.

Same dependence of the cleavage structures with crack propagation velocity was observed and the five zones described in section 4.3 were found in the region between two stopped crack fronts.

Fig.4.37 shows a typical tartan pattern. Although decoration is not as good as for the sodium chloride crystals, the pattern is quite similar for both materials. Even bundles of longitudinal steps steming from a transverse slip line and ending in a weak slip band were observed as illustrated in Fig. 4.38.

Stop band zones are shown in Fig . 4.39. All the characteristic features described for this zone for the sodium chloride crystals can be observed. In particular it is to be noted the jogged structure of relatively low cleavage steps at their intersection with dense transverse slip bands and with the stop bands. Some evaporations effects are visible in these photographs as a consequence of the heating of the specimen during the decoration process.

Although the investigation on lithium fluoride was less exhaustive as it was performed only for comparison purposes, from

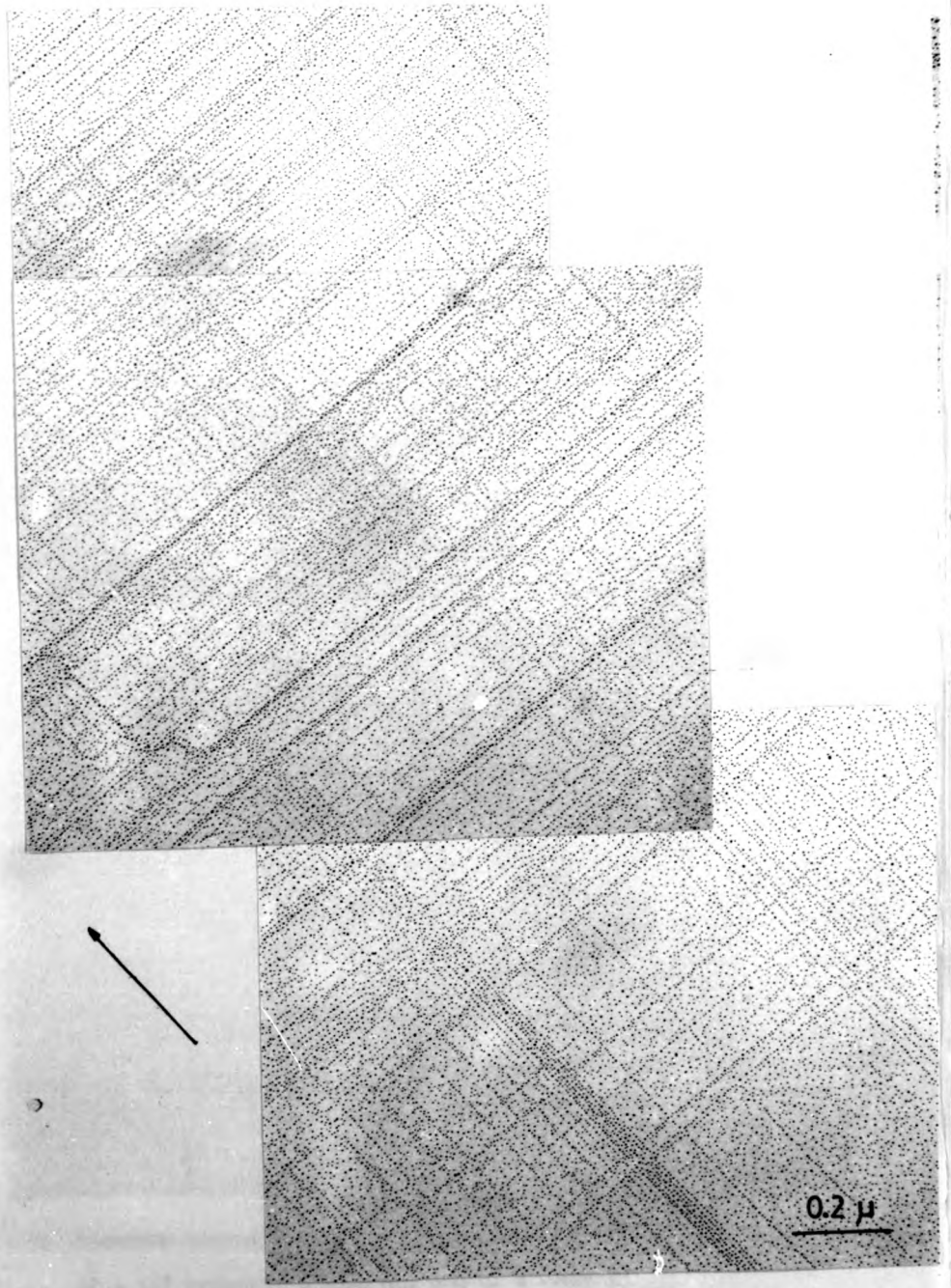

Fig. 4.37. Tartan pattern zone. Standard decorated replica of a LiF crystal.

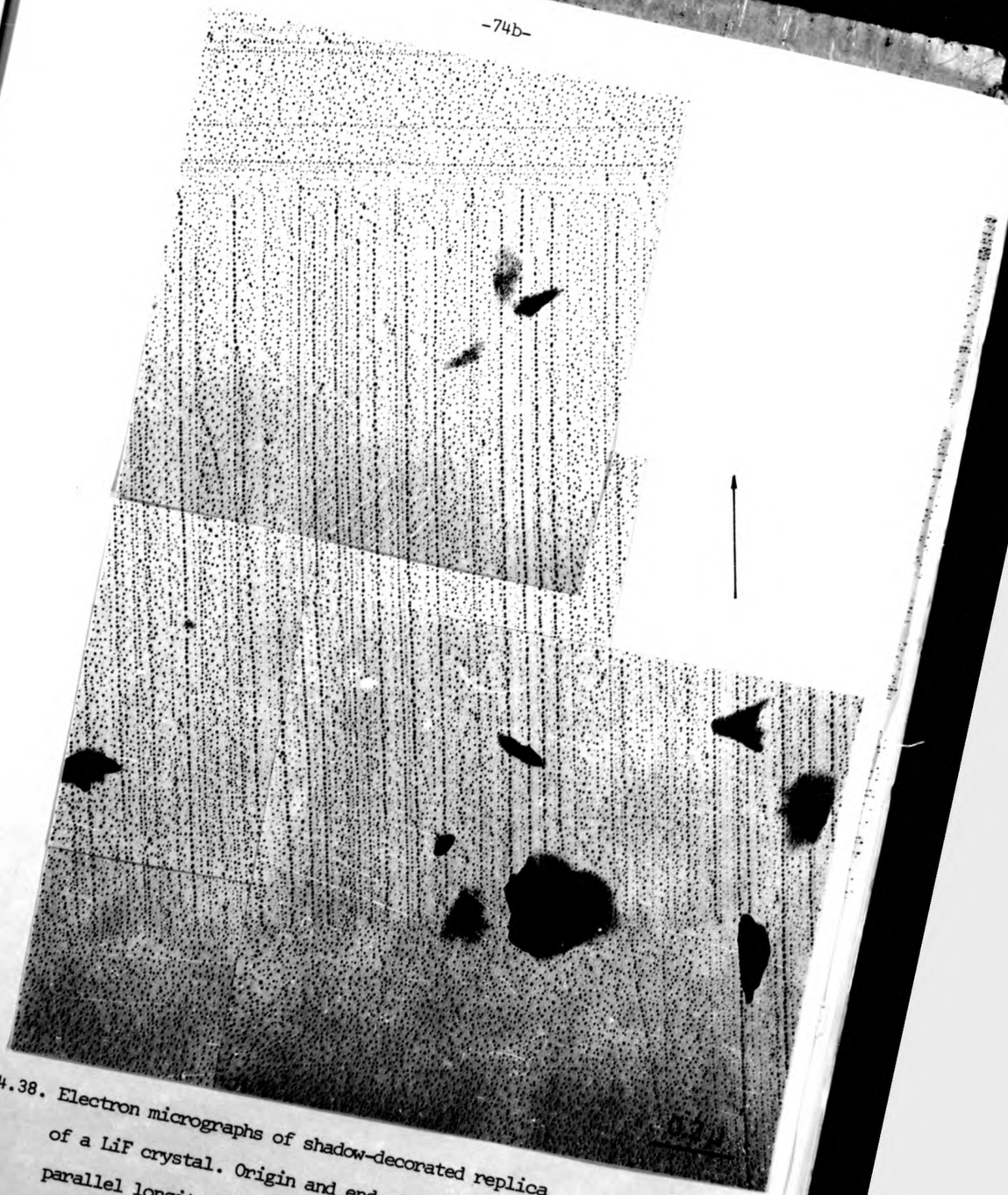

Fig. 4.38. Electron micrographs of shadow-decorated replica of a LiF crystal. Origin and end of a bunch of parallel longitudinal lines.

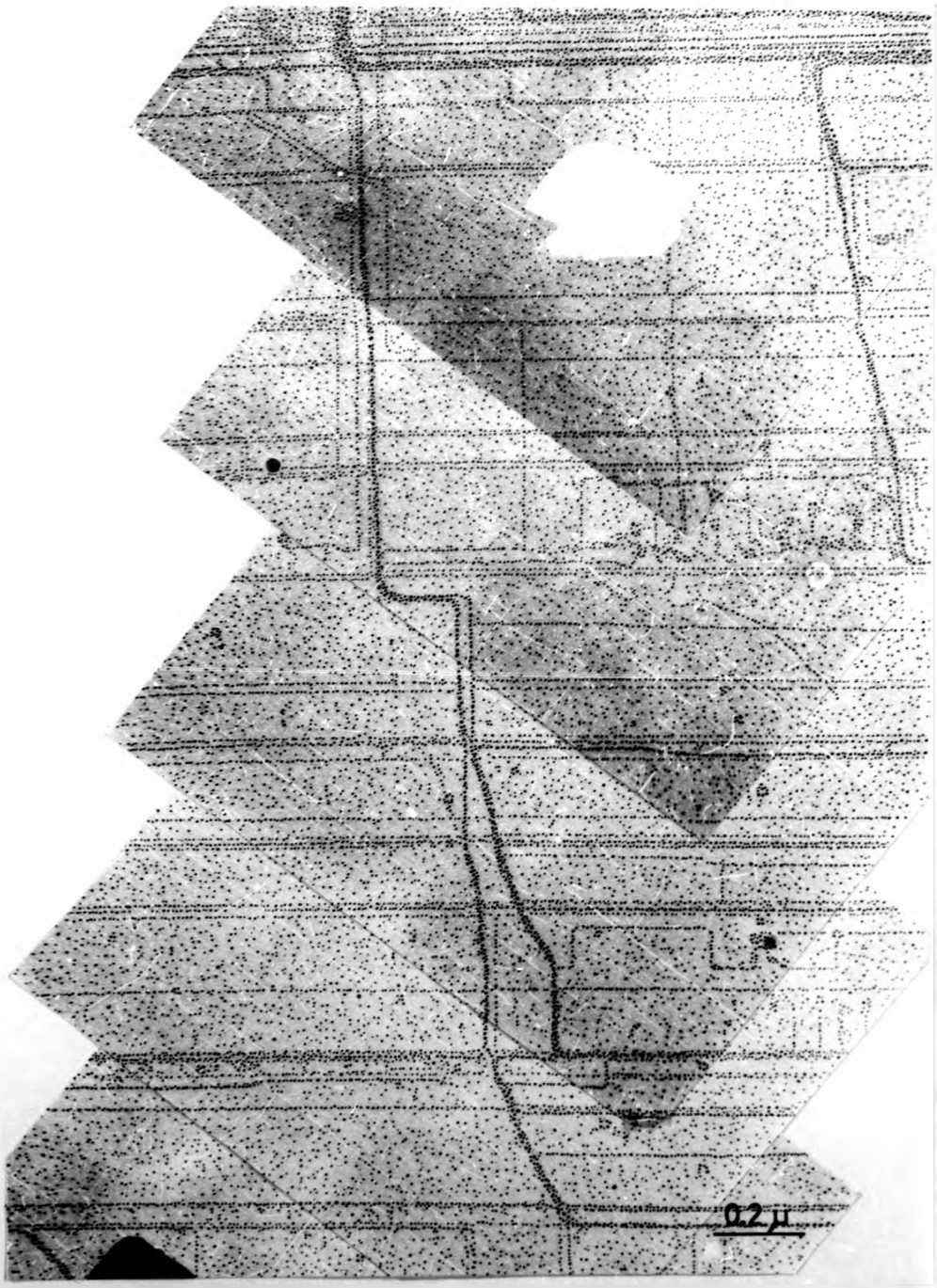

Fig. 4.39. Stop band zone. Standard decorated replica of a LiF crystal.

the seven crystals studied, it seems that the density of transverse slip bands is lower for lithium fluoride than for sodium chloride.

the seven crystals studied, it seems that the density of transverse slip bands is lower for lithium fluoride than for sodium chloride.

R.4. References

(1) Forty A.J., Proc. Roy. Soc. A, vol 242, 392 (1957).

(2) Forty A.J., Forwood C.T., Trans. Brit. Ceram. Soc, 62, 715 (1963).

(3) Forwood C.T., PhD Thesis, University of Bristol (1966).

(4) Burns S.J., Phil. Mag. 18, 625 (1968).

(5) BurnsS.J., Webb W.W., J. Appl. Phys. 41, 2086, (1970).

(6) Gilman J.J., Trans. Met Soc. AIME 449, April (1957).

(7) Gilman J.J., Trans. Met Soc. AIME 310, (1958).

(8) Lange F.F., Phil.Mag. 16, 761 (1967).

(9) Lange F.F., Lambe K.A.D., Phil. Mag. 18, 129 (1968).

(10) SwainM.V., Lawn.B.R., Burns S.J., J. Mat. Sci. 9, 175 (1974).

(11) Bassett G.A., Phil. Mag. 3, 1042 (1958).

(12) Bethge H.,Phys. Stat. Sol. 2, 3 and 775 (1962).

(13) Bethge H.,Physical Basis of Yield and Fracture , Conference Proceedings, pag. 17, Oxford (1966).

(14) Forwood C.T., Forty A.J., Phil. Mag. 11, 1067 (1965).

(15) Stirland D.J.,Phil. Mag. , 1181 (1966).

(16) Robins J.L., Rhodin T.N., Gerlarch R.L., J.Appl. Phys. 37, 3893 (1966).

(17) Appel F., Messerschmidt U.,Phys. Stat. Sol. 35, 1003 (1969).

(18) Levi L., Phil. Mag. 28, 427 (1973).

Chapter 5

X-RAY TOPOGRAPHY

5.1. Introduction

While attempting to understand the relationship between the surface structures described in chapter 4 and the dislocations nucleated by the crack, some doubts arose on the slip systems that comprise plastic deformation. X-ray topography is a good complementary technique to electron microscopy observations. It is not as effective in revealing small details as electron microscopy is, but it is capable of giving a good survey of dislocations arrangement in a large volume of the crystal, provided dislocation density is not very high.

Dislocation distribution is made visible through several contrast mechanisms. Wilkens (1) reviewed the mechanisms of contrast formation acting as sources of image contrast in the Berg-Barrett technique. Two of these mechanisms arise from local rotations of the crystal lattice: a) when the rotation axis is parallel to the intersection of the plane of incidence of the X-rays with the reflecting planes "displacement contrast" appears; b) "orientation contrast" appears as a consequence of lattice rotations around an axis normal to the plane of incidence. Reduction of the periodicity d_{hkl} of the diffracting planes reduces the primary extinction of the X-rays and gives rise to another image contrast mechanism, generally called "extinction contrast" (2). This extinction contrast is a maximum when the reduction of periodicity is in a direction normal to the diffracting planes, i.e. when $\vec{g}.\vec{b}=1$ (g= diffracting planes, b= Burgers vector of the dislocations).

Plastic deformation in lithium fluoride single crystal has been intensively studied by X-ray topography (2, 3, 4, 5, 6) but some specific experimental problems arise when working with sodium chloride crystals, due to its hygroscopic character and its relatively high plasticity, as has been stated in section Besides, even single crystals grown under very careful conditions exhibit many subgrain boundaries, which make it very difficult to observe the traces of activated slip planes simultaneously in every region of the crystal.

Recently Strunk (6) has studied, by X-ray topography, sodium chloride crystals plastically deformed under compression but to our knowledge the results to be described in this chapter, are the first X-ray topography study of the deformation introduced by unsteady cleavage in sodium chloride single crystals.

Direct comparison of X-ray topography and electron microscopy studies is possible by using both halves of the same crystal as already mentioned in section 2.2.

An X-ray topography study of lithium fluoride was carried out under the same experimental conditions in which the sodium chloride topographs were obtained, in order to elucidate whether plastic deformation accompanying crack propagation is similar in sodium chloride and lithium fluoride, and whether the experimental conditions used in this research are comparable to those used by other workers in lithium fluoride

5.2.0. Experimental

A Lang A3 * camera installed on a Rigaku Denki Microfucus

---

* Rigaku Denki Co. Ltd. Tokyo - Japan.

X-ray generator * was used to obtain both back reflection and transmission topographs (fig. 5.1). It is possible to use either a line or a point focus. A line focus was used throughout this work to minimize exposure times. The apparent size of the focus is approximately 0.1 x 0.5 mm.

The X-ray beam is directed onto a crystal previously oriented so that the Bragg reflecting conditions can be obtained for a predetermined set of crystallographic (hkl) planes. The divergence of the incident beam is adjusted by a system of collimating slits so as to obtain only the Bragg reflection from the $K\alpha_1$ characteristic radiation.

A sketch of Lang's camera and X-ray source for back reflection geometry is shown in fig. 5.2. The camera collimating tube has two slits. Slit S_1, near the window of the X-ray tube, is fixed and throughout this work a width of 100μ was chosen; slit S_2 was used with several widths ranging from 50μ to 100μ. The diffracted beam is recorded on a photographic plate. The Lang camera is designed so that the crystal-photographic plate system has translation movement; in this way the X-ray beam may sweep the whole crystal. The plate is placed perpendicular to the diffracted beam to avoid a broadening of the image.

The Lang camera is intended for transmission topography, so it has some geometric limitations when used in reflection geometry. The crystal-photographic plate distance was minimized in order to

---

* Rigaku Denki Co. Ltd. Tokyo - Japan

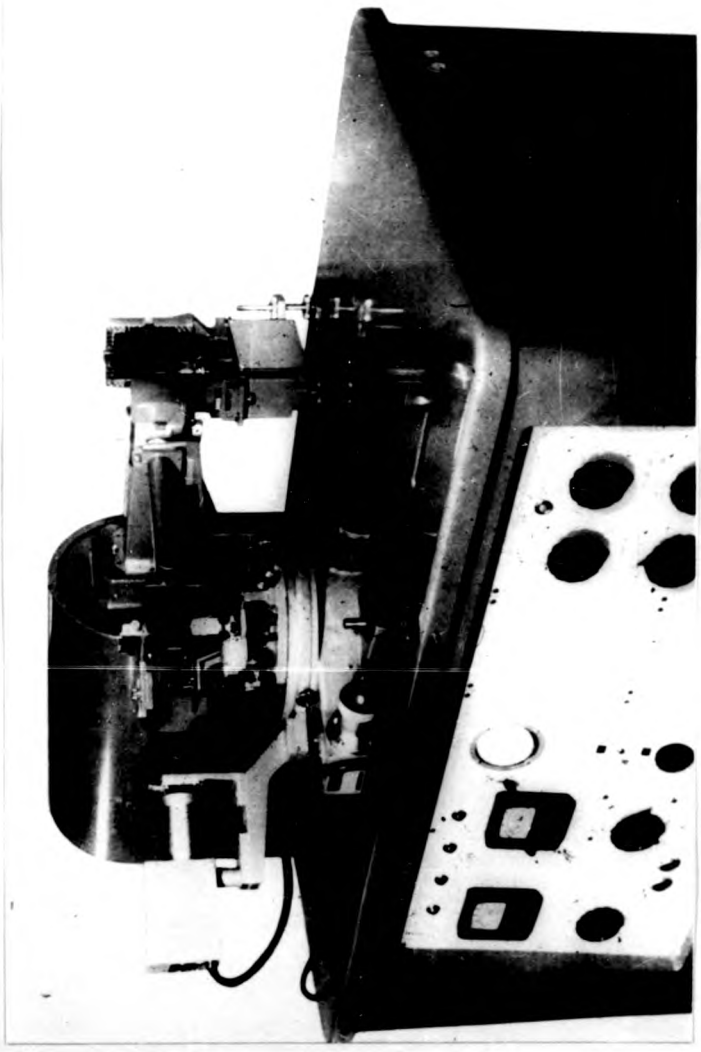

Fig. 5.1. Photograph of Lang's camera and the Rigaku Denki X-ray generator.

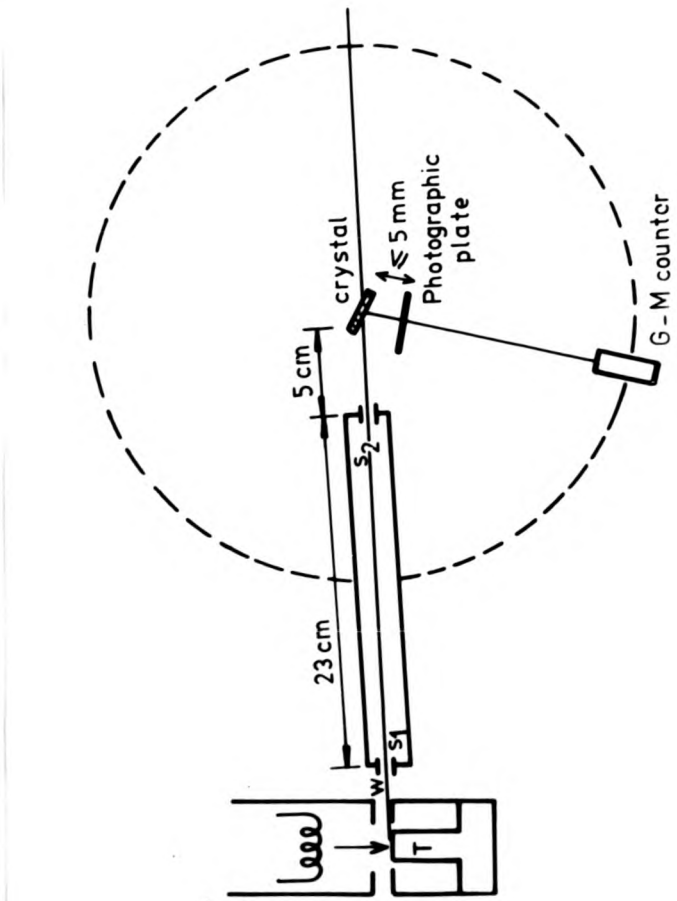

Fig. 5.2. Schematic diagram of Lang's camera and X-ray source for back reflection topography.

improve the resolution of the reflection topographs. A smaller specimen holder was constructed to bring the film closer to the crystal. High resolution Ilford L4 50μ plates were used.

The sodium chloride crystals were kept under a dry nitrogen flux while the X-ray topographs were taken to avoid surface attack by humid air.

5.2.1. Back-reflection topography

Information on the surface distribution of dislocations is obtained from reflection topography. Fig. 5.3 shows the geometry of the back reflection topographs.

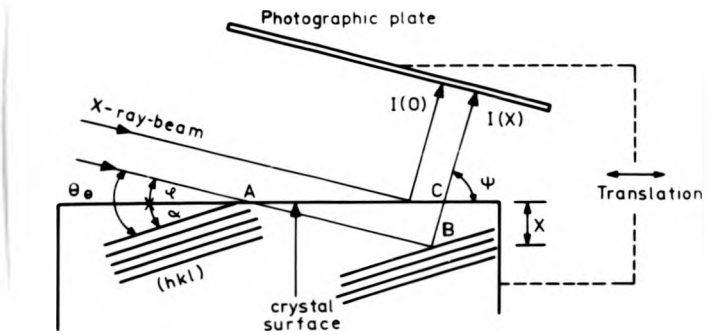

Fig. 5.3. Geometry of the back-reflection X-ray topography.

The following geometry considerations were borne in mind in order to obtain maximum contrast and resolution in the imaging of crystals:

1) The angle of incidence of X-rays, ϕ, must be small; $\theta > \alpha$ to obtain a reflected beam.

2) The exit angle of X-rays ψ, should be approximately 90°. The photographic plate, perpendicular to the diffracted rays is then approximately parallel to the surface of the crystal. In this way, the compression of the scaling factor on the film, parallel to the plane of incidence is decreased, the crystal-photographic plate distance can be very small with this geometry.

3) Small penetration depth of the X-rays, t_p, is required (t_p is a function of the absorption coefficient of the sample and of the geometry of the reflection).

Best experimental conditions for the sodium chloride crystals were obtained with Cu $K\alpha_1$ radiation for the (044) reflections. For these reflections

$$d\ (044) = 0.997\ \text{Å}$$

$$\theta_B = 50°30'$$

$$\alpha = 45°$$

$$\phi = \theta_B - \alpha = 5°30'$$

$$\psi = \theta_B + \alpha = 95°30'$$

$$t_p = 12\mu$$

Best experimental conditions for the lithium fluoride crystals were obtained with Cr $K\alpha_1$ radiation for the (022) reflections.

5.2.2. Transmission X-ray topography

Information on the volume distribution of defects is gained with transmission X-ray topography. Good kinematic contrast is obtained for $\mu t = 1$ (t=thickness of the crystals, μ = absorption coefficient). Mo $K\alpha_1$ radiation and (200) reflections were selected for transmission X-ray topographs of lithium fluoride crystals; a

symmetric reflection was chosen to minimize the horizontal distortion of the image.

If the defect density throughout the crystal is very high, this technique fails to give much information. X-ray tomography (or depth limited X-ray topography) circumvents this difficulty.

Fig. 5.4 is a sketch of the geometry involved in X-ray tomography. Slit S_3 can be modified to intercept the rays diffracted by one of the crystal surfaces. By selecting a small S_3 slit, only a narrow slice of the crystal is imaged, improving the resolution. For lithium fluoride crystals good tomographs were obtained with Mo $K\alpha_1$ radiation and (200) reflections.

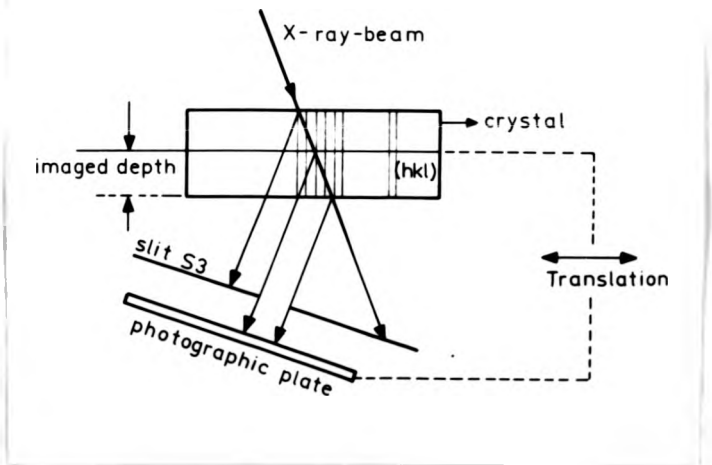

Fig. 5.4. Geometry of the X-ray tomography

For sodium chloride it was impossible to obtain good transmission topographs or well resolved tomographs due to the relatively high plasticity of the crystals; the cleaved fragments

symmetric reflection was chosen to minimize the horizontal distortion of the image.

If the defect density throughout the crystal is very high, this technique fails to give much information. X-ray tomography (or depth limited X-ray topography) circumvents this difficulty.

Fig. 5.4 is a sketch of the geometry involved in X-ray tomography. Slit S_3 can be modified to intercept the rays diffracted by one of the crystal surfaces. By selecting a small S_3 slit, only a narrow slice of the crystal is imaged, improving the resolution. For lithium fluoride crystals good tomographs were obtained with Mo $K\alpha_1$ radiation and (200) reflections.

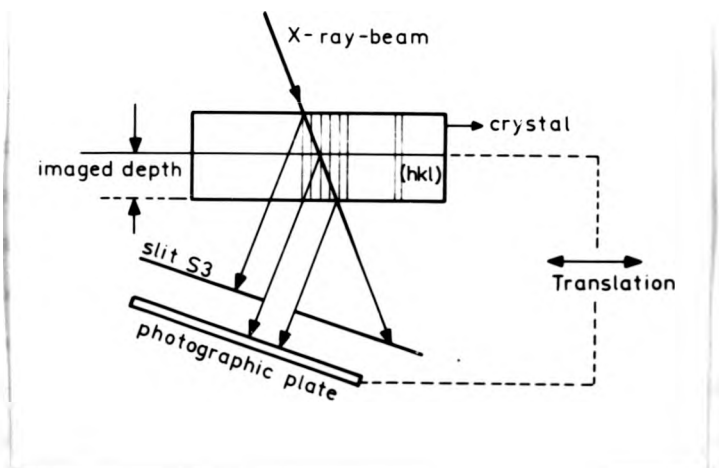

Fig. 5.4. Geometry of the X-ray tomography

For sodium chloride it was impossible to obtain good transmission topographs or well resolved tomographs due to the relatively high plasticity of the crystals; the cleaved fragments

are severely bent as explained in section 1.1.2 and it is impossible to image relatively large areas of the crystal.

5.3.0. Results

A description will be given now of the main features observed in the X-ray topographs of sodium chloride and lithium fluoride cleavage surfaces, the discussion of which will be given in section 5.4.

5.3.1. Sodium chloride

Fig. 5.5 shows a topograph from a zone of a crystal in which cleavage was started from the top left corner. It is possible to observe:

a) Cleavage steps SS following the local crack propagation direction.

b) Stopped crack fronts AA, BB.

c) Traces of transverse slip systems (reinforced at the intersection with the stopped crack fronts).

d) Weak traces of one of the longitudinal systems (the contrast is weak, the traces are observed as streaks, strengthened at the intersections with diagonal systems).

e) Neat traces of the diagonal systems. Traces of the diagonal systems are generally observed near the crystal edges, probably activated by prior cleavages and propagated inside the crystal by misalignment of the cleavage tool.

This is confirmed in Fig. 5.6, which shows most of the cleavage surface of another crystal in which the traces of the diagonal systems stem from the edge of the crystal.

In this photograph transverse systems are also observed and there are weak traces of the activated longitudinal system.

Fig. 5. 5. Reflection X-ray topograph of (001) NaCl cleavage surface, Cu $K_{\alpha 1}$ radiation $\vec{g}$ = (044). Arrow indicates general cleavage direction.

Fig. 5.6. Reflection X-ray topograph of (001) NaCl cleavage surface, Cu $K_{\alpha 1}$ radiation $\vec{g} = (044)$.

Misorientation of the subgrains is so large that some of them are out of reflection. It is quite evident in this photograph the poor quality of the initial crystals. One of the subgrains which is slightly misorientated in fig. 5.6, is shown in fig. 5.7 after reorientation of the specimen to get maximum contrast.

Parallel to the stopped crack fronts AA, BB there are in fig. 5.8 some short traces similar to those which appeared in Newkirk's (2) work on lithium fluoride and were interpreted by him as the outcrops of individual dislocations.

Although reflecting planes in all the topographs of the twelve crystals studied were chosen so that one of the longitudinal systems should appear with maximum contrast ($\vec{g}.\vec{b} = 1$), a longitudinal system appears neatly as continuous lines only in one of the crystals (fig. 5.9). This last figure is a topograph from a crystal in which there is only one subgrain in the Bragg condition.

X-ray topography of sodium chloride crystals shows with great clarity that although the longitudinal systems are activated, the main activated systems for a slowly propagating crack are the transverse slip systems.

5.3.2. Lithium fluoride

Fig. 5.10 shows a reflection topograph from a cleavage surface of a lithium fluoride single crystal with $\vec{g}$ = (022). Longitudinal systems should appear with maximum contrast. Cleavage steps and stopped crack fronts are neatly observed. Weak traces of the longitudinal systems and some segments of the transverse systems are observed.

A region of the same crystal imaged by limited transmission topography can be seen in fig. 5.11. Only one third of the specimen

Fig. 5.7. Reflection X-ray topograph of (001) NaCl cleavage surface $CuK\alpha_1$ radiation $\vec{g}$= (044).

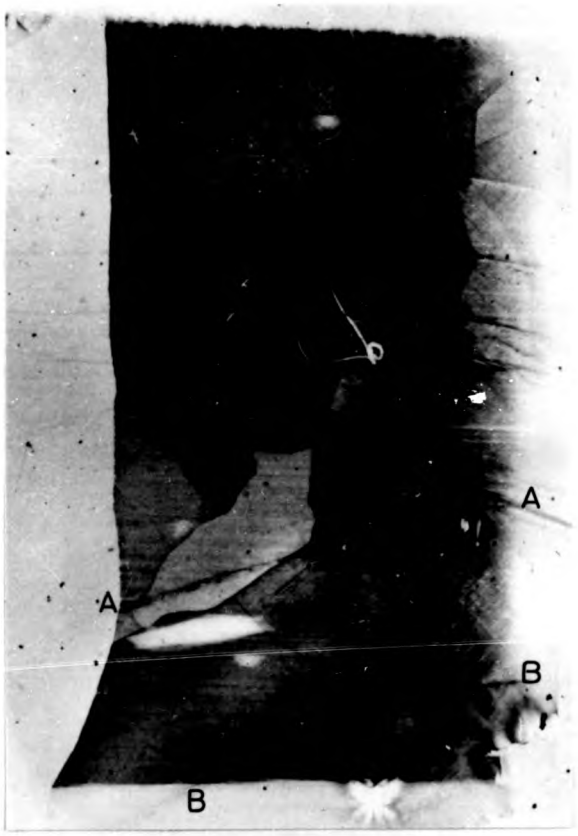

Fig. 5.8. Reflection X-ray topograph of (001) NaCl cleavage surface, Cu K_α radiation $\vec{g}$ = (044).

Fig. 5.9. Reflection X-ray topograph of (001) NaCl cleavage surface Cu K_{α_1} radiation $\vec{g}$= (044)

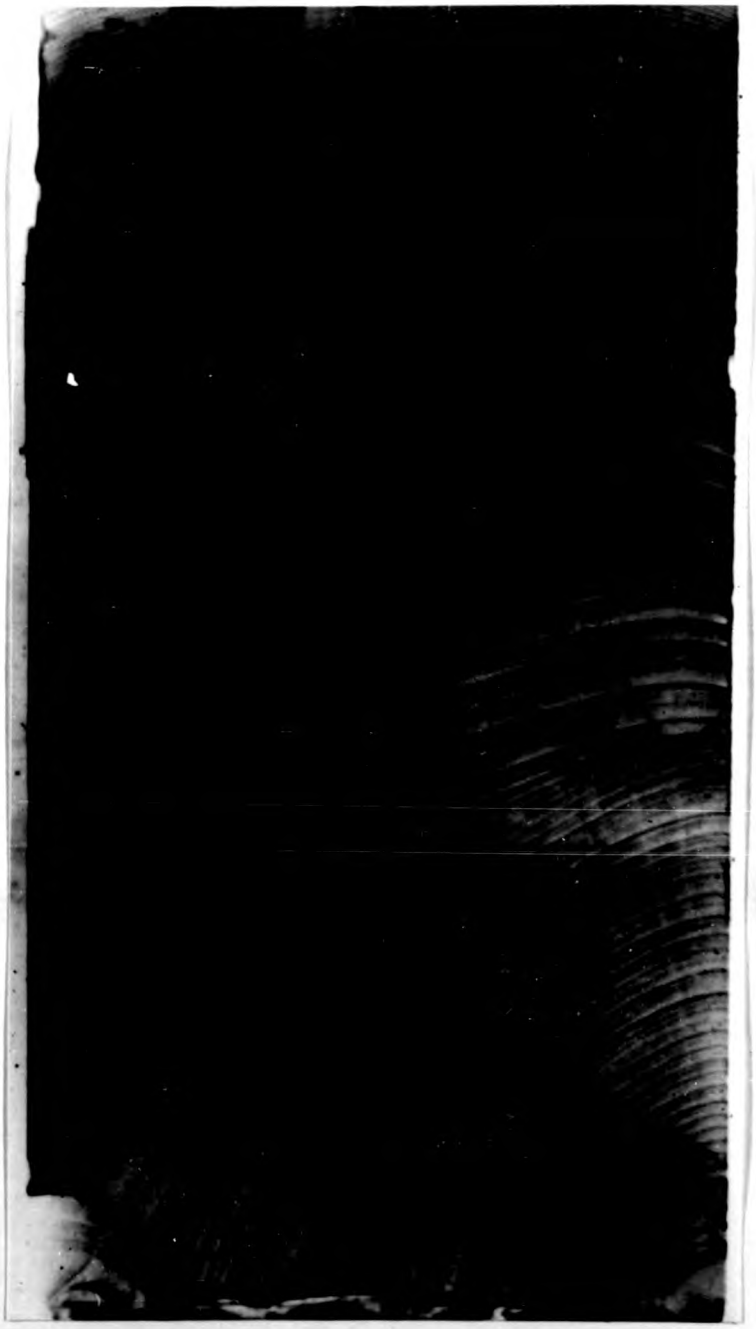

Fig. 5.10. Reflection X-ray topograph of (001) LiF cleavage surface, Cr K_{α_1} radiation

$\vec{g}$= (022)

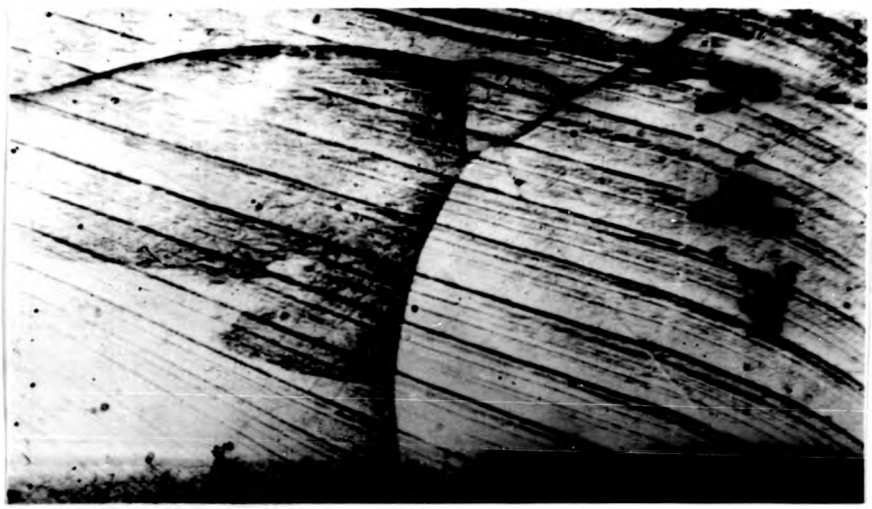

Fig. 5.11. Transmission X-ray limited topograph from a region of same crystal as in Fig. 5.10 Mo K_{α_1} radiation; $\vec{g}$= (200)

depth contributed to the image. In this photograph the specimen was tilted 90° and the reflecting plane was chosen ($\vec{g}$ = (200)) so that the transverse systems should appear with maximum contrast. These can be observed at the stopped fronts.

The contrast dependence on the selected reflecting planes is evident in fig. 5.12a and 5.12b. These are two reflection topographs of the same region of a lithium fluoride crystal with diffraction vectors $\vec{g}$ = (022) and $\vec{g}$ = (202) respectively. It is evident that the longitudinal and transverse systems are both activated, but their traces are not visible when $\vec{g}.\vec{b} = 0$.

These results are in agreement with previous investigations (3, 4, 5) on lithium fluoride.

5.4. Conclusions

The main conclusions to be drawn from X-ray reflection topographs of sodium chloride cleavage surfaces is that, for slowly propagating cracks, the principal activated systems are the transverse slip systems. These are observed with enhanced contrast at the stopped crack fronts.

The activation of the longitudinal slip systems was observed in most of the topographs as weak and discontinuous streaks, although experimental conditions were chosen so that each of the longitudinal systems should appear with maximum contrast (reflecting planes $\vec{g}$ = (044) and $\vec{g}$ = ($0\bar{4}4$)).

A possible explanation to the fact that the longitudinal systems are not always observed is that the strong activation of the transverse slip systems, leading to an inhomogeneous intense plastic deformation of the sodium chloride crystals, gives origin to macroscopic changes

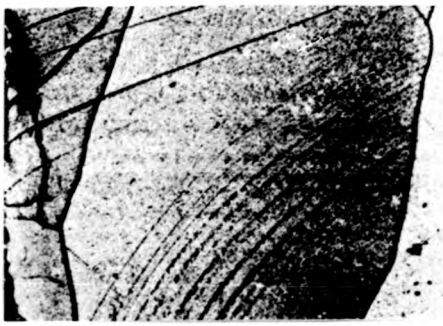

a)

b)

Fig. 5.12. Reflection X-ray topographs from a LiF cleavage surface obtained with different reflections. Cr $K_{\alpha 1}$ radiation

a) $\vec{g}$ = (022)

b) region enclosed in a) with $\vec{g}$ = (202)

and the extinction contrast conditions are no longer valid.

No conclusions can be drawn about the distribution of dislocations in the activated systems. Local lattice rotations, due to the presence of layers or walls of dislocations which can normally be deduced through the analysis of orientation and displacement contrast mechanisms, could not be carried out, because the bending of the sodium chloride crystals made it impossible to obtain topographs from reflecting planes others than (044 and ($0\bar{4}4$).

The transmission and reflection topographs of lithium fluoride crystals described in section 5.3.2 show the expected contrast dependence on the selected reflecting planes. In the stopped crack fronts both longitudinal and transverse systems are activated; they can be observed when the proper reflecting planes are selected.

Comparison between sodium chloride and lithium fluoride topographs shows that the transverse systems are much more activated in sodium chloride than in lithium fluoride as can be expected from the higher plasticity of the sodium chloride crystals.

Thanks are due to Lic. E. Manghi and CITEFA staff for making available the X-ray diffractometer and cameras and for several useful discussions during the course of collecting the data.

R.5. References

(1) Wilkens M., Ca. J. Phys. 45, 567, (1967).

(2) Newkirk J.B., Trans. Met. Soc. AIME, 215, 483, (1959).

(3) Yoshimatsu M., Kohra K, J. Phys. Soc. Japan, 15, 1760, (1960).

(4) Burns S.J., Webb W.W., Trans. Met. Soc. AIME, 236, 1165, (1966).

(5) Forwood C.T., Lawn B.R., Phil. Mag. 13, 595, (1966).

(6) Strunk N., Thesis Univ. of Stuttgart (1973).

R.5. References

(1) Wilkens M., Ca. J. Phys. 45, 567, (1967).

(2) Newkirk J.B., Trans. Met. Soc. AIME, 215, 483, (1959).

(3) Yoshimatsu M., Kohra K, J. Phys. Soc. Japan, 15, 1760, (1960).

(4) Burns S.J., Webb W.W., Trans. Met. Soc. AIME, 236, 1165, (1966).

(5) Forwood C.T., Lawn B.R., Phil. Mag. 13, 595, (1966).

(6) Strunk N., Thesis Univ. of Stuttgart (1973).

Chapter 6

DISCUSSION

6.1. Introduction

A discussion of the dislocation processes which give rise to those surface structures associated with unsteady cleavage crack propagation will be given in this chapter. The relationship between the dislocation processes and crack propagation direction will also be considered.

The surface features characteristic of crack propagation at different velocities, as observed by complementary techniques, have been described in detail in chapters 4 and 5. From this description, a clear understanding of the main features associated with each stage in the unsteady propagation of a cleavage crack has been gained. A considerable amount of fine scale detail, sometimes at an atomistic scale, is accessible through the thin film decoration techniques. Although it is not possible at present to understand every single feature thus observed, many of the microstructures have been interpreted. Some of these structures have been related to the main features and elucidate the dislocation processes which give rise to the macrostructures.

6.1.1. General features of an unsteady propagating crack.

The different features left on the cleaved surfaces of a crystal by an unsteady propagating crack have been described in chapter 4 and a sketch is given in Figs. 4.2 and 4.7. When a cleavage crack is introduced in an alkali halide crystal in the manner described in chapter 2, it usually starts from a corner and

runs at high velocity straightening its front to accommodate the applied stresses. The cleavage surface is scratched and strongly damaged where the cleavage wedge is first introduced in the crystal as already described by Gilman (1) and Forwood (2) and this zone will not be considered in the following discussion.

The whole process of unsteady crack propagation includes the crack running freely, slowing down, stopping, retreating, and healing slightly (including some surface hardening), restarting and repeating the entire sequence until the crystal is finally cleaved. These different stages correspond to the zones described in section 4.2.

Each time the crack is stopped and restarted, the cleavage crack nucleates at the center of the stopped front, because of the drag exerted by the crystal edges. It then spreads at high velocity sideways and forwards as illustrated in Fig. 4.2. Cleavage steps generally form a fan pattern steming from the point where the crack nucleates (except at the sites of very high cleavage steps). The angle which the cleavage steps form with the stop band depends on its position along the crack front.

Imperfect healing of the zones immediately ahead of the stop band, gives rise to a surface hardening and higher stresses are required to restart the cleavage crack.

It is this surface hardening, together with the large number of unit cleavage steps originating at dislocation loops, which comprise the stop band and build up a rough non-crystallographic surface.

While the crack is gaining velocity, river patterns are formed, considerably reducing the number of steps and leaving a smoother surface.

The crack runs then freely again in a (001) plane at high

velocity, at an angle with the 100 general direction of crack propagation.

As the velocity of the crack decreases, cleavage steps straighten up and become parallel to the crystallographically preferred [10 0] direction. In effect, in this case the risers of the steps are the (010) cleavage planes, and less energy is required to propagate a step. This decrease in the velocity of the crack is accompanied by the onset of plastic deformation, becoming only slightly visible as traces of the transverse and longitudinal slip systems at an optical microscopy scale, although clearly established in the "tartan pattern" observed in the electron micrographs of decorated replicas and in the X-ray topographs.

The crack finally stops and retreats to the stop band accompanied by imperfect healing of the two cleavage surfaces. During the time the crack is at rest, some relaxation of the stresses concentrated at the tip of the crack occurs by the expansion of dislocation loops; some surface induced movement of dislocation also takes place.

Each time the crack is restarted, additional plastic deformation occurs in the already torn up part of the crystal, leading to an enhancement of the existing slip bands and to a polygonization of the stop bands.

The relationship between these main features and the more detailed structures observed mainly at an electron microscopy level will be discussed in the following sections.

6.1.2. Detailed surface structures left by an unsteady propagating crack.

It is important for the following discussion to define clearly some of the terms to be used in the interpretation of the electron

velocity, at an angle with the 100 general direction of crack propagation.

As the velocity of the crack decreases, cleavage steps straighten up and become parallel to the crystallographically preferred [10 0] direction. In effect, in this case the risers of the steps are the (010) cleavage planes, and less energy is required to propagate a step. This decrease in the velocity of the crack is accompanied by the onset of plastic deformation, becoming only slightly visible as traces of the transverse and longitudinal slip systems at an optical microscopy scale, although clearly established in the "tartan pattern" observed in the electron micrographs of decorated replicas and in the X-ray topographs.

The crack finally stops and retreats to the stop band accompanied by imperfect healing of the two cleavage surfaces. During the time the crack is at rest, some relaxation of the stresses concentrated at the tip of the crack occurs by the expansion of dislocation loops; some surface induced movement of dislocation also takes place.

Each time the crack is restarted, additional plastic deformation occurs in the already torn up part of the crystal, leading to an enhancement of the existing slip bands and to a polygonization of the stop bands.

The relationship between these main features and the more detailed structures observed mainly at an electron microscopy level will be discussed in the following sections.

6.1.2. Detailed surface structures left by an unsteady propagating crack.

It is important for the following discussion to define clearly some of the terms to be used in the interpretation of the electron

microscopy structures.

Surface structures previously described can be divided into two main groups: cleavage steps and slip steps. Cleavage steps monoatomic or only a few units high are related to dislocations only at their origin: no movement of dislocations is involved along the path of a cleavage step. On the other hand slip steps are always derived from the movement of dislocations. Slip steps are often grouped in bands. It is convenient to distinguish between dislocation filled bands and slip bands as discussed by Argon and Orowan (3) for lithium fluoride and magnesium oxide crystals. They state that the slip bands arise in an already dislocation filled crystal by the gradual concentration of slip in bands (resulting in slip in a macroscopic scale). Examples of high transverse slip steps have already been described in chapter 4 and are readily visible in shadow-decorated and in etched specimens.

The same zones described in section 4.2 will be considered in this chapter to facilitate comparison between the description of the characteristic features and their interpretations.

6.2.0. Tartan pattern zone: active slip systems.

From observations described in chapter 4 it is inferred that the tartan pattern zone observed by electron microscopy techniques is associated in alkali halide crystals, with deceleration of a cleavage crack. When the crack velocity decreases, plastic relaxation of the stresses concentrated at the tip of the crack can take place. This plastic relaxation occurs through the nucleation and multiplication of dislocations of the transverse and longitudinal slip systems. Cleavage structures produced as a consequence of the

nucleation and multiplication of dislocations of both slip systems will be discussed in sections 6.2.1. and 6.2.2 for a crack propagation direction parallel to [100]and in section 6.2.3 for a crack propagation direction nearly parallel to [110].

Care must be taken not to overlook that the observed cleavage structures are the final picture resulting both from the processes involved in the deceleration of a cleavage crack and those related to the wedge opening of the crystal arms.

Comments on the etch pit distribution will be given in section 6.3.3.

6.2.1. Analysis of cleavage structures produced by the activation of the transverse slip systems.

From X-ray topography studies, it was shown (see chapter 5), that the transverse slip systems are the main activated systems for a decelerating crack.

Numerous dislocation loops are present in the (101) and ($\bar{1}$01) planes as a consequence of the activation of the transverse slip systems ahead of the crack tip; once the crack has passed through the activated slip plane, residual stresses move these dislocations in their slip plane, image forces attract them to the surface and a slip trace is formed. Transverse lines forming the tartan pattern are thus generated.

Further plastic deformation resulting from the wedge opening of the crystal arms contributes to the characteristic transverse slip bands forming the tartan pattern.

It was observed that the transverse slip lines are inhomogeneously distributed. Some of them appear as isolated single lines but most of them form bands of various widths as described in

sections 4.3.1. a) and b).

Their grouping in bands provides a verification that the most active mechanism for the multiplication of dislocations introduced by cleavage is the infection of neighbouring planes by double cross-slip. This mechanism was first suggested by Koehler (4) and observed by Gilman and Johnston (5) for lithium fluoride crystals.

By using the shadow-decoration technique (section 4.3.3.b) it has been possible to demonstrate that both of the transverse slip systems are activated by a decelerating crack.

It is to be expected from the anisotropy of the stress field of the propagating crack that one of the transverse slip systems should appear more frequently. This has been confirmed by the presence of a larger number of slip lines, appearing either in isolation or as wide bands, belonging to the (101) $[\bar{1}01]$ system (which are positive steps for the figures of chapter 4) than of slip lines of the conjugate system.

As neither isolated slip lines of the $(\bar{1}01)$ [101] system nor wide bands consisting mostly of lines of this system were observed, it can be inferred that the (101) $[\bar{1}01]$ system was activated first and acted as a barrier to dislocations of the second activated system.

The presence of both slip systems has been observed in groups or bands.

A common feature observed in many of the transverse slip bands (see section 4.3.3.b), is the occurrence of closely spaced groups of negative (or down) steps bounded by two positive (or up) steps. This distribution can be understood in terms of the preferential activation of the (101) $[\bar{1}01]$ system which gives origin to the two positive steps. Dislocations of the conjugate system produced at or near the surface of the crystal, are held up when they

sections 4.3.1. a) and b).

Their grouping in bands provides a verification that the most active mechanism for the multiplication of dislocations introduced by cleavage is the infection of neighbouring planes by double cross-slip. This mechanism was first suggested by Koehler (4) and observed by Gilman and Johnston (5) for lithium fluoride crystals.

By using the shadow-decoration technique (section 4.3.3.b) it has been possible to demonstrate that both of the transverse slip systems are activated by a decelerating crack.

It is to be expected from the anisotropy of the stress field of the propagating crack that one of the transverse slip systems should appear more frequently. This has been confirmed by the presence of a larger number of slip lines, appearing either in isolation or as wide bands, belonging to the (101) $[\bar{1}01]$ system (which are positive steps for the figures of chapter 4) than of slip lines of the conjugate system.

As neither isolated slip lines of the $(\bar{1}01)$ [101] system nor wide bands consisting mostly of lines of this system were observed, it can be inferred that the (101) $[\bar{1}01]$ system was activated first and acted as a barrier to dislocations of the second activated system.

The presence of both slip systems has been observed in groups or bands.

A common feature observed in many of the transverse slip bands (see section 4.3.3.b), is the occurrence of closely spaced groups of negative (or down) steps bounded by two positive (or up) steps. This distribution can be understood in terms of the preferential activation of the (101) $[\bar{1}01]$ system which gives origin to the two positive steps. Dislocations of the conjugate system produced at or near the surface of the crystal, are held up when they

impinge on the slip planes of the primary system, already activated, and cross-slip and multiply in the narrow zone between the two planes of the primary system (see Fig. 6.1).

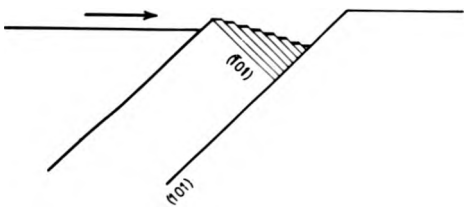

Fig. 6.1

This behaviour can be related to that described by T. Suzuki (cited by Nabarro (6))for potassium chloride single crystals deformed in compression.

That both transverse systems are active can also be inferred from the observation of electron micrographs of standard decorated replicas through the deflection, on opposite directions, of slip lines at their intersection with a cleavage step. (e.g. see Fig. 4.20). In Fig. 4.20 the preferential activation of one of the transverse slip systems is also evident.

It is believed that the remarkable sudden change in the height of some lines of very dense transverse bands and the jogged path of some cleavage steps when traversing the bands (section 4.3.3 b and 4.3.4 b) are related to the interaction of conjugate systems. This sudden change in the height of transverse lines can be accounted for by the presence of small (100) cracks nucleated at the intersection of the orthogonal transverse systems.

The mechanism of crack formation as a consequence of the interaction of conjugate slip systems has been described and explained for magnesium oxide crystals by Argon and Orowan (3) though a different interpretation was given by Stokes et al. (7). Argon and Orowan state that the basic cause of cracking in magnesium oxide is that a dislocation band, if not too narrow, represents a serious obstacle to the penetration of an intersecting band. The high stresses present at the intersections can be partially accommodated by kinking and in many cases this is sufficient to avoid crack formation. In unfavourable cases kinking is not enough to relax the resulting stresses and cracks are nucleated. These cracks are along (001) or (100), or more often, along (101) or ($\bar{1}$01) depending on the relative width of the intersecting bands. In these last cases they run for a distance along (101) or ($\bar{1}$01) before they swing into the usual cleavage planes (001) or(100).

Argon and Orowan took the view that the formation of cracks at the intersection of dislocation bands is related to certain features of plastic deformation of magnesium oxide crystals which differ distinctly from those of other softer ionic crystals of the sodium chloride structure. In the same year Davidge and Pratt (8) found that a common feature of sodium chloride crystals deformed in compression is that slip commences on two orthogonal planes one of which becomes inactive. The planes of the inactive system act as barriers to dislocations on the main system, leading to kink bands. These kink bands are similar to those described by Argon and Orowan for magnesium oxide crystals.

If the stresses originating in sodium chloride by the interaction of orthogonal transverse dislocation bands cannot be

The mechanism of crack formation as a consequence of the interaction of conjugate slip systems has been described and explained for magnesium oxide crystals by Argon and Orowan (3) though a different interpretation was given by Stokes et al. (7). Argon and Orowan state that the basic cause of cracking in magnesium oxide is that a dislocation band, if not too narrow, represents a serious obstacle to the penetration of an intersecting band. The high stresses present at the intersections can be partially accommodated by kinking and in many cases this is sufficient to avoid crack formation. In unfavourable cases kinking is not enough to relax the resulting stresses and cracks are nucleated. These cracks are along (001) or (100), or more often, along (101) or ($\bar{1}$01) depending on the relative width of the intersecting bands. In these last cases they run for a distance along (101) or ($\bar{1}$01) before they swing into the usual cleavage planes (001) or(100).

Argon and Orowan took the view that the formation of cracks at the intersection of dislocation bands is related to certain features of plastic deformation of magnesium oxide crystals which differ distinctly from those of other softer ionic crystals of the sodium chloride structure. In the same year Davidge and Pratt (8) found that a common feature of sodium chloride crystals deformed in compression is that slip commences on two orthogonal planes one of which becomes inactive. The planes of the inactive system act as barriers to dislocations on the main system, leading to kink bands. These kink bands are similar to those described by Argon and Orowan for magnesium oxide crystals.

If the stresses originating in sodium chloride by the interaction of orthogonal transverse dislocation bands cannot be

The mechanism of crack formation as a consequence of the interaction of conjugate slip systems has been described and explained for magnesium oxide crystals by Argon and Orowan (3) though a different interpretation was given by Stokes et al. (7). Argon and Orowan state that the basic cause of cracking in magnesium oxide is that a dislocation band, if not too narrow, represents a serious obstacle to the penetration of an intersecting band. The high stresses present at the intersections can be partially accommodated by kinking and in many cases this is sufficient to avoid crack formation. In unfavourable cases kinking is not enough to relax the resulting stresses and cracks are nucleated. These cracks are along (001) or (100), or more often, along (101) or ($\bar{1}$01) depending on the relative width of the intersecting bands. In these last cases they run for a distance along (101) or ($\bar{1}$01) before they swing into the usual cleavage planes (001) or(100).

Argon and Orowan took the view that the formation of cracks at the intersection of dislocation bands is related to certain features of plastic deformation of magnesium oxide crystals which differ distinctly from those of other softer ionic crystals of the sodium chloride structure. In the same year Davidge and Pratt (8) found that a common feature of sodium chloride crystals deformed in compression is that slip commences on two orthogonal planes one of which becomes inactive. The planes of the inactive system act as barriers to dislocations on the main system, leading to kink bands. These kink bands are similar to those described by Argon and Orowan for magnesium oxide crystals.

If the stresses originating in sodium chloride by the interaction of orthogonal transverse dislocation bands cannot be

completely relieved by kinking, they would nucleate cracks similar to those described by Argon and Orowan in magnesium oxide. Cracks of this type are thought to be the origin of the sudden change in the height of lines in very dense transverse slip bands.

6.2.2.0. Analysis of the cleavage structures produced by the activation of the longitudinal slip systems.

The origin of the longitudinal lines forming the tartan pattern is not so evident. As unit cleavage steps run, in this zone, along the crystallographically preferred [100]direction, it is necessary to seek additional evidence to elucidate which of the longitudinal lines are slip steps and which are cleavage steps.

It is assumed that most of the isolated longitudinal lines are cleavage steps, monoatomic or only a few units high. Most of these lines are those arms of Vs which reach the tartan pattern zone and are deflected into the [100] direction (see tracing 4.7 and section 6.5).

The number of isolated monoatomic cleavage steps which have their origin in grown-in dislocations is negligible. There is also a small number of longitudinal lines which stem from the screw components of transverse dislocation loops.

Longitudinal lines that do not originate by the previous mechanisms, can be accounted for by the nucleation of dislocation loops of the longitudinal systems. As described in section 4.3.3.b) they are inhomogeneously distributed. Most frequently they are grouped in bands of various widths. Here again, double cross-slip appears to be the most likely multiplication mechanism in longitudinal band formation. Longitudinal lines of both signs have been observed in shadow-decorated replicas. The fact that although

some pairs of lines have been observed, most of the longitudinal lines do not alternate in sign (see section 4.3.3.b) is not in agreement with Burns and Webb's (9) interpretations of decorated cleavage structures of lithium fluoride crystals for cracks propagating at low velocities. The high density of longitudinal lines shown in Burns and Webb's paper (Fig.8) is by no means typical of a decelerating crack. Though localized regions of the crystal with such a density of longitudinal lines have been observed as illustrated in chapter 4, the distribution of longitudinal lines along the full extent of the crack front is not at all homogeneous, neither for the sodium chloride nor for the lithium fluoride crystals studied.

Some isolated segments of longitudinal lines have been observed. It is believed that these segments are formed when dislocation loops of the longitudinal system, nucleated by the stress field of the crack tip, emerge at the cleaved surface. Loops from approximately 0.5μ diameter have been observed. It is very difficult to venture an estimate of the possible upper limit for the size of the longitudinal loops. Though a very good resolution was obtained in the shadow-decorated replicas of sodium chloride crystals, the possibility that these short segments, which are visible as single lines, were formed by unresolved pairs of lines like the ones described by Robins et al. (10) for magnesium oxide crystals cannot be ruled out. If that were the case, the distance between lines of a pair would be less than approximately 20 Å.

From the large number of specimens observed, no evidence was found of the presence of more than one longitudinal segment along the same slip plane. On the other hand Burns and Webb have observed in replicas of lithium fluoride crystals decorated with the standard thin film technique (specimen heated to 125°C) the appearance of

several segments on the same slip trace. The fact that no reappearance of a loop in the same slip plane has been observed in any of the shadow-decorated replicas, prepared at room temperature, of sodium chloride or lithium fluoride crystals, rules out their explanation of this effect in terms of dislocations moving with the crack tip and supports their alternative suggestion that it is due to deterioration of the crystal surface before the metal condensation. Observation of Burns and Webb's micrographs shows the presence of small thermal evaporation structures and further supports the latter hypothesis.

6.2.2.1. Bundles: a peculiar structure of the longitudinal lines

An explanation of the origin of the bundles of parallel longitudinal lines characteristic of the tartan pattern zone is not trivial. This is partly due to the fact that it is impossible to distinguish in this zone between longitudinal unit cleavage steps and slip steps as mentioned above.

Two possible mechanisms for their formation will be discussed:

a) A mechanism in which the bundles are assumed to be formed as a consequence of the nucleation and multiplication of dislocations of the transverse slip system.

b) A mechanism in which the bundles are assumed to be formed by the activation of the longitudinal slip systems.

a) It could be assumed that the longitudinal steps of a bundle are formed when the crack cuts through the screw components of transverse dislocation loops. Such a high density of dislocation loops in a short segment of a transverse slip line could be accounted for by the precipitation of impurities or by the presence of a Frank-Read type

of dislocations source. As many concentric dislocation loops are formed by the Frank-Read mechanism, it would be consistant with the distribution of signs sometimes found in the bundles. (see Fig. 6.2).

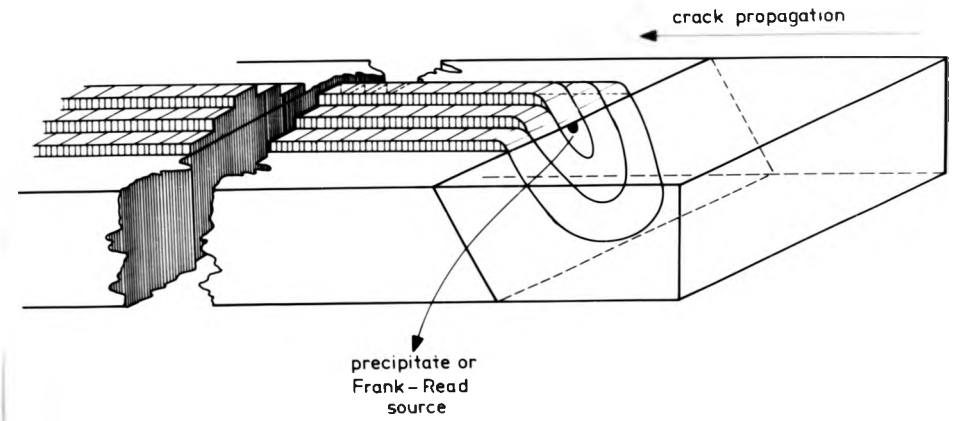

Fig. 6.2.

No convincing explanation can be found for the common end of the steps of a bundle at a transverse slip band. In effect, cleavage steps are formed at the crack front, while slip steps are formed after the crack front has passed; therefore, slip steps cannot be the obstacles blocking the propagation of cleavage steps. On the other hand, it is inconceivable for every cleavage step of a bundle to encounter a dislocation of opposite sign at the same transverse band so that annihilation could take place.

These arguments rule out the hypothesis that bundles are formed by cleavage steps which originate in dislocation loops of the transverse slip systems.

b) The hypothesis that bundles appear as a consequence of the activation of the longitudinal slip systems is supported by X-ray

of dislocations source. As many concentric dislocation loops are formed by the Frank-Read mechanism, it would be consistant with the distribution of signs sometimes found in the bundles. (see Fig. 6.2).

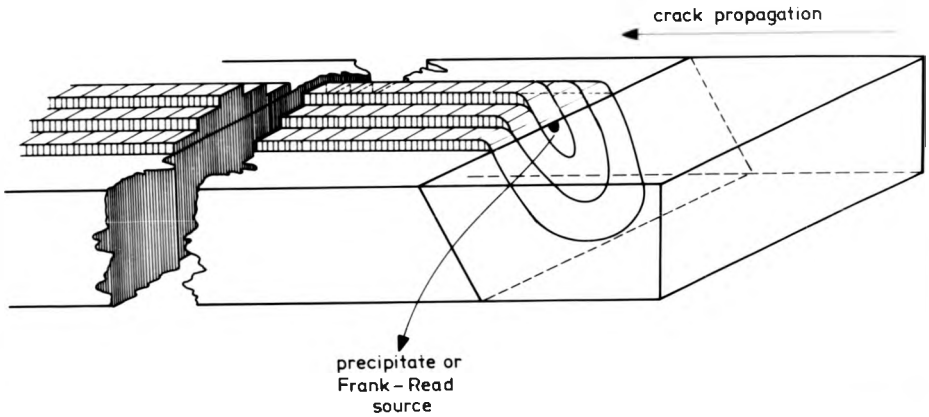

Fig. 6.2.

No convincing explanation can be found for the common end of the steps of a bundle at a transverse slip band. In effect, cleavage steps are formed at the crack front, while slip steps are formed after the crack front has passed; therefore, slip steps cannot be the obstacles blocking the propagation of cleavage steps. On the other hand, it is inconceivable for every cleavage step of a bundle to encounter a dislocation of opposite sign at the same transverse band so that annihilation could take place.

These arguments rule out the hypothesis that bundles are formed by cleavage steps which originate in dislocation loops of the transverse slip systems.

b) The hypothesis that bundles appear as a consequence of the activation of the longitudinal slip systems is supported by X-ray

topography observations: X-ray topographs show the localized activation of the longitudinal slip system in the zone immediately before a stopped crack front.

Most of the isolated longitudinal lines observed in the electron micrographs can be followed back to their origin and have been interpreted as cleavage steps. Bundles are the only feature of the tartan pattern zone that can be related to the activation of the longitudinal slip systems.

It is believed that the following is the more likely mechanism for the origin of the bundles; it bases on the idea that they are a characteristic feature of the activation of the longitudinal systems and it can explain the length which a bundle of longitudinal dislocation loops can attain, as well as the fact that both ends are along [010] transverse lines.

It is assumed that a side of a longitudinal dislocation loop is cut by the crack and a cleavage step is formed, which follows the crystallographically preferred [100] direction. The other side of the dislocation loop is carried over by the stresses ahead of the crack tip for distances sometimes as long as 150μ. Eventually the interaction with kinks at the intersection of two orthogonal transverse systems, or the interaction with the debris left by the multiple cross-slip of dislocations of the transverse system, slows down the dislocation. This is then cut by the crack, giving rise to a cleavage step of opposite sign which annihilates the previous one (see Fig. 6.3.a). Most frequently the first side of this dislocation loop cross-slips in the (010) plane. This surface-induced cross-slip of one side of the dislocation originates

topography observations: X-ray topographs show the localized activation of the longitudinal slip system in the zone immediately before a stopped crack front.

Most of the isolated longitudinal lines observed in the electron micrographs can be followed back to their origin and have been interpreted as cleavage steps. Bundles are the only feature of the tartan pattern zone that can be related to the activation of the longitudinal slip systems.

It is believed that the following is the more likely mechanism for the origin of the bundles; it bases on the idea that they are a characteristic feature of the activation of the longitudinal systems and it can explain the length which a bundle of longitudinal dislocation loops can attain, as well as the fact that both ends are along [010] transverse lines.

It is assumed that a side of a longitudinal dislocation loop is cut by the crack and a cleavage step is formed, which follows the crystallographically preferred [100] direction. The other side of the dislocation loop is carried over by the stresses ahead of the crack tip for distances sometimes as long as 150μ. Eventually the interaction with kinks at the intersection of two orthogonal transverse systems, or the interaction with the debris left by the multiple cross-slip of dislocations of the transverse system, slows down the dislocation. This is then cut by the crack, giving rise to a cleavage step of opposite sign which annihilates the previous one (see Fig. 6.3.a). Most frequently the first side of this dislocation loop cross-slips in the (010) plane. This surface-induced cross-slip of one side of the dislocation originates

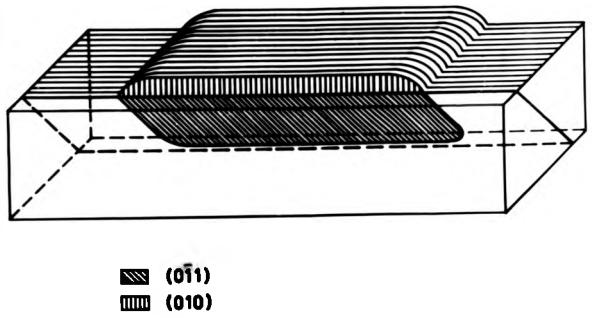

a

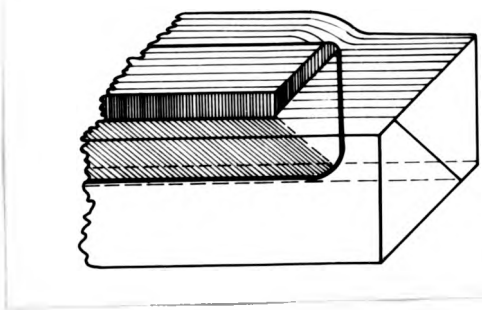

b

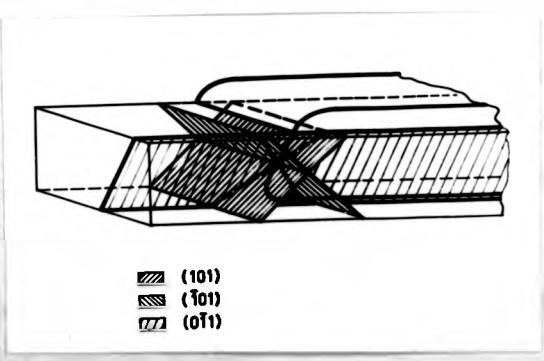

c

Fig. 6.3 Schematic diagram showing the proposed mechanisms for the origin and end of bundles.

a [010] slip line (segment AB, Fig. 6.3.b).

Infection of neighbouring longitudinal planes by multiple cross-slip of a few of these longitudinal dislocation loops accounts for the appearance of the bundles. Both longitudinal slip systems are activated: as each longitudinal dislocation loop gives rise to several longitudinal loops of the same sign, it is possible to explain with the model the observed distribution of signs of steps along a bundle such as in Fig. 4.18 for example. Residual stresses and the stresses introduced by the wedge opening of the crystal arms are the origin of this multiple cross-slip; they also expand the resulting dislocation loops back to the cross-slip segment AB on one side, and on the other side up to the intersecting obstacle which halted the original dislocation loop (Fig. 6.3.c). This explains why both ends of all the loops of a bundle are aligned along a [010] direction. It also explains the L-shaped structure observed at the beginning of the bundles (see diagram 6.3.b).

It is worth noting the fact that the bands of transverse lines intersected by the bundles, have been formed in stages after most of the expansion of the longitudinal loops of the bundles has taken place. These transverse bands are formed at each advance of the wedge by multiplication of the existing transverse loops. So that it is quite possible that the expanding longitudinal loops do not actually cross the dense transverse bands observed in the electron micrographs.

6.2.3. Cleavage structures for a crack propagation direction nearly parallel to <110>

Main features of the tartan pattern zone are the same for

a crack propagating in a [110]direction as for a crack propagating along [100] as described in section 4.3.3.a).

The fact that longitudinal bundles parallel to [100]appear even for cracks propagating in a [110] direction further supports the hypothesis that they appear as a consequence of the activation of the longitudinal slip systems.

A remarkable feature is that most of the monoatomic or only a few atomic units high cleavage steps run almost or exactly parallel to the crystallographically preferred [100] direction while higher cleavage steps generally follow the [110] local direction of crack propagation. The fact that monoatomic steps run parallel to [100] is in agreement with Burns and Webb's (9) observations for lithium fluoride crystals when the crack propagation direction differs less than 20°from the [100] crystallographic direction (as can be inferred from their description of the angle between small and large cleavage steps). Burns and Webb also observed that steps travelling just slightly off the [110]direction are composed of [100]and [010] segments, but these structures have not been observed in any of the replicas of the sodium chloride nor lithium fluoride crystals studied. They cannot be considered a typical feature of atomic steps running slightly off the [110] direction for a decelerating crack.

6.3.0. Stop band

The characteristic features of the stop band, which comprises the last stage of the deceleration process, the immediate healing and the first stage of the restarting process, have been described in sections 4.3.4 .a and b. These features will be discussed in sections 6.3.1 , 6.3.2 and 6.3.3.

6.3.1. Transverse bands associated with the deceleration process

Dislocation processes associated with the transverse bands included in the stop band are the same as those described for the tartan pattern zone: both transverse systems are active and multiplication by multiple cross-slip of dislocations occurs both by deceleration of the cleavage crack and by the stresses introduced by the wedge opening of the crystal arms.

A characteristic feature of the stop bands is the strong interaction between both transverse systems which give rise to the marked relief already described in section 4.3.4 b) leading even to the displacement of entire crystal blocks. Crack nucleation by the interaction of conjugate systems by an Argon and Orowan (3) mechanism, as already proposed for the tartan pattern zone, is considered to be responsible for the roughness of the stop bands. It is believed that the stresses introduced by the wedge opening of the crystal arms when restarting the cleavage crack are the main cause of the strong interaction of conjugate systems at the stop band. But the influence of the stresses ahead of a decelerating crack tip on the interaction of conjugate systems should not be underestimated. The jogged paths of high cleavage steps at the stop band are examples of crack nucleation by this kind of interaction; in effect as cleavage steps are formed at the crack tip, the stresses introduced by the wedge opening of the crystal arms cannot influence their previous paths.

6.3.2. Short straight longitudinal lines: relationship with dislocations.

After the crack stops, the healing process takes place reaching nearly to the last deformation band. The healing process becomes clearly evident in the intricate pattern of inclined

restarting steps found at the beginning of the zone following the stop band (see section 4.3.5). More inferential evidence of this healing is the presence of the steps that follow the short straight segments stemming from the last slip line of the stop band, and which are strikingly clear in the curved stopped fronts (see for example Fig. 4.3). It is proposed that these short straight segments are due to surface induced cross-slip on the (010) plane of one end of the (101) $\langle\bar{1}01\rangle$ dislocation loops to reduce their line length. The mechanism of cross-slip near a surface has been described by Gilman (11) and Appel and Messerschmidt (12). The surface-induced cross-slip cannot proceed farther than the place where both cleavage surfaces are united. When the crack restarts, a unit cleavage step stems from each cross slipped dislocation.

The observed sequence of signs of the short segments stemming from the stop band, can be understood in terms of this model. If two neighbouring dislocations of opposite sign are very close together, the corresponding steps run together for a short time until they annihilate, giving rise to the pairs described in section 4. 3. 4.b) (Fig. 4.29). Pairs belonging to adjacent loops have always the same sequence of signs (positive-negative or viceversa), while the presence of some pairs with the opposite sequence (negative-positive or viceversa) can be accounted for by the annihilation of steps stemming from both ends of small dislocation loops. (Fig. 6. 4. a and 6.4.b).

Isolated short longitudinal segments are frequently observed in crack fronts roughly parallel to [010] and have not been observed for crack fronts which differ appreciably from [010] e.g. Figs. 4.22 and 4 .29. It is suggested that they result from small longitudinal loops nucleated ahead of the crack tip that could later expand slightly under residual stresses up to the last transverse slip line. The fact that none of these segments have been observed for inclined

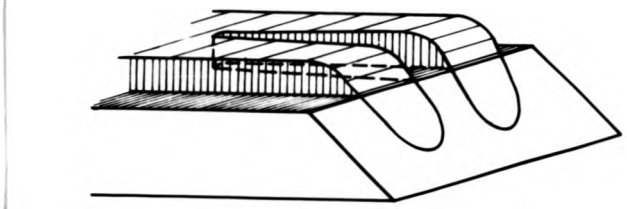

a)

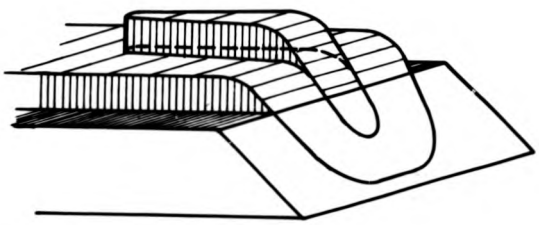

b)

Fig. 6.4 a and b. Stop band. Annihilation of pairs of short lines.

stop bands is consistent with this suggestion; the longitudinal systems are less active for cracks propagating off the [100] direction, as already discussed for the bundles of longitudinal lines appearing in the tartan pattern zone.

The behaviour of the short segments included in the stop band near high cleavage steps, described in section 4.3.4 a) can be understood in terms of the two mechanisms mentioned above: the cross-slip of the end of transverse dislocation loops and the presence of small longitudinal dislocation loops. In effect, cleavage steps stemming from the short longitudinal segments support the assumption that the surface-induced cross-slip mechanism is operative. Where the crack front is deflected from the [010] direction towards the [100] direction by the inhomogeneous stress distribution associated with a high cleavage step (see Fig. 4.24), the presence of isolated [010] segments can be explained by the expansion of small transverse loops. These transverse loops originate ahead of the stopped crack front which is here parallel to [100]. They tend to expand under the strong stresses created by the high cleavage step rather than to cross-slip to reduce their line length.

6.3.3. Etch pits

The relationship between the etch pit distribution described in section 4.4 and the microstructures observed by electron microscopy of decorated replicas will be discussed in this section.

It is believed that the absence of etch pits in the slip bands is the result of macroscopic slip which must have occurred by the stresses introduced by the wedge opening of the crystal arms. In effect the curvature of the cleavage halves observed even by the naked eye when cleavage is completed, must be related to localized macroscopic slip. Moreover slip bands observed in etched specimens

must correspond to macroscopic slip, because relatively small slip steps are dissolved during etching.

Dislocation filled bands like the one shown in Fig. 4.36 have often been observed at stop bands, particularly where they are slightly inclined to the [010] direction. These dislocation bands mark the at-rest position of a crack front. The dislocation loops are here displaced in parallel planes along the curved front and cannot give rise to macroscopic slip unlike dislocations lying along non-curved sections of the crack front.

It is not easy to reconcile the apparent absence of aligned etch pits in the tartan pattern zone with the mechanism proposed to explain the presence of bundles of longitudinal slip lines in decorated replicas. In order to further investigate whether or not there are dislocations emerging at both ends of longitudinal bundles it is proposed to analyze matching cleavage surfaces, one of which would be etched and the other decorated.

6.4. Restarting zone with inclined steps

Decorated replicas of sodium chloride cleavage surfaces show, in the zone immediately ahead of the stop band, an intricate pattern formed simultaneously by a river pattern and something similar to a lightning pattern (see section 4.3.5). This intricate pattern arises from the imperfect healing which is usually present when the crack is halted. As the crystal surfaces become more intimately united, there is a variable mismatch at numerous sites of the cleavage surfaces. When cleavage is restarted, it must cut through these faulted regions producing a multitude of unit cleavage steps. The rough surfaces observed in Figs. 4.8. and 4.24, for example, are produced in this manner

must correspond to macroscopic slip, because relatively small slip steps are dissolved during etching.

Dislocation filled bands like the one shown in Fig. 4.36 have often been observed at stop bands, particularly where they are slightly inclined to the [010] direction. These dislocation bands mark the at-rest position of a crack front. The dislocation loops are here displaced in parallel planes along the curved front and cannot give rise to macroscopic slip unlike dislocations lying along non-curved sections of the crack front.

It is not easy to reconcile the apparent absence of aligned etch pits in the tartan pattern zone with the mechanism proposed to explain the presence of bundles of longitudinal slip lines in decorated replicas. In order to further investigate whether or not there are dislocations emerging at both ends of longitudinal bundles it is proposed to analyze matching cleavage surfaces, one of which would be etched and the other decorated.

6.4. Restarting zone with inclined steps

Decorated replicas of sodium chloride cleavage surfaces show, in the zone immediately ahead of the stop band, an intricate pattern formed simultaneously by a river pattern and something similar to a lightning pattern (see section 4.3.5). This intricate pattern arises from the imperfect healing which is usually present when the crack is halted. As the crystal surfaces become more intimately united, there is a variable mismatch at numerous sites of the cleavage surfaces. When cleavage is restarted, it must cut through these faulted regions producing a multitude of unit cleavage steps. The rough surfaces observed in Figs. 4.8. and 4.24, for example, are produced in this manner

Etching of these faulted regions yields shallow, rounded large pits (see section 4.4) showing that the "healed in" dislocations are of a different nature than those introduced when stressing a crystal either by propagating a decelerating crack or by applying compressive or tensile stresses.

Atomic mechanisms involved in the healing process cannot be further investigated by electron microscopy of decorated replicas due to the roughness of the surfaces.

6.5. V or lightning zone

It is widely known that the V or lightning pattern is the surface structure left by a cleavage crack running freely at high velocities in a direction different from 100 in alkali halide crystals.

Different mechanisms have been proposed (by Forwood (2), Forwood and Forty (13), Robins et al. (10), Burns and Webb (9), Levi (14), Bethge (15)) to explain the formation of this type of structure.

Most of the authors proposed the hypothesis that the Vs are formed by a cleavage step and a slip step although two different mechanisms were suggested. This hypothesis sounds convincing for Vs in which one of the arms is parallel to the [100]direction. But for Vs in which both arms are curved or follow irrational directions, this hypothesis implies that a large number of dislocations are cross-slipping following parallel irrational paths. No other situation is known where a large number of neighbouring individual dislocations cross-slip along parallel curved or irrational paths and it is hard

to believe in such a uniform behaviour for dislocations not moving in their usual slip planes.

Furthermore, any proposed mechanism should be able to explain the nearly identical behaviour of both arms of the Vs when the crack is running at slower velocities: as described in section 4.3.2 they both tend to align parallel to the crystallographically preferred [100] direction.

No alternative mechanism can be proposed at present for the formation of this widely known pattern, but the accepted mechanisms do not meet all the types of patterns observed in practice.

6.6. High cleavage steps

The asymmetry of the microstructures observed by electron microscopy at both levels of a high cleavage step described in section 4.3.4.a), has been studied by Forwood (2), who, based on observations of decorated replicas, stated that the front of the crack is only distorted on one side of a high cleavage step. He suggested that the localized distortion of the crack front is not symmetrical about a cleavage step slightly inclined to the direction of crack propagation.

It is believed that a complete study of this asymmetry must take into account the undercut existing beneath high cleavage steps and the subsequent appearance of "healed-in" dislocations. Fig. 6.7 is a schematic diagram of typical structures observed in optical micrographs of high cleavage steps such as in Fig. 4.4. It can be seen the overlapping of the crack fronts preceeding the formation of a high cleavage step.

Following Swain et al. (16) it is considered that the cracks on adjacent planes approach each other from mutually opposing directions

to believe in such a uniform behaviour for dislocations not moving in their usual slip planes.

Furthermore, any proposed mechanism should be able to explain the nearly identical behaviour of both arms of the Vs when the crack is running at slower velocities: as described in section 4.3.2 they both tend to align parallel to the crystallographically preferred [100] direction.

No alternative mechanism can be proposed at present for the formation of this widely known pattern, but the accepted mechanisms do not meet all the types of patterns observed in practice.

6.6. High cleavage steps

The asymmetry of the microstructures observed by electron microscopy at both levels of a high cleavage step described in section 4.3.4.a), has been studied by Forwood (2), who, based on observations of decorated replicas, stated that the front of the crack is only distorted on one side of a high cleavage step. He suggested that the localized distortion of the crack front is not symmetrical about a cleavage step slightly inclined to the direction of crack propagation.

It is believed that a complete study of this asymmetry must take into account the undercut existing beneath high cleavage steps and the subsequent appearance of "healed-in" dislocations. Fig. 6.7 is a schematic diagram of typical structures observed in optical micrographs of high cleavage steps such as in Fig. 4.4. It can be seen the overlapping of the crack fronts preceeding the formation of a high cleavage step.

Following Swain et al. (16) it is considered that the cracks on adjacent planes approach each other from mutually opposing directions

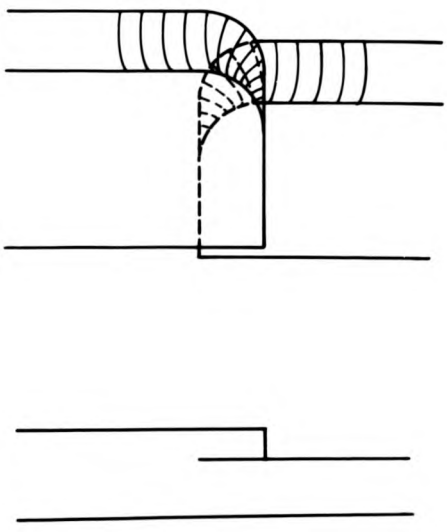

Fig. 6.5 High cleavage steps: overlapping of the crack fronts preceding its formation and resulting undercut.

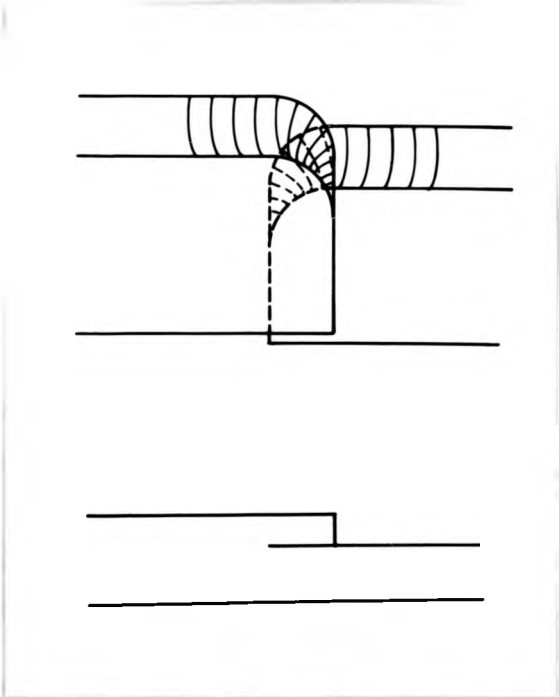

Fig. 6.5 High cleavage steps: overlapping of the crack fronts preceding its formation and resulting undercut.

transverse to the main crack front. It is proposed that small and monoatomic cleavage steps at both levels of a high cleavage step are formed at this stage, before the complete separation of the cleavage halves takes place. They are perpendicular to the crack fronts, thereby resulting perpendicular to the riser of the high cleavage step as was observed in Fig. 4,4 and is sketched in Fig. 6.5. The deflected portions of the steps at the lower level remain in the undercut surface of the steps and cannot be observed in the decorated replicas. This is considered to be the origin of the apparent asymmetry of the cleavage step microstructures observed by electron microscopy at both levels of a high cleavage step. This does not imply that all microstructures at both levels should be strictly symmetrical. It supports the view expressed by Swain et al. on the need of extreme caution in the interpretation of deformation patterns associated with high cleavage steps.

Plastic deformation arising when the high cleavage step is formed could bring about some kind of asymmetry in the slip microstructures. It remains to be studied whether this kind of asymmetry takes actually place. This study is complicated because it is necessary to distinguish between three kinds of structures: small cleavage steps, posterior plastic deformation and " healed-in " dislocations.

6.7. Cross-slip structures

It has previously been reported (2, 11, 12) that individual dislocations with a screw component can cross-slip along different crystallographic planes as well as following curved paths. For example, Forwood observed cross-slip structures in sodium chloride crystals which he suggested should have been the result of dislocation cross-slip

along a plane of the type 122 . He proposed that this cross-slip took place due to heating during preparation of the replica.

An effort was made to ascertain which of the cross-slip structures observed in decorated replicas are an artifact due to the heating of the specimen and which correspond to other mechanisms, such as surface-induced cross-slip or cross-slip due to the presence of obstacles in the path of a moving dislocation.

Non-crystallographic cross-slip of individual dislocations occurs mostly in heated specimens and is negligible in shadow-decorated replicas.

Some of the decoration structures found at room temperature have been interpreted in section 6.3.2 as due to surface-induced cross-slip of dislocations after the new surfaces have been created. Appel and Messerschmidt (12) stated that cross-slip of individual dislocations occurs mostly when they are immobile. This seems to be true for the surface-induced cross-slip of dislocations, but it is not the case for the frequently observed cross-slip structures such as the one shown in Fig. 4.21 which must be related to mobile dislocations.

Enclosed polygonal figures such as those described by Robins and Rhodin for magnesium oxide, were sometimes observed in the tartan pattern zone of replicas of sodium chloride crystals. They are probably related to cross-slip but they are not frequent enough to be considered representative of the surface structures associated with unsteady crack propagation.

It has been possible by observation of shadow-decorated replicas, to distinguish between thermal activated cross-slip due to heating of the specimen and surface-induced cross-slip or cross-slip due to intensive plastic deformation.

R.6 References

(1) Gilman J.J., Trans. A.I.M.E. 209, 449 (1957).

(2) Forwood C.T., Ph.D. Thesis, Bristol University (1966).

(3) Argon A.S., Orowan E., Phil. Mag. 9, 1023 (1964).

(4) Koehler J.S., Phys. Rev. 86, 52 (1952).

(5) Gilman J.J., Johnston T.C., J. Appl. Phys. 31, 632 (1960).

(6) Nabarro F.R.N., Theory of Crystal Dislocations, Oxford, Clarendon Press (1967).

(7) Stokes R.J., Johnston T.L., Li C.H., Phil. Mag. 4, 920 (1959).

(8) Davidge R.W., Pratt P.L., Phys. Stat. Sol. 6, 759 (1964).

(9) Burns S.J., Webb W.W., J. Appl. Phys. 41, 2086 (1970).

(10) Robins J.L., Rhodin T.N., Gerlach R.L., J. Appl. Phys. 37, 3893 (1966).

(11) Gilman J.J., Phil.Mag. 6, 159 (1961).

(12) Appel F., Messerschmidt U., Phys. Stat.Sol 35, 1003 (1969).

(13) Forwood C.T., Forty A.J., Phil. Mag. 11, 1067 (1965).

(14) Levi L., Phil. Mag. 28, 427 (1973).

(15) Bethge H., Phys. Stat. Sol. 2, 775 (1962).

(15) Swain M.V., Lawn B.R., Burns S.J., J. Mat. Sci. 9, 175 (1974).

Chapter 7

CONCLUSIONS

7.1. Summary

In this chapter the conclusions derived from the descriptions of previous chapters will be summarized and discussed.

From the outset the aim of this research has been to study the atomic mechanisms involved in the plastic deformation accompanying accelerations and decelerations of cleavage cracks in alkali halide crystals. For this reason a comprehensive study was made of the surface markings left by the propagation of a hesitating crack in sodium chloride.

Arguments have been presented which indicate the necessity to integrate the partial information already available.

A special apparatus was designed to study surface structures by optical and electron microscopy. It included facilities to control the atmosphere during specimen preparation.

It was found that the study of surface features characteristic of crack propagation at different velocities could be suitably performed on a crystal by stopping a cleavage crack several times and observing the zones between successive stopped fronts.

From this study five zones with distinctive characteristic surface features were considered both at a macroscopic and at a microscopic level, and different relative velocities were assigned to each of them.

The good reproducibility of the results justifies making further experiments to extract quantitative measurements of the velocities acting in each zone. An attempt was made to measure crack

velocities and a brief description of the experiments both performed and planned is included in the next section.

Many arguments have been presented in favour of the hypothesis that the longitudinal mode of deformation is the one which contributes most to the transverse bands associated with a stopped crack. However it is evident from the X-ray topography and the electron microscopy results that what characterizes the deceleration process is the activation of the transverse system. Using the knowledge which has been obtained of the processes involved in the deceleration of cleavage cracks, a simplified model was constructed. It illustrates the manner in which the activated transverse system is the origin of the cleavage structures observed at the stop bands. A limited correlation has been established between etch pit density and the density of surface structures at the same zone.

The presence of the longitudinal system in the deceleration zone is observed mainly through the presence of bundles of longitudinal slip lines. In order to discern whether both longitudinal conjugate systems are active, a new and improved decoration technique was developed. Previous models could not account for the characteristics revealed by this new technique and a new mechanism has been proposed to correlate the activation of the longitudinal systems with the observed characteristic structures. Interactions between orthogonal and oblique slip systems were taken into account in the proposed mechanisms.

To test the generality of the derived conclusions, electron microscopy and X-ray topography studies were carried out on lithium fluoride. Qualitatively the same results were obtained, although less transverse deformation was found due to the lesser plasticity of the lithium fluoride crystals. It is most probable that these surface

structures are common to a large number of materials with similar crystalline structure.

In conclusion: the present work constitutes the first stage of a research programme into the atomic mechanisms involved in the plastic deformation associated with decelerations of cleavage cracks in ionic materials. A clear overall picture of the surface structures generated by accelerations and decelerations of cleavage cracks in sodium chloride and lithium fluoride has been gained. Some tentative models have been proposed. Quantitative measurements and a theoretical analysis of the proposed mechanisms are justified by the generality of the observed surface structures.

7.2. Future work

In order to measure crack propagation velocity it is necessary to cleave the crystal in a reproducible fashion. One of the simplest ways to propagate cracks with reasonably reproducible velocities is by the use of an apparatus similar to that described by Gilman. In this device crystals are cleaved by a chisel fitted to a pendulum arm (Fig. 7.1). The chisel is released from a predetermined height and strikes the crystal with a known momentum.

The simple circuit of Fig. 7.2 was used to determine crack propagation velocities. For this purpose a series of parallel silver stripes were evaporated on a lateral surface of the crystal; these stripes are connected by an evaporated silver stripe on one side and by a resistive stripe of a painted Dag carbon on the other. During cleavage silver stripes are successively broken and resulting changes in resistance are displayed in a Tektronix 565 oscilloscope provided

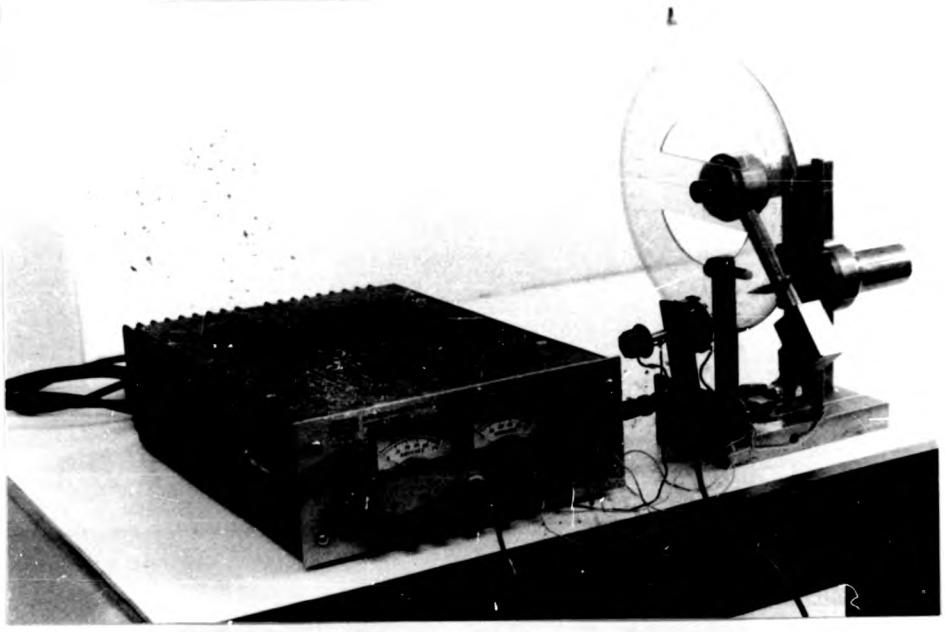

Fig. 7.1. Cleavage device

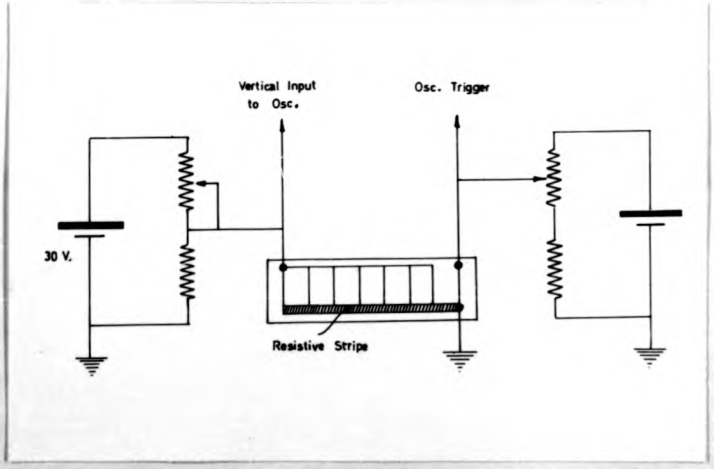

Fig. 7.2. Circuit used to determine crack propagation velocity

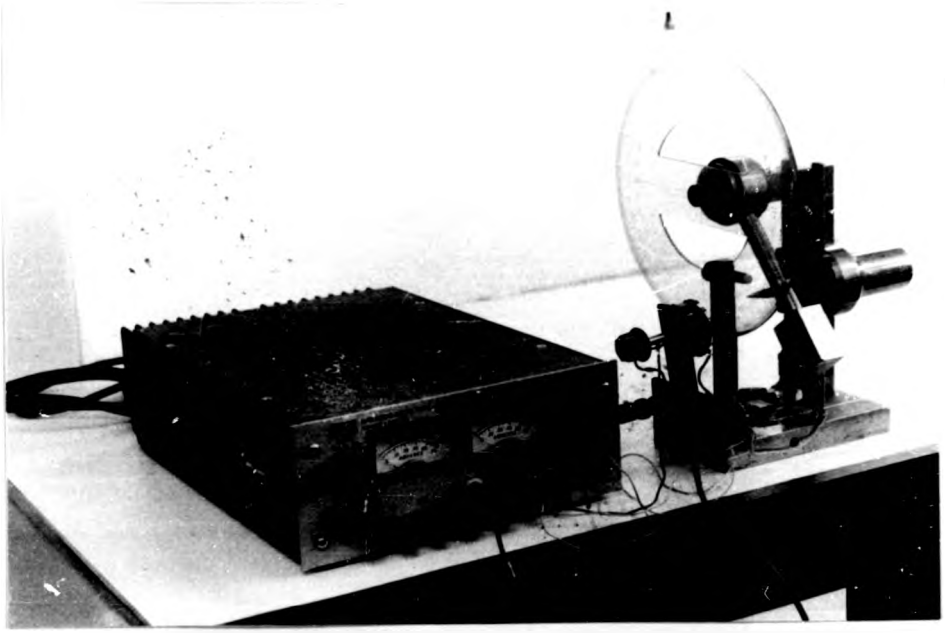

Fig. 7.1. Cleavage device

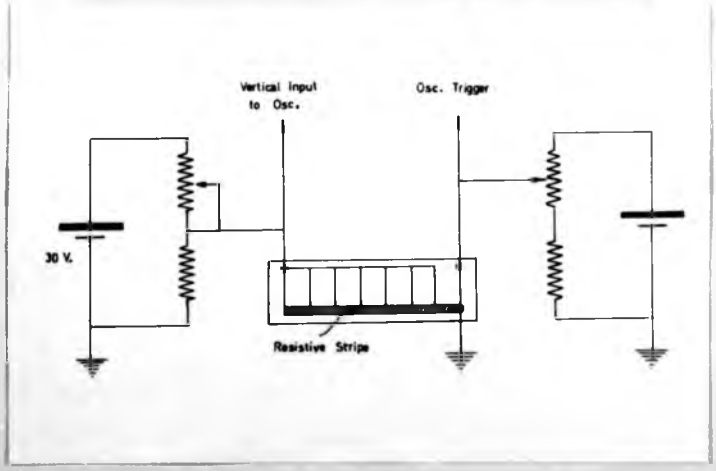

Fig. 7.2. Circuit used to determine crack propagation velocity

with a Polaroid camera. By recording the time between successive ruptures of the silver stripes an average velocity of the crack between the positions of two stripes can be determined. Fig. 7.3 illustrates a typical oscillogram showing the change of resistance as each stripe was broken. This oscillogram was obtained with a circuit evaporated with a mask in which stripes were 0.2 mm wide and were separated by 1.5 mm.

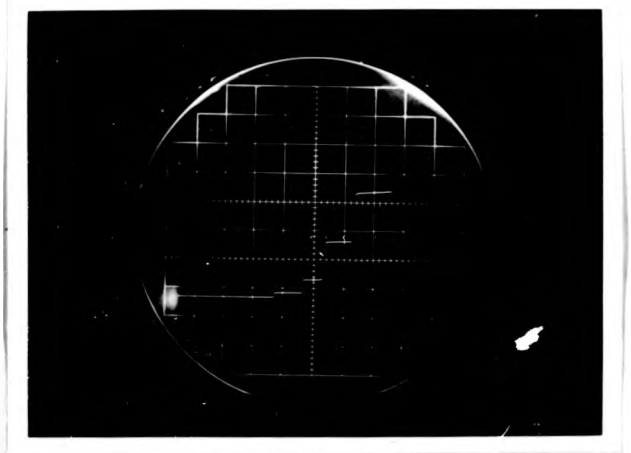

Fig. 7.3. Oscillogram showing the change of resistance as four silver evaporated stripes were broken.

Good reproducible results have been obtained.

The resolution of the velocity record depends on the width and spacing of the stripes.

It is impossible with the facilities presently available in the Argentine Atomic Energy Commission to construct a mask adequate to provide enough resolution to measure crack propagation velocities in the zones described in Chapter 4, whose lengths are of the order

of a hundred microns or less; in principle the method could achieve the required result.

The necessary facilities to measure the crack propagation velocities operative in the experiments described in this research could be provided only by an institution with advanced electronic technology. These measurements should be accompanied by the determination of other variables intervening in crack propagation theory as well as in plastic deformation theory (e.g. applied force). Only when these data are available the proposed mechanism can be quantitatively compared with theories on plastic deformation associated with crack propagation.

Besides, in order to make a theoretical analysis of observed cleavage structures, it is necessary to discriminate between elementary cleavage steps and slip steps. This discrimination is particularly difficult for elementary cleavage steps trailing out of a cleavage crack propagating nearly parallel to [100] .

This problem can be approached by the application of the nucleation theory analysis to the observation of decorated replicas obtained under very carefully controlled conditions.

As mentioned in Chapter 3, the effectiveness of the decoration process, as given by the ratio of the nucleation rates on steps and on flat surfaces, is a function of the included angles of the steps. It should be different for cleavage steps (included angle: 90° and for slip steps (included angle: 135°).

In order to determine this ratio with great accuracy, it would be necessary to study replicas decorated with very small nuclei

so that coalescence of neighbouring nuclei does not take place.

Only when all these problems are solved will an accurate comparison with theory be possible.

APPENDIX

Thin Solid Films, *21* (1974) S31–S32

Short Communication

On a shadow decoration technique

LELIA S. DE WAINER
Comisión Nacional de Energía Atómica, División Cristalografía, Buenos Aires (Argentina)
(Received January 24, 1974; accepted February 17, 1974)

The thin film decoration technique was first developed by Bassett[1] for the study of cleavage surfaces in ionic crystals. The original technique consists of the evaporation of a metal in a vacuum of 10^{-4}–10^{-5} Torr, the metal atoms impinging perpendicularly on a freshly cleaved surface of the crystal maintained at about 120 °C. An extremely light deposit develops in the form of small particles predominantly nucleated on the imperfections of the surface. Details of the surface structure on an atomistic scale are thus rendered visible. The decoration mechanism depends on the mobility of the metal atoms on the substrate and on the high density of nucleation sites along the surface steps. When the sample is heated thermal agitation increases and nucleation and growth of the metal clusters are enhanced. Poor results are obtained on crystals kept at room temperature.

We have found that very good decorations can be obtained at room temperature if the metal atoms strike the crystal surface at near grazing incidence, say 2°–3°. Under such conditions the principal component of the kinetic energy of the arriving atoms lies in the plane of the surface; these metal atoms may travel for long distances on the surface and a larger proportion of them are collected at steps. Since nucleation occurs almost exclusively on these preferential sites, a very low density of nuclei is obtained on the flat areas and resolution is improved (Fig. 1). This constitutes an important advance in technique, since possible modification of cleavage structures due to the heat-activated movement of the dislocations is avoided by decorating the crystals at room temperature.

An additional asset of this shadow decoration technique is the possibility of determining the sense of some of the steps running perpendicularly to the propagation direction of the arriving gold atoms. While the size of nuclei along one and the same step is approximately constant, there are basically two sizes of nuclei that condense on different monatomic steps. This difference in size may be related to the sense of the steps: on what we call a positive monatomic step, the atoms arrive at a re-entrant angle and large nuclei are condensed; although no shadow can be observed on monatomic negative steps, diffusing atoms render them visible through the condensation of small nuclei. In order to make this difference more evident it is advisable to evaporate slightly larger amounts of gold than those necessary to obtain an optimum decoration (Fig. 2). It is then possible to determine the sense of the steps provided they are not too closely spaced. In this last case, the size of nuclei is fairly uniform.

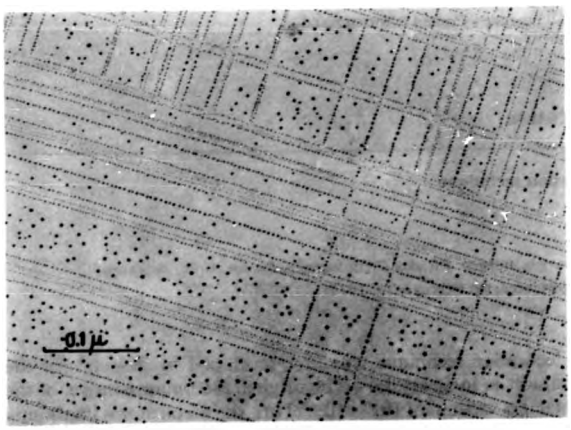

Fig. 1. Typical gold shadow decoration at room temperature and 10^{-5} Torr of a cleaved rocksalt surface. Glancing angle: 2°.

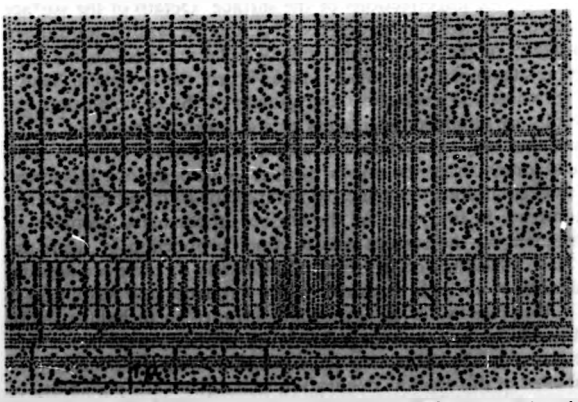

Fig. 2. Shadow decoration at room temperature and 10^{-5} Torr of a cleaved rocksalt surface. The amount of gold evaporated was about three times that necessary for optimum decoration.

As even monatomic steps lying in the shadow of large steps are near decorated, it is possible to compare slip lines appearing on the two levels of cleavage step.

The author wishes to thank Professor G. A. Bassett for valuable advice.

1 G. A. Bassett, *Phil. Mag.*, *3* (1958) 1042.

IV CONGRESSO

GRUPO IBEROAMERICANO

DE

CRISTALOGRAFIA

5ª REUNIÃO

SOCIEDADE BRASILEIRA

DE

CRISTALOGRAFIA

JUNHO 30 - JULHO 5, 1975

UNIVERSIDADE ESTADUAL DE CAMPINAS

CAMPINAS, S. P., BRASIL

LOCAL DA REUNIÃO

CATI - Av. Brasil 2340

PROGRAMA

E

RESUMOS

[illegible] I.U.C.A.

[illegible] Catiucha Ellis (Brasil) Presidente
[illegible] Gesto Gallon) (Argentina)
[illegible] Rittle (Chile)
[illegible] Font Altaba (Espanha)
[illegible] Bueno (Peru)
[illegible] Lima de Faria (Portugal)
[illegible] Estrella Laredo (Venezuela)

[illegible] BRASILEIRA

[illegible] Catiucha Ellis (Coordenador)
[illegible] Dório Dávora
[illegible] da Silva
[illegible]
[illegible]
[illegible]
[illegible] de Almeida
[illegible] Tanabura

[illegible] UNIDOS

[illegible], Universidade de Tokyo
[illegible] Prof. Polytechnic Institute of New York
[illegible] Prof. Stanford University
[illegible], Rutgers University

IV CONGRESSO IBEROAMERICANO DE CRISTALOGRAFIA

A Comissão Executiva solicita o envio dos resumos até a data de 30 de maio, com o objetivo de facilitar a sua impressão. Dentro do programa científico haverá uma seção especial de Aplicações a Problemas Tecnológicos, à qual é dada muita importância pelas suas implicações no desenvolvimento dos países da Zona.

EXPOSIÇÃO COMERCIAL

Várias das mais importantes empresas fabricantes de equipamentos usados nas técnicas cristalográficas e correlatas [illegible] os seus mais modernos equipamentos.

EXPOSIÇÃO NÃO COMERCIAL

Os participantes são convidados a enviar para a exposição, fotografia de interesse científico e/ou artístico ligadas ao campo da cristalografia, assim como aparelhos não comerciais recentemente projetados e construídos.

PROGRAMA SOCIAL E TURÍSTICO

Está sendo organizada a programação social e turística para os participantes e acompanhantes.

DATAS LIMITES

Envio de resumos: 30 de maio de 1975
- Prof. S. Catiucha Ellis
Instituto de Física - UNICAMP
CP 1170 - 13100 Campinas - SP.
Brasil

Reserva de Hotel: 20 de junho de 1975
- GRUNAPE
Rua dos Morães, 596 - Vila Madalena
05434 São Paulo - SP.
Brasil

[illegible]

S. Caticha Ellis (Brasil) Presidente
[illegible]esto Galloni (Argentina)
[illegible] Wittke (Chile)
[illegible] Font Altaba (Espanha)
[illegible] Bueno (Peru)
[illegible] Lima de Faria (Portugal)
Estrella Laredo (Venezuela)

[illegible] BRASILEIRA

[illegible]
[illegible]
[illegible] da Silva
[illegible]
[illegible]

[illegible]
[illegible]
[illegible]
[illegible]
[illegible]
[illegible] C. de Almeida
[illegible] Tsukahara

[illegible] CONVIDADOS

[illegible], Universidade de Tokyo
[illegible] Post, Polytechnic Institute of New York
[illegible], Stanford University
[illegible], Rutgers University

IV CONGRESSO IBEROAMERICANO DE [illegible]

A Comissão Executiva solicita o envio dos resumos até a data de 30 de maio, com o objetivo de facilitar a sua impressão. Dentr[illegible] do programa científico haverá uma seção especial de Aplicações [illegible] Problemas Tecnológicos, à qual é dada muita importância pelas suas implicações no desenvolvimento dos países da Zona.

EXPOSIÇÃO COMERCIAL

Várias das mais importantes empresas fabricantes de equipamento[illegible] usados nas técnicas cristalográficas e correlatas exibir[illegible] seus mais modernos equipamentos.

EXPOSIÇÃO NÃO COMERCIAL

Os participantes são convidados a enviar para a exposição, [illegible]grafia de interesse científico e/ou artístico ligadas ao [illegible] da cristalografia, assim como aparelhos não comerciais recentemente projetados e construídos.

PROGRAMA SOCIAL E TURÍSTICO

Está sendo organizada a programação social e turística para [illegible] participantes e acompanhantes.

DATAS LIMITES

Envio de resumos: 30 de maio de 1975
- Prof. S. Caticha Ellis
Instituto de Física - UNICAMP
CP 1170 - 13100 Campinas - SP.
Brasil

Reserva de Hotel: 20 de junho de 1975
- GRUNASE
Rua dos Morás, 696 - Vila Madalena
05434 São Paulo - SP.
Brasil

B10 SINGLE CRYSTAL LINE PROFILE ANALYSIS II. APPLICATION TO NEUTRON IRRADIATED LiF SINGLE CRYSTALS.(*)

Cecília A. Pimentel, Instituto de Física, Universidade de São Paulo, CP 20517, São Paulo - SP. Brasil, and S. Caticha Ellis. Instituto de Física, Universidade Estadual de Campinas, CP 1170, Campinas - SP - Brasil.

Line profile analysis of single crystal reflections of LiF irradiated under well controlled conditions in the core of a swimming pool reactor are compared with the profiles given by non-irradiated LiF.

The influence of such parameters as the temperature of the sample during irradiation, neutron spectra and background gamma radiation on the line profile is described and analyzed. The complexity of the changes involved precludes a complete interpretation in terms of specific defects and their distribution. An interpretation in terms of the dynamics of the damaging process is attempted as well as a correlation of some profile parameters with those of the corresponding crystal planes.

(*) Research sponsered by BNDE,CNPq,FAPESP,BID.

B11 MEDICION DE ALTA DENSIDAD DE DISLOCACIONES EN CRISTALES DE NaCl.

Victoria Míguez (1), Lelia S. de Wainer (2).

Se desarrolló un método de ataque químico para medir altas densidades de dislocaciones en superficies de cristales de ClNa.
Las réplicas de las superficies atacadas se fotografiaron en el microscopio electrónico y se midieron densidades del orden de 10^{9} disloc./cm^{2} en zonas en que se habían frenado grietas de clivaje.

A chemical etchant was developed to measure dislocation density in highly plastically deformed zones of cleavage surfaces of NaCl crystals.
Replicas of the etched surfaces were observed in the electron microscopy. Densities of approx. 10^{9} dislocations/cm^{2} were measured in zones where a cleavage crack had been stopped.

(1) UTN Fac. Reg. Bs.As., CIT y Dto. de Física. Medrano 951. Buenos Aires, Argentina.
CNEA. División Cristalografía y Fisicoquímica de Sólidos.
Avda. del Libertador 8250. Buenos Aires, Argentina.
(2) CNEA. División Cristalografía y Fisicoquímica de Sólidos.
Avda. del Libertador 8250. Buenos Aires, Argentina.

Proceedings in press

P1 TOPOGRAFIA DE RAYOS X EN CRISTALES HALUROS ALCALINOS.

E. Manghi (1) y L.S. de Vainer (2)

En el presente trabajo se estudiaron por topografía de rayos X las estructuras de dislocaciones producidas por clivaje en cristales de ClNa y FLi y se compararon con las obtenidas en FLi por otros autores.

Dislocation structures generated by cleavage in NaCl and LiF single crystals were studied by X-ray topography and compared with previous results on LiF as reported by different authors.

(1) CITEFA. Laboratorio de Física del Sólido. Zufriategui y Varela, Villa Martelli, Prov. Bs.As.

(2) CONEA. División Cristalografía y Fisicoquímica de Sólidos. Avda. del Libertador 8250, Buenos Aires.

P2 MEDIDAS DE CORREÇÃO DE DISPERSÃO PARA O ZR POR INTERFEROMETRIA DE RAIOS-X, M. Hart, H.H.Wills Physics Laboratory, University of Bristol, C.Cusatis, Departamento de Física, Universidade Federal do Paraná.

Desenvolveu-se um interferômetro de raios-x de varredura em que o deslocamento relativo de uma das placas é feito por força eletrostática. Elimina-se assim a vibração transmitida pelo contacto mecânico existente nos modelos anteriores.

Utilizando-se êste interferômetro e o método de determinação de espessura, cujo êrro é predominante nêste caso, sujerida pelos autores em 1974 mediu-se o índice de refração para o Zr no comprimento de onda da raia MoKα e encontrou-se

$$\Delta f' = 2{,}64 \pm 0{,}48.$$

Mostra-se que a precisão pode ser incrementada por um fator de 10.

Proceedings in press

P1 TOPOGRAFIA DE RAYOS X EN CRISTALES HALUROS ALCALINOS.

E. Manghi (1) y L.S. de Vainer (2)

En el presente trabajo se estudiaron por topografía de rayos X las estructuras de dislocaciones producidas por clivaje en cristales de ClNa y FLi y se compararon con las obtenidas en FLi por otros autores.

Dislocation structures generated by cleavage in NaCl and LiF single crystals were studied by X-ray topography and compared with previous results on LiF as reported by different authors.

(1) CITEFA. Laboratorio de Física del Sólido. Zufriategui y Varela, Villa Martelli, Prov. Bs.As.

(2) CONEA. División Cristalografía y Fisicoquímica de Sólidos. Avda. del Libertador 8250, Buenos Aires.

P2 MEDIDAS DE CORREÇÃO DE DISPERSÃO PARA O ZR POR INTERFEROMETRIA DE RAIOS-X, M. Hart, H.H.Wills Physics Laboratory, University of Bristol, C.Cusatis, Departamento de Física, Universidade Federal do Paraná.

Desenvolveu-se um interferômetro de raios-x de varredura em que o deslocamento relativo de uma das placas é feito por força eletrostática. Elimina-se assim a vibração transmitida pelo contacto mecânico existente nos modêlos anteriores.

Utilizando-se êste interferômetro e o método de determinação de espessura, cujo êrro é predominante nêste caso, sujerida pelos autores em 1974 mediu-se o índice de refração para o Zr no comprimento de onda da raia MoKa e encontrou-se

$$\Delta f' = 2{,}64 \pm 0{,}48.$$

Mostra-se que a precisão pode ser incrementada por um fator de 10.